2001

# Development and Characterization of Velocity Workspaces for the Human Knee.

John Eric Fuller
*Louisiana State University and Agricultural & Mechanical College*

# DEVELOPMENT AND CHARACTERIZATION OF VELOCITY WORKSPACES FOR THE HUMAN KNEE

A Dissertation

Submitted to the Graduate Faculty of the
Louisiana State University and
Agricultural and Mechanical College
in partial fulfillment of the
requirements for the degree of
Doctor of Philosophy

in

The Department of Mechanical Engineering

by
John Eric Fuller
B.S., Louisiana State University, 1995
December, 2001

*For my Father, my Mother and my Sister—*

*my foundation,*

*my sanctuary,*

*my motivation,*

*my inspiration.*

# ACKNOWLEDGEMENTS

This dissertation represents what I have been doing with my life for the past six years but these were things that I could not have done alone. As I consider those who have stepped up to lend me support, assistance, and guidance, it suddenly occurs to me that the current resurgence of patriotism, generosity, and humanity is not something that has been absent during my research. In fact, it has blessed me my entire life.

With that the first people I must thank are those who gave me life. My parents brought me into this world, protected me from it, gave me the tools to survive in it, and the inspiration and courage that have kept me going. Thanking them almost seems absurd, for how do you communicate infinite gratitude with mere words?

My sister kept me honest, suffered my moodiness, been an incredible role model, and taught me more than she will ever know and for that I will never be able to thank her enough. She has set the bar high and I hope one day I might be able to see just how high she has leapt.

To Dr. Michael C. Murphy, my appreciation for the unwavering example, the opportunity, and for being more than a teacher and mentor. Thank you for being a friend and listening to what I had to say, no matter how ridiculous. Dr. Warren N. Waggenspack, Jr., also more than a teacher and mentor, you trusted me with your home and while it might just seem *fair enough* to you, that kind of trust is not something I regard lightly.

For the remainder of my committee, Dr. Madden, Dr. Kerwin, and Dr. Welsch, thank you for the guidance, the patience, and the time you have given to this work.

Rob, Donovan, Jake, Garrett, and Danny...for being true friends, and the subjects of way too many stories that I am sure will be further embellished with time, my eternal gratitude and, understandably, my continued silence.

My gratitude must also be extended to those who have made specific technical contributions to the research. These include: Chris Schwehm for his assistance in accessing data, Timothy Morgan for the use of his thresholding code, and Anna Omeltchenko and Mingli Zhang for their preliminary development of the concepts of displacement workspaces.

Specific acknowledgements for data collection include: (1) ***Massachusetts Institute of Technology Data Collection and Manipulation***-Dr. Murali Jasty of Massachusetts General Hospital for arranging CT scans, Jane Pardy of Massachusetts General Hospital for operating the CT scanner, Professor Derek Rowell from the Massachusetts Institute of Technology for initial aid with CT scan imaging, Michael Stracher of the Orthopaedics Research Laboratory at Massachusetts General Hospital for data conversion, Mingli Zhang from Louisiana State University for data conversion, Timothy Morgan from Louisiana State University for preliminary coding (2) ***University of Minnesota Data Collection and Manipulation***-Dr. Greg Brown of the University of Minnesota and Regions Hospital for specimen acquisition, specimen dissection, marker placement, setting up the CT scans, general clinical guidance, and putting up with me for four days, Paul Grunhovd, R.T. of Regions Hospital for operating the CT scanner, Fred Wentorf from the Biomechanics Department of the University of Minnesota for specimen storage and handling, Synthes Corporation (Paoli, PA) for the donation of titanium screws (3) Those with the ***Visible Human Project*** (4) ***Health South***

***Diagnostic Center Data Collection and Manipulation***-Dr. Charles Greeson of Heath South Diagnostic Center for setting up the MRI scans and general clinical guidance David Frye of Heath South Diagnostic Center for operating the MRI scanner Chris Schwehm from the Remote Sensing and Image Processing Lab at Louisiana State University for data conversion.

I also need to extend thanks to the people of the College of Engineering Dean's Office, including: Vicki Hannan, Mickey Adler, Lisa Hebert, Shea Dunigan, Cathy Hill, Lisa Bergens, Lisa Launey, Cathy Harrison, Dr. Julius Langlinais, and the office student workers over the years. Their suggestions, help, employment, and indulgences for my benefit have helped enormously over the years.

Last but certainly no least, I would be derelict in my gratuities if I did not acknowledge my fellow students who put up with my shenanigans, kept me on my toes, and kept our lab an entertaining place to work. To all of you, my sincere gratitude: Yohannes Desta, Tim Morgan, Jim O'Bryan, Anna Omeltchenko, Jim Rodgers, Christophe Marques, Fred Majkut, Kevin Zanca, Gary Templet, Mircea Despa, Dawit Yemane, Proyag Datta, Summer Johnson, Abhinav Bhushan, Tracy Morris, Catherine Oropeza, Dinakar Palaparti, John Williams, Madhulika Sathe, Michael Mitchell, Dwhyte Barrett, Lyle Breaux, Chris Cowart, and John Breeden.

# TABLE OF CONTENTS

# LIST OF TABLES

# LIST OF FIGURES

# LIST OF SELECTED SYMBOLS AND ACRONYMS

| Symbol | Description |
|---|---|
| $\hat{S}$ | Unit screw coordinate vector |
| $\vec{s}$ | unit vector in the direction of the screw axis |
| $\vec{s}_0$ | vector to any point on the screw axis |
| $\lambda$ | pitch of a screw |
| $\beta$ | general wrench |
| $\alpha$ | general twist |
| $\varpi_{\alpha\beta}$ | virtual coefficient of twist $\alpha$ and wrench $\beta$ |
| g | gravity |
| X, Y, Z | principle Cartesian coordinate axes |
| $x, y, z$ | Cartesian coordinates |
| $M$ | Constraint matrix |
| $\$_{ij}$ | $j^{th}$ screw coordinate of the $i^{th}$ constraint |
| $n$ | dimension of the constraint space |
| ACL | Anterior Cruciate Ligament |
| PCL | Posterior Cruciate Ligament |
| FCL | Fibular Collateral Ligament |
| TCL | Tibial Collateral Ligament |
| CT | Computed Tomography |
| MRI | Magnetic Resonance Imaging |
| $M_L$ | Longitudinal magnetization |
| $M_T$ | Transverse magnetization |
| $T_1$ | Longitudinal relaxation time |
| $T_2$ | Transverse relaxation time |
| TR | Time between repetitions |
| TE | Time 'til echo |
| $C$ | Machine and environment constant for MRI intensity |
| $I$ | MRI intensity |
| MIT | Massachusetts Institute of Technology |
| MGH | Massachusetts General Hospital |
| NLM | National Library of Medicine |
| VHP | Visible Human Project |
| UMN | University of Minnesota |
| VODW | Variable Orientation Displacement Workspace |
| FODW | Fixed Orientation Displacement Workspace |
| $\tilde{\alpha}$ | Twist with first three coordinates switched with last three |
| $N(\beta)$ | Null space of the matrix $\beta$ |
| $P(\beta)$ | Repelling space of the matrix $\beta$ |
| $X_H$ | Homogeneous solution basis |
| $X_P$ | Repelling solution basis |
| $r$ | rank of the constraint matrix |

| | |
|---|---|
| $m$ | Number of constraining wrenches |
| $n$ | dimension of the constraint space |
| $d$ | dimension of the null space |
| $q$ | distinct $d$+1-face partitions of the constraint matrix |
| $\lambda_i$ | any real scalar |
| $\gamma_i$ | any positive scalar |
| $\tilde{X}$ | General velocity workspace element |
| $A$ | Negative of the constraint matrix |
| $\vec{b}$ | tolerance vector for minimization solution |
| $\$_i$ | $i^{th}$ constraining wrench |
| $\tau_i$ | $i^{th}$ velocity workspace twist |
| $a,b$ | Homogeneous Euclidean 3-space vector |
| $x_a, y_a, z_a$ | Cartesian coordinates of a point $a$ |
| $e_i$ | $i^{th}$ geometric algebra basis vector |
| $[L,M,N,P,Q,R]$ | Plücker Coordinates |
| $A$ | General multivector |
| $W_C$ | Pure couple wrench |
| $W_F$ | Pure force wrench |
| $T_\omega$ | Pure rotation velocity |
| $T_v$ | Pure translation velocity |
| $\overline{W}$ | general wrench |
| $\overline{T}$ | general twist |
| $I$ | unit pseudoscalar |

# ABSTRACT

The knee joint is the most complex joint in the human body. A complete understanding of the physical behavior of the joint is essential for the prevention of injury and efficient treatment of infirmities of the knee. A kinematic model of the human knee including bone surfaces and four major ligaments was studied using techniques pioneered in robotic workspace analysis. The objective of this work was to develop and test methods for determining displacement and velocity workspaces for the model and investigate these workspaces.

Data were collected from several sources using magnetic resonance imaging (MRI) and computed tomography (CT). Geometric data, including surface representations and ligament lengths and insertions, were extracted from the images to construct the kinematic model. Fixed orientation displacement workspaces for the tibia relative to the femur were computed using ANSI C programs and visualized using commercial personal computer graphics packages. Interpreting the constraints at a point on the fixed orientation displacement workspace, a corresponding velocity workspace was computed based on extended screw theory, implemented using MATLAB™, and visually interpreted by depicting basis elements.

With the available data and immediate application of the displacement workspace analysis to clinical settings, fixed orientation displacement workspaces were found to hold the most promise. Significant findings of the velocity workspace analysis include the characterization of the velocity workspaces depending on the interaction of the underlying two-systems of the constraint set, an indication of the contributions from passive constraints to force closure of the joint, computational means to find potentially

harmful motions within the model, and realistic motions predicted from solely geometric constraints. Geometric algebra was also investigated as an alternative method of representing the underlying mathematics of the computations with promising results.

Recommendations for improving and continuing the research may be divided into three areas: the evolution of the knee model to allow a representation for cartilage and the menisci to be used in the workspace analysis, the integration of kinematic data with the workspace analysis, and the development of *in vivo* data collection methods to foster validation of the techniques outlined in this dissertation.

# CHAPTER 1. INTRODUCTION

## 1.1 Motivation

Without question, the significance of physical activity has boomed in the past century. From physical and emotional health concerns to lucrative business ventures, exercise and athletics have become aspects of life that affect virtually every member of civilized society. Athletic endeavors permeate politics, religion, education, the economy, crime, family, entertainment, international relations, and the environment as well as many other aspects of human life. Along with this rise in the significance of sports has come the escalation of the number of people participating in them. A natural companion of any sport is injury, which can manifest itself in many forms ranging from minor cuts and abrasions, to muscle, tendon, and ligament injuries, to fractured and broken bones to serious neurological damage. Cuts and abrasions generally do not preclude a person's participation in a sport for any significant amount of time, while muscle, tendon, and ligament injuries tend to be repairable but often remove the participant from the sport while healing. Fractured and broken bones almost always interrupt a persons participation in athletics, generally taking longer times to heal depending on the course of treatment, while neurological injuries can spell the end of a person's athletic involvement altogether.

Athletic involvement, however, is not the only segment of life where physical injury is a significant concern. Increased risk for physical injury can be found in many other aspects of life including the workplace or simply as a result of natural aging. In an effort to reduce the number of workplace-related injuries, the United States Government created the Occupational Safety and Health Administration (OSHA) in

1971 to prevent workplace injuries, illnesses, and deaths. Such an organization naturally pursues the causes and mechanisms of workplace trauma for many purposes, including fault assessment, punitive action, and policy drafting. Injuries have become more common among the elderly as advances in medicine and nutrition have increased the possible service time for the human body. Deterioration of the human body as one gets older carries multiple threats of physical injury from factors such as natural wear, reduced strength, and fading senses.

### 1.1.1 Clinical Significance

The human skeletal system is the frame for the human body. It provides the structural scaffold on which the body is built. Among its many functions, it provides protection to delicate internal organs, supplies rigid supports through which forces can be transmitted, provides the frame for the human biomechanical system, and furnishes production facilities for various life-sustaining elements. In essentially all of these duties, there is some element of mechanical interaction, specifically the absorption, transmission, or sensing of force, and from this observation we may generalize that the main functions of bones are to manage the forces and motion encountered and initiated by the human body. Thus, it is not surprising that investigations into the movement of the human body begin with the study of the movement of the skeletal system.

The biomechanics of the human knee are no exception to this generalization. According to an American Academy of Orthopaedic Surgery report, in the United States of America during the calendar year 1994, there were approximately 6.4 million people who sought physician attention regarding knee problems. From 1990 to 1994 the number of knee procedures performed rose from 234,000 to 311,000 while the

number of total knee replacements rose from 129,000 to 209,000 that same year (AAOS, 1997). In a separate report from the Bureau of Labor Statistics of the United States Department of Labor, knee injuries accounted for 149,100 cases of nonfatal occupational injuries that resulted in a median nine days away from work in 1994 (Hoyle, 1996). From these numbers it is clear that knee problems affect a significant number of Americans either personally or professionally. For that reason, along with the fact that the human knee is the largest and perhaps most complex joint in the body, the function and movement of the joint are two of the most active areas of research in human biomechanics.

When the human knee is injured, damage may be incurred by any of the structures in and around the knee including bone, soft tissue, surrounding vascular supplies and nervous tissues. Strained or torn ligaments, cartilage damage, strained and ruptured tendons and an assortment of auxiliary soft tissue impairments are the most commonly diagnosed results of knee trauma. Many of the partially torn (strained) injuries will heal on their own given adequate rest and nutrition. In some cases, even fully torn tissues may repair themselves as exemplified by the study reported by Tewes et al. (Tewes, et al., 1997) concerning the spontaneous reattachment of the chronically injured posterior cruciate ligament. It was noted, however that in these cases, the ligament appeared to be "arcuate or hyperbuckled", in contrast to typical uninjured ligament structure.

Tewes' study is an example of research that gives rise to the question of the necessity and or advantages of surgical intervention versus less invasive therapies. Are the benefits of surgical intervention worth the invasiveness of the procedure with

respect to other options available to the patient? Another study, investigating the effects the posterior cruciate ligament had on tibio-femoral gap in total knee arthroplasties (Mihalko and Krackow, 1999) used data collected *in vitro* from cadaver specimens. A major concern of this type of study is how well the cadaver specimen data correlates to *in vivo* human performance. The development of some method to correlate the findings of clinical investigations with everyday life is necessary to put the results in a proper context. Many such *in vitro* studies have investigated the roles of ligaments in the function of the human knee. Some of the subjects studied include the role ligaments play in the stability of the human knee joint (Piziali, et al., 1980) as well as the results of removing individual ligaments or ligament sections from the system entirely (Shoemaker and Markolf, 1985).

The human knee is a joint in the musculoskeletal system, and as such, its main function is to allow motion between the thigh and shank of the human lower limb. The development of an analysis technique that, given a set of constraints, maps out all possible knee motions, could offer much information and insight into studies of knee biomechanics. The study of the kinematics of the human knee is one discipline where the construction of this type of information could provide new perspectives on old problems, meaningful information on current questions, and possible direction to future work. Once a model has been developed, the natural place to begin with respect to kinematic analysis is position analysis. The construction of all possible positions and orientations one rigid body may assume relative to some other rigid body is a general description of what displacement workspace analyses attempt to accomplish. It is highly probable that information useful to the study of the biomechanics of the human

knee is inherently contained within workspace analyses based on the constraint system of the joint. Investigation of a relatively simple model, including representations for constraints dictated by the four major ligaments, gives insight into many aspects of the joint biomechanics. For example, the addition and exclusion of ligaments to a workspace model showed noticeable changes in the shape, geometry and size of the two dimensional cross-sections of the displacement workspace. Such information may allow investigators to develop strategies for affecting the allowable displacements and trajectories in similarly constrained joints, *in vivo* (Fuller, et al., 2000).

Normally, *in vivo* studies look at the statistical effects on injury rates or some type of performance metric. Often these studies look at geometric comparisons between subjects. Comparison of specific ligament failure as related to activity or gender are popular areas of interest as exemplified in a study by Arendt and Dick (Arendt and Dick, 1995). In this study, knee injury patterns between men and women basketball and soccer players were analyzed for trends. It was concluded that women are more susceptible to anterior cruciate ligament (ACL) injuries in these sports than their male counterparts due to an amalgamation of reasons. A study by LaPrade and Burnett investigated the statistical link between intercondylar notch stenosis, as measured by the subjects NWI (notch width index), with the frequency of ACL injury. The statistics showed that a lower NWI, or a more prominent narrowing of the intercondylar notch, was an indication of an increased risk for ACL injury (LaPrade and Burnett, 1994). From a kinematic perspective the study of workspaces based on the geometric parameters observed in these studies could provide a method for confirming or invalidating these types of purely statistical studies.

Another characteristic of this past century is the increase in litigation involving physical injuries related to both the work environment as well as leisure activities. As the monetary compensation has steadily increased for those injured and their advocates, considerable interest has been directed toward the determination of the mechanisms of injury for litigation involving common injuries. The identification of those mechanisms responsible for specific injuries could lead to alterations of the environment or the activity in order to eliminate or minimize the risk of injury, thus saving corporations money, improving employee quality of life, and freeing up court time for other applications. Workspace analysis may provide a window through which these mechanisms and their augmentation could be studied.

Not to be overlooked due to the general occupational occurrences, organized athletics represent the realm where physical injury produces the most visible losses, financial or otherwise, both to the individual and the organization. The NCAA reported an injury rate for varsity football during the fall of 1999 of 44.9 injuries per 1000 athlete-exposures. Fifteen percent of injuries sustained during practice involved the knee while twenty-one percent of those occurring during games were knee injuries (N.C.A.A., 1999). Data also indicated that in practices as well as games, the knee was the body part most often injured. In professional sports, or any career, significant injuries translate into lost revenue through the cost of treatment, and in some instances can lead to legal problems involving contract disputes, safety regulations, fraud, and the loss of patrons.

### 1.1.2 Workspaces in Medicine

In a 1986 perspective on the different levels of knee research, Noyes catalogued some of the more prevalent problems associated with clinical knee research, many of which remain with us today. One of the shortcomings he cited was poor epidemiological (the investigation of the causes, distribution, and control of infirmities) analysis in clinical studies, referring to the poor design, inadequate control and limited scope of the majority of clinical studies reported in "current" literature (Noyes, 1986). Workspace analysis of a model of the human knee is a direct investigation into the kinematic epidemiology of injuries to the modeled structures. Studies of the cause of injury (constraint violation), distribution of injury (statistical analysis of geometries), and control (modeling treatment procedures) are all aspects that may be addressed through information communicated by workspace analyses.

Noyes also addressed the problem of inadequate data, particularly among studies concerning corrective procedures. Much of this problem stems from ambiguous terminology such as "partial" tears, "severe" pain, or "normal" knee. Other sources of ambiguity come from the highly subjective knee injury classification systems (Noyes, 1986). Using the displacement and velocity workspaces as educational tools, agreement between clinician assertions of terminology and more universal assessments of functional results of procedures may be acquired. In his closing statements, Noyes called for research of the forces communicated by ligaments, the assessment of varying techniques of knee reconstruction, and investigation into control issues, specifically, stability and injury compensation mechanisms (Noyes, 1986). Workspace analysis

presents itself as an organization of kinematic information that can be harvested to address these concerns.

The human machine, like all other machines, from time to time, breaks down and is in need of repair. Repairs to injuries of the human knee come in various forms from rest and temperature therapy to total knee arthroplasty (TKA) with procedures such as ligament grafting and arthroscopic surgery falling somewhere in between. While devices such as implants, artificial ligaments, and knee braces are made from various engineering materials, they do not possess the regenerative abilities seen in their equivalent human part. Wear, fatigue, and loading characteristics, among other factors, will always play roles in the life of an artificial biomedical device. Computer simulation of the causes and potential solutions to these problems necessarily must draw from information found during workspace analysis of the human knee joint model. For example, Chen, et al, track the likely path of contact between femoral and tibial prosthetics, effectively mapping out a path contained within the displacement workspace of the human knee, in an attempt to predict the wear behavior of the implants (Chen, et al., 2000). Their analysis is the only known work to date that includes both surface contact and ligament constraint to investigate arbitrary displacements of the human knee, however the authors make no attempt to map out all possible relative displacements.

There are many occurrences where robotics and related sciences play key roles in medicine. Computer-aided surgery takes advantage of automated scanning techniques to diagnose, plan, and execute some surgical procedures. Simulations of surgery with robotic analysis techniques allow physicians to plan, practice, and evaluate

procedures before committing to specific courses of action. During surgery, models are used to identify and visualize structures, paths, and progress of the physicians' work. These techniques improve the efficiency of doctors and minimize the trauma a patient incurs from time spent in the operating theater. Postoperatively, robots are used to simulate the resulting kinematics of the surgical procedure and in some cases, directly assist in patient rehabilitation (Ellis, 2000). Perhaps some day robots will be employed to perform surgical tasks whose precision or stability requirements are beyond the capabilities of human doctors. A research group at Johns Hopkins University has developed one of several robots capable of assisting in surgery or delivering therapies. This particular example was capable of being controlled either remotely by a human user or based on radiologically determined guidance (Stoianovici, et al., 1998). Employing the same techniques to study both the human aspect and the robotic aspect within the medical field, namely workspace analysis, naturally leads to more seamless integration of the two with the progression of technology.

### 1.1.3 Scientific Interest

Workspace analysis has a strong foundation in the field of robotics, however the human knee presents interesting challenges when extending workspace concepts to its study. The detection of displacement workspaces based on both ligament-style constraints and arbitrary surface contact constraints is a new and relatively unaddressed topic of study in either the robotics or medical communities. The application of Ohwovoriole's characterization of total freedom of a rigid body based on extended screw theory to the study of biomechanics of the human knee is also relatively

unexplored. There is scientific value to the study of both of these topics that will be beneficial to the fields of robotics and medicine alike.

Injuries are inevitable in any form of repetitive physical activity. The method of treatment and the preventative techniques developed from analysis of those injuries are always candidates for improvement. The investigation into the types and ranges of motion that cause injury to the human knee joint is one way to make a significant contribution to the understanding of the function and performance of both the human knee joint as well as its prosthetic replacements. It is exactly this task that the notions of displacement and velocity workspaces address both by definition and evaluation. This is the focus of this dissertation, and its goal is to bring to the forefront some novel information that may be understood and applied to the improvement of treatment and the reduction of injury associated with the human knee.

**1.2 Objectives**

While it is mathematically possible to generate a velocity workspace based solely on ligament constraints, preliminary results of the ligament-based displacement workspace have indicated that significant portions of the resulting workspace were not feasible due to bone-to-bone surface interactions. A velocity workspace generated by the constraints imposed by ligaments alone would produce large amounts of information characterizing unattainable conditions and do more to confuse the issue than to elucidate it. The surface interaction between the tibia and femur initially appears to provide a considerable constraint to the displacement workspace of the human knee. Thus, it is necessary to include the contribution of the two main articulating bones of the knee in the description of the displacement workspace. With

the surfaces included, the efficiency of the computation of the resulting velocity workspaces will be significantly improved by the elimination of unreachable configurations of the rigid bodies representing the tibia and the femur in the knee model. In addition to the contribution to efficiency, the range of application for the model is expanded by providing an avenue for the model to be altered to represent a total knee replacement or some other type of surgical procedure for similar analysis.

The first objective of this dissertation was to determine the displacement constraints contributed by the contact between the tibia and femur. This determination yielded the surface constrained displacement workspace of the human knee. The second objective of this dissertation was to combine the displacement workspace defined by the surface interaction between the two major bones of the human knee with the displacement workspace defined by the interactions of the four major ligaments of the human knee. The construction of the combined surface contact and ligament-constrained workspace allowed the analysis of the passive or reactionary forces that were present along the workspace boundaries. The characteristics of these forces along with their interactions are the focus of the third objective of this dissertation, to determine the inequalities that define the velocity workspaces of the human knee. The final objective of this dissertation was to investigate the properties of the velocity workspace of the human knee as well as the application of various mathematical and graphical techniques that may be used to interpret and visualize the velocity workspace of the human knee.

# CHAPTER 2. BACKGROUND

## 2.1 Robotics

### 2.1.1 History

It is interesting to note that the word robot was first used in 1921 in the play R. U. R. (Rossum's Universal Robots) by Czech playwright Karel Capek. In Capek's play, the "robots" were machines whose physical forms and movements resembled those of humans, establishing the stereotype that has remained throughout both scientific and recreational literature regarding robots in general (Murray, et al., 1994). Perhaps the vanity of mankind along with the impressive complexity of the human body have led to the imitation of the human form as the optimum design for early robots. As such, in the development of robotics, the classification of a machine as a robot was often connected to its ability to operate autonomously or its flexibility to perform several distinct operations, as human workers might.

Both the form and operation of robots progressed, with technological advances, to more closely mimic human characteristics. This has led to the identification of many robotic components with terms typically used to describe human attributes such as elbows and wrists, or human actions such as grasping and manipulation. The science of robotics, however, has advanced beyond human forms to better tailor the machine to the required task. The more recent development of robots and machines in general has progressed largely by the motivation to perform complex or hazardous tasks that are beyond the physical limitations of human labor, rather than simply mimicking human behaviors.

Today's robotic manipulators seldom resemble human anatomy, and many applications have moved from solitary serial link mechanisms to multiple cooperating serial chains or parallel link configurations. In step with the development of robots and manipulators, the interest in describing and defining the mathematics associated with these machines has gained considerable momentum. Various mathematical genres have been revived, including Screw Theory, Lie Algebra, Geometric Algebra, and Projective Geometry, to handle the modeling and simulation of robotics and to take advantage of the recent, considerable improvements in computers and instrumentation. The result is that robotic analysis has become a science in its own right. Many techniques and algorithms have been produced to handle the rigorous geometry and kinetics of today's robots. It is the application of these methods to the study of the "ultimate living robot", the human being, that is the basis for the establishment of the field of biomechanics.

### 2.1.2 Workspaces

The very concept of a workspace comes from the definition of its root words "work" and "space". In the most general sense, a workspace can be defined as a region (space) where specified operations (work) can be performed. The nature of the region is directly dependent on the type of operation for which it is defined. For example, an office workspace consists of the general area where the business of the office is carried out. Similarly, a displacement workspace will generally be defined within the realm of angular and/or linear displacements and velocity workspaces will find their basis as some subset of angular and linear velocities. For the remainder of this section, the discussion will use the term workspace to describe some type of displacement workspace.

The first notable work discussing a "working spaces" approach to the analysis of robots came from Roth (Roth, 1976) while investigating serial link robot manipulators. Several others have made contributions to workspace analysis in robotics including Kumar and Waldron (Kumar and Waldron, 1981), Sugimoto and Duffy (Sugimoto and Duffy, 1981a; 1981b), Gupta and Roth (Gupta and Roth, 1982), and Yang and Lee (Lee and Yang, 1983; Yang and Lee, 1983), along with many others. Gupta (Gupta, 1986) provides a concise summary of the early contributions made by these and other authors.

Workspace determination has been extensively investigated regarding mechanical manipulators along with many other classes of robots. Much of the work has been focused on devices with some component attached to a fixed reference frame such that the workspace determination is dependent solely on the geometry of the mechanism. Sugimoto et al. looked at special configurations of single-loop mechanisms using screw theory to deduce limitations on the permissible, instantaneous trajectories of an end effector (Sugimoto, et al., 1982). In contrast, the workspaces of free-floating manipulators, or manipulators whose base is not attached to a fixed inertial frame, were addressed by Agrawal and Garimella (Agrawal and Garimella, 1994). In their work, inertial property data for the mechanism links were required to determine the manipulator workspace boundaries, which were determined by force-based constraints similar to fixed-base manipulator analyses.

Methods for determining workspaces of general mechanisms vary in their techniques from purely geometric construction, to force analysis, to energy minimization. Yang and Haug investigated workspaces by solving a set of kinematic constraint equations using numerical solution techniques to handle nonlinear systems

(Yang and Haug, 1994a; 1994b). Davidson and Hunt, and Davidson and Pingali (Davidson and Hunt, 1987b; Davidson and Pingali, 1987) used a sweeping process to map out the plane-workspaces of 2-revolute manipulators and extended the method to describe n-revolute manipulators by generating the corresponding plane-workspace envelopes or boundaries. The authors then developed classifications for 3-revolute manipulators for which the outermost two axes intersect.

Madhani and Dubowsky introduced the Force Workspace Approach to the design of multi-limb robots, such as walking machines. This method effectively mapped constraint obstacles into the mechanism configuration space to determine link and joint limitations as well as plan mechanism motion (Madhani and Dubowsky, 1992). Cai and Rovetta used a modified Boolean approach, similar to a spatial decomposition method, to map out the workspaces of multiple link serial mechanisms (Cai and Rovetta, 1990). Huang and Schimmels realized the geometric limits of a rigid body constrained by simple, parallel springs using screw theory (Huang and Schimmels, 1998). Bulca et al. constructed workspaces for spherical wrists and spherical platforms by mapping out the space of singular configurations using the Euler-Rodrigues parameters defining the orientation transformation of the end effector (Bulca, et al., 1999). Abdel-Malek, et al. compared two methods of mapping out the workspace boundary based on the analytic Jacobian of the manipulator. The first method used a numerical method to determine the boundary based on continuation criteria while the second searched for singularity surfaces both on the workspace boundary and in its interior (Abdel-Malek, et al., 1997). Bicchi et al. studied the properties of cooperating robots, looking at mobility, kinematics, and velocity behaviors of robotic systems under the assumption of force

closure in the kinematic chains (Bicchi, et al., 1995). Considering only manipulators capable of representation by rigid links, prismatic joints, and revolute joints, Kumar and Patel developed a computer graphics-based technique employing transformation matrices to map out the workspace boundary of a mechanism (Kumar and Patel, 1986). Lee presented an algorithm for determining the minimum $l_\infty$-norm for a set of under constrained, consistent linear equations, borrowing on techniques from convex analysis and linear programming. Lee applied his algorithm to determine velocity workspaces of serial-link robots of varying configurations in two and three dimensions (Lee, 2001).

#### 2.1.2.1 As Design Tools

Workspace analysis has proven valuable in robotics both as a design and as an evaluation tool. A workspace can represent various combinations of forward kinematic solutions for a manipulator allowing for performance adjustments, prediction of singularity configurations, and synthesis with the working environment. An algorithm for the synthesis of a manipulator to fit specific two-dimensional workspace geometries has been developed by Gosselin and Guillot (Gosselin and Guillot, 1991). This method optimizes the geometry of the manipulator workspace to coincide with some predetermined workspace and the authors hypothesize that it should be possible to extend this algorithm to spatial workspaces. Merlet presented an algorithm that sought out all possible geometries of a class of parallel manipulators known as Gough-platforms, which would generate workspaces that contained some predetermined workspace. Using the specified workspace, which was made up of a set of points and lines representing the location of the center point of the moving platform, the algorithm

addressed such synthesis issues as joint range of motion and link interference (Merlet, 1997).

Sen and Mruthyunjaya presented a method of synthesizing planar mechanisms with resulting workspaces that included a predetermined workspace using an optimization method known as simulated annealing (Sen and Mruthyunjaya, 1999). Rao and Anne looked at the comparison of the workspaces of general serial kinematic chains, among other characteristics, as a method of design (Rao and Anne, 1998), while Davidson and Hunt searched for the minimum number of actuators necessary to cover a given workspace in order to simplify the complexities associated with spherical wrist joint structures (Davidson and Hunt, 1987a).

#### 2.1.2.2 As Evaluation Tools

From an evaluation perspective, workspace analysis allows the prediction of performance characteristics such as the relationship between primary and secondary workspaces and the effect of manipulator configurations (Gupta and Roth, 1982). Yang and Haug have investigated the kinematic dexterity of mechanisms in order to specify the workspace necessary to perform some task (Yang and Haug, 1994a). In a similar application of workspace analysis for the purpose of evaluation of mechanisms, Kieffer and Litvin studied the spatial interference between two or more objects through the determination of end effector swept volumes (Kieffer and Litvin, 1991). Intersection volumes indicated a potential for contact between the generating end effectors and often this type of analysis is used as a method of detecting collisions or simulating machining processes.

#### 2.1.2.3 Visualization of Workspaces

There are many methods for communicating the results of workspace analysis including mathematical expressions, discrete surface patches, planar projections and point cloud representations. The representation of a workspace depends heavily on the type of workspace that is under investigation. There are numerous distinct definitions for robotic workspaces, however the most widely accepted and studied include the complete workspace, reachable workspace, and dexterous workspace. The complete workspace is defined as the set of all displacements and orientations of the end effector of a mechanism. The reachable workspace is defined as the set of all positions an end effector may obtain with no specification being placed on orientation. The reachable workspace is actually the boundary of the complete workspace. The dexterous workspace is defined as the set of all positions an end effector may take while maintaining the ability to achieve all permissible orientations (Murray, et al., 1994).

Cai and Rovetta chose to display two-dimensional contours (slices) of their reachable workspace as well as some interior contours of the complete workspace in some arbitrary, but preestablished plane (Cai and Rovetta, 1990). Gosselin, et al, in their study of six degree of freedom, parallel manipulators, developed a wireframe representation of the reachable manipulator workspace based on analytic representations for the workspace boundaries (Gosselin, et al., 1992). Zhang et al. subdivided the complete workspace of a walking machine into two categories. These were the position workspace where orientation is constant and the orientation workspace where position is constant, leading to graphical visualizations including both

two- and three-dimensional plots of position or orientation with respect to a Cartesian coordinate frame (Zhang, et al., 1996a; 1996b).

Haug et al. presented algorithms for determining reachable workspaces, citing a planar serial manipulator example. For the visualization of the workspaces, the authors plotted the limiting contours of the manipulator's path (Haug, et al., 1995). Spanos and Kohli looked at workspaces for a class of manipulators that had revolute joints, with axes intersecting orthogonally at a point, as the last three joints in the serial chain. They chose to present their results in the form of tables and equations for each of the regional structures studied (Spanos and Kohli, 1985).

The displacement workspaces studied in this dissertation consist of reachable workspaces, eventually concentrating on the simplified case arising when the orientation of the end effector is fixed. The terms variable-orientation workspace and fixed-orientation workspace will be used to distinguish between the two, respectively.

There are numerous other studies that have been published that investigated different aspects of robotic workspaces, so numerous in fact that discussion is beyond the scope of this literature review. Some examples of the additional research dedicated to the evaluation of parallel and platform type manipulators include (Huang, et al., 1999; Ji, 1994; Masory and Wang, 1992; Merlet, 1995; Merlet, et al., 1998; Romdhane, 1994), while examples of additional work that investigated different configurations of serial robotic manipulators include (Abdel-Malek, et al., 1999; Ceccarelli, 1995; Ceccarelli and Vinciguerra, 1995; Karger, 1996). In addition to studies that focused on geometric configuration, workspace research has been conducted regarding binary actuators (Ebert-Uphoff and Chirikjian, 1995), while Merlet has investigated actuator

forces of manipulators and velocities of mechanism components from a workspace perspective (Merlet, 1998a; 1998b).

### 2.1.3 Workspaces Applied to the Knee

In order to identify the active constraints for a given configuration of the human knee joint, Murphy studied the constraint space of the human knee. Assuming ligament and bone surface contact constraints, Murphy presented and partially implemented a method for mapping out the displacement workspace of the human knee (Murphy, 1990). Zhang continued the development of the displacement workspace of the human knee, including ligament constraints and bone surface contact constraints. He modeled the ligaments as single inextensible filaments, the bones as rigid bodies, and computed the displacement workspace using an octree based spatial decomposition analysis. The ligament insertions into the bones were modeled as spherical joints while the surfaces of the femur and tibia were modeled as discrete spherical patches through points measured by Murphy (Zhang, 1995; Zhang and Murphy, 1995).

Omeltchenko addressed computational, continuity, and user interface concerns in her continued development of the displacement workspace. An energy minimization method was constructed to map out the extreme displacements of the human tibia relative to the femur for both fixed and variable orientations based on ligament constraints modeled as linear springs. She also developed a novel interface for viewing and manipulating the results of her workspace construction, which communicated information such as ligament constraint activity and relative bone orientation. Surface contact constraints were not modeled (Omeltchenko, 1997; Omeltchenko and Murphy, 1998).

Chen, et al., employed a similar energy based algorithm to study the passive knee kinematics of surgical implants including the implant surface contact constraints. Rather than map out a complete workspace, the method located individual minimum energy positions for specified orientations of the joint that produced one medial compartment contact point and one lateral compartment contact point between the articulating surfaces (Chen, et al., 2000).

Murphy and Mann also investigated the total freedom of the knee based on extended screw theory. The idea was an extension of the displacement workspace concept that looked at the possible motions of the human knee under various configurations of its passive constraint system (Murphy and Mann, 1988; Murphy and Mann, 1990). In earlier work that related the geometry and kinematics of the human knee, Langrana, et al., developed a computer graphics model of the joint based on computerized axial tomography (CAT) scans. Using this model, the authors simulated rotations of the human knee that supported kinematic investigations without bone-to-bone interference (Langrana, et al., 1982).

### 2.1.4 Robotic Components

In order to discuss the properties of robots, it is necessary to look at the components that comprise the majority of robotic systems. The basic robot can be broken down into three categories of components. These include the driving source, the linkages through which that impetus is applied, and the joints that transform and transmit the impetus between links. The driving source has many forms but typically manifests itself as some type of actuator, providing a known input (force, velocity, displacement, etc.) to a linkage structure. The linkages themselves consist of some type

of physical transmitter of that actuation and can take the form of beams, gears, cables, and so on. The joints are the interfaces between links where the actual transmission and redirection of the movements are accomplished and ultimately define the mobility of the robot.

Under this general description of robotic components, one might ask about the difference between robots and mechanisms. Mechanisms are generally designed to perform a single function while robots often possess many degrees of freedom and are adaptable to many different functions. However, that being said, the kinematic analysis of robots is virtually the same as that of mechanisms (Selig, 1996). The kinematic analysis of mechanisms is a widely studied topic with a large envelope of subject areas addressed by authors such as Hunt, Goldstein, Phillips, and others, however the area of interest for this dissertation will focus mainly on kinematic analysis of manipulators.

For the purpose of kinematic analysis, the links of a manipulator are generally considered to be rigid. A rigid link is defined by Guillet (Guillet, 1956) as a part of a machine or mechanism capable of transmitting both a thrust and a pull. A better definition, however, of a rigid link is an embodiment of points that do not move relative to one another. Some links, however, are flexible, and their contributions must also be included in the geometric model. These non-rigid links can normally be classified as either tension or compression links. Tension links such as ropes, chains, or cables cannot effectively transmit a thrust load yet readily support a tension load, while compression links, such as the incompressible fluid in a hydraulic system, are generally only useful when relaying a thrust load. When applying classical kinematic analyses,

flexible links are usually considered as "momentarily" rigid links, effectively performing the same function as a rigid link when they do transmit a load.

Links interact with one another through joints, which provide some level of physical constraint to the interaction between the links, dependent on the nature of the contacting surfaces. Tsai gives the following classification standards for the joints most commonly encountered in robotic analysis. The surface on a link, which makes contact with another link, is termed a pair element of that link. The presence of two pair elements interacting forms a kinematic pair or joint between the links of the pair elements. Reuleaux first showed how kinematic pairs could be used to simplify analyses of mechanisms (Hunt, 1978), leading to kinematic pairs being classified as lower pairs if there is substantial surface area contact between the pair elements, or higher pairs if there is simple point or line contact between the pair elements. The six basic lower pairs encountered in robotic analysis consist of the revolute joint (rotation about a single axis: hinge-type) prismatic joint (translation along a axis: slider type), cylindrical joint (rotation about and translation along the same axis), helical joint (rotation about and translation along the same axis in constant proportion: screw type), spherical joint (rotation about three orthogonal axes: ball and socket type), and planar pairs (two-dimensional translation in a plane with rotation about axes normal to the plane). The two basic higher pairs encountered in robotic analysis are the gear pair and cam pair (Tsai, 1999).

The end-effector of a robot is the link that serves to transmit the activity of the robot to its surrounding environment (Murray, et al., 1994). The end-effector is mounted on what is generally termed the output link and often takes the form of some

type of grasping, lifting or otherwise manipulating-type device. While they may be assigned to any of the robot's rigid links or joint centers, a reference frame is some type of coordinate object whose purpose is to provide an organized method of mathematically describing the physical or geometrical status of the mechanism. Robots may be classified by their configuration as well. Serial manipulators are mechanisms with open kinematic chains, parallel mechanisms consist of one or more closed kinematic chains, and hybrid mechanisms are mechanisms with both open and closed kinematic chains describing the system (Tsai, 1999).

## 2.2 Screw Theory

The fundamental theorems of Chasles (1834) and Poinsot (1809), taken together, form the basis of screw theory (Fischer, 1998). Chasles's theorem states that any displacement of a rigid body in Euclidean three-space can be represented by a translation parallel to an axis coupled with a simultaneous rotation about that axis. Poinsot's theorem, readily seen as an analog to Chasles, states that any set of forces and moments acting on a rigid body can be resolved into a single force and couple acting about the same axis (Roth, 1983). It was based on these two principles that Ball developed his historic treatise, mapping out the basic definitions, axioms, and relationships characterizing Screw Theory (Ball, 1900).

### 2.2.1 Pitch

Several parameters must be defined in order to adequately discuss screws, their relationships, and characteristics. First of these is the notion of pitch. The pitch of a screw was defined by Ball as the ratio between the linear displacement and angular displacement described by the screw. For the impetus analog (or wrench), the pitch is

defined as the ratio between the moment component and the force component of the wrench. Finally, for the velocity analog (or infinitesimal twist), the pitch is defined as the ratio between the linear velocity component and angular velocity component of the twist. In all three cases, displacement, velocity, and impetus, the pitch is always a parameter having dimensions of length and is one of the defining characteristics of a screw. In fact, Ball used the idea of pitch to initially define the term screw. In his treatise, Ball stated, "A screw is a straight line with which a definite linear magnitude termed the pitch is associated" (Ball, 1900). Using this definition of screw, the notions of a twist on a screw and wrench on a screw may be made clear. A twist is described as the combined, (uniformly applied) linear and angular motion along a screw as constrained by a scalar multiple of the associated pitch. In the position altering sense, a twist is often termed a screw displacement. A wrench is simply the combination of a linear force and an angular moment with coincident axes (Tsai, 1999). However, using the previous definition for screws, a wrench can also be described as the application of a force and moment along a screw axis constrained by a scalar multiple of the associated pitch (Ball, 1900).

### 2.2.2 Screw Representation

There are many different methods used to describe screws and screw transformations. Beggs, using a homogeneous Cartesian coordinate system, represented screw displacements as affine transformation matrices (Beggs, 1983). Yang showed that dual Euler angles could be used to represent screw motions, (Yang, 1974) while others have used some form of Hamilton's quaternions as their language for the discussion of screw motions (Murphy, 1990), (Etzel and McCarthy, 1999).

For the sake of future developments, and for clarity, the definition of a unit screw in this document will be developed from concepts of line geometry, bearing particular affinity to Plücker coordinate representations for lines. A rigorous discussion of line geometry and Plücker coordinates may be found in Hunt's text (Hunt, 1978) as well as in Ohwovoriole's dissertation with an extension to the screw motion representation (Ohwovoriole, 1980). Appendix B contains a brief development of the mathematics from the usual Cartesian reference frame.

A unit screw can be described with the aid of two Cartesian vectors, $\vec{s}$ and $\vec{s}_0$, where $\vec{s}$ is a unit vector in the direction of the screw axis and $\vec{s}_0$ is any vector from the origin to a point that lies on the line coincident with the screw axis. The unit screw, $\hat{S}$, is then defined by the following relationship where $\lambda$ is the pitch of the screw.

$$\hat{S} = \begin{bmatrix} \vec{s} \\ \vec{s}_0 \times \vec{s} + \lambda \vec{s} \end{bmatrix} = \begin{bmatrix} S_1 \\ S_2 \\ S_3 \\ S_4 \\ S_5 \\ S_6 \end{bmatrix} \qquad 2.1$$

The resulting six components are known as the screw coordinates of the unit screw, however, owing to the condition that $\vec{s} \cdot (\vec{s}_0 \times \vec{s}) = 0$, only five of the coordinates are independent (Tsai, 1999).

In addition to providing a very clean and compact notation to describe displacements, instantaneous velocities, and rigid body forces, screws provide a unique tool for the investigation of the interrelations of rigid body forces, freedoms, and displacements. Screw coordinates also alleviate the problem of coordinate system

dependence found in many other representations including eigenvalue decomposition methods (Huang and Schimmels, 2000).

### 2.2.3 Wrenches and Twists

Recognizing screw coordinates to be a mathematical representation of the combinations of linear and angular components naturally evolves into their application to the description of quantities commonly represented by vector notation such as displacement, velocity, and force. Ball defined a twist about a screw axis as a uniform angular displacement about the screw axis performed concurrently with a uniform linear displacement parallel to that axis through a distance equal to the product of the angular displacement and the pitch of the screw. Ball later described a wrench as the combination of a force parallel to a screw axis with a couple about that screw axis with the constraint that the couple be equal to the product of the force and pitch of the screw (Ball, 1900).

In dealing with the composition of twists and wrenches one notable point must be made. In order to combine two or more wrenches into a resultant wrench, the screw coordinates are simply summed as one would normally sum a six-dimensional vector. Finite twists do not behave in this manner. Consistent with other representations of rigid body motion, the order in which multiple finite twists are applied to a rigid body has a meaningful effect on the final destination of the body. For that reason, when dealing with screw theory and extended screw theory, Ball and Ohwovoriole both set forth the condition that the twists be "small" or infinitesimal such that a twist applied to a point can be regarded as a rectilinear displacement (Ball, 1900), (Ohwovoriole, 1980). These infinitesimal twists, when observed in the context of differential displacements

are akin to "velocities" or trajectories and are in fact the fundamental members of the spaces that are to be defined as Velocity Workspaces. As such, these infinitesimal twists play a key role in the development of the concept of virtual work and, subsequently, the definition of the virtual coefficient.

In an analogous study of spatial displacement, investigating novel ways to represent rigid body motion, Etzel and McCarthy introduced the concept of double quaternions as approximations of spatial motions through the sum of very small finite rotations (Etzel and McCarthy, 1999). This was a direct application of the theory of instant centers, which showed that the instantaneous motion of a rigid body could be represented by rotation only about the instantaneous axis of rotation (Seely and Ensign, 1933). A brief discussion of the basic quaternions can be found in Appendix A.

Murray expanded the idea of twists to describe finite velocities of a rigid body, in both spatial as well as body fixed coordinate systems. In his application, Murray was employing the compactness of screws to aid in the analysis of the propagation of manipulator joint velocities through a mechanism. Here the order of the joints, and subsequently the order of the application of velocities, was fixed, allowing for finite representation of velocities, unlike the case of general spatial motion addressed by screw theory (Murray, et al., 1994). Taking velocity screws to be infinitesimal twists allows the composition of multiple velocity screws irrespective of the order of application. With this in mind, a twist space basis may be constructed, allowing the specification of twists within the space without regard to the order in which the bases are combined.

### 2.2.4 Virtual Coefficient

Work is done by an action on a rigid body when that body undergoes a displacement along the axis of the action. Such actions can be linear (force) or angular (moment), as well as constant or variable. In the case of a linear force, work is done when the body being acted upon undergoes a translation in the direction of the linear force. In the case of a moment, work is done when the body being acted upon undergoes an angular displacement about an axis parallel to that of the applied moment (Seely and Ensign, 1933). Using the nomenclature of screws to describe the actions (wrenches) and displacements (twists), the work done by a wrench on a rigid body that undergoes a screw displacement as a result of that wrench is easily computed.

Taking advantage of screw coordinates, consider a wrench given by $\beta$ as shown in Equation 2.2.

$$\beta = \{\beta_1, \beta_2, \beta_3, \beta_4, \beta_5, \beta_6\} \qquad 2.2$$

Now suppose this wrench acts upon a rigid body that undergoes an infinitesimal twist $\alpha$ given by Equation 2.3

$$\alpha = \{\alpha_1, \alpha_2, \alpha_3, \alpha_4, \alpha_5, \alpha_6\}, \qquad 2.3$$

The virtual work, $\varpi_{\alpha\beta}$, done by the wrench, $\beta$, acting through the twist, $\alpha$, is given by Equation 2.4.

$$\varpi_{\alpha\beta} = \beta_1\alpha_4 + \beta_2\alpha_5 + \beta_3\alpha_6 + \beta_4\alpha_1 + \beta_5\alpha_2 + \beta_6\alpha_3 \qquad 2.4$$

$\varpi_{\alpha\beta}$ was called the virtual coefficient in Ball's original treatise and it is readily apparent that the screws of the wrench and twist may be commuted in Equation 2.4 without altering the value of $\varpi_{\alpha\beta}$ (Ball, 1900). Equation 2.4 is the principle tenet of Ball's

screw theory and the foundation of extended screw theory as set forth by Ohwovoriole (Ohwovoriole and Roth, 1981). Equation 2.4 will also serve as the foundation of the definition of velocity workspaces of the human knee.

Ball defined a screw as being reciprocal to another screw when the virtual coefficient vanished ($\varpi_{\alpha\beta}$ equal to zero). Physically this signifies that the wrench $\beta$ performs zero work if the rigid body undergoes the (infinitesimal) twist $\alpha$. Consider a rigid sphere resting on a perfectly horizontal, frictionless plane under the influence of gravity as shown in Figure 2.1.

For convenience, take the Cartesian x- and y-axes to lie within the horizontal plane and the z-axis, normal to the plane, positive in the direction opposite gravity. The only wrench applied to the sphere under these conditions is the normal force (zero pitch) inthe vertical direction through the contact point (a, -b, 0). This force has the wrench coordinates {0, 0, 1, -b, -a, 0}. Suppose the sphere undergoes an infinitesimal

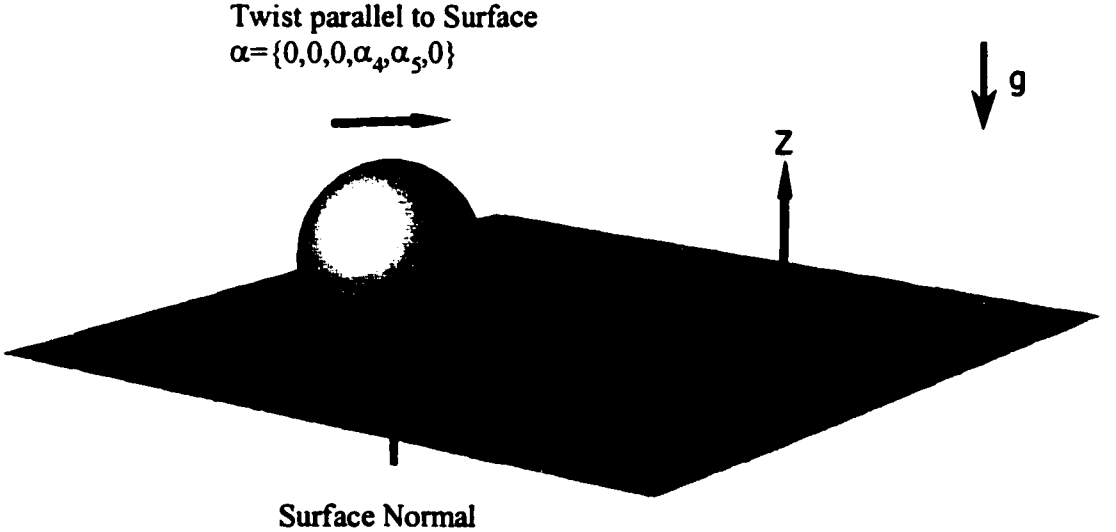


Figure 2.1 Basic example showing a simple reciprocal twist-wrench pair.

twist of pure translation (infinite pitch) parallel to the horizontal surface. By definition, this displacement must have the twist coordinates {0, 0, 0, $\alpha_4$, $\alpha_5$, 0}. Calculating the virtual work (coefficient),

$$\varpi_{\alpha\beta} = 0\cdot\alpha_4 + 0\cdot\alpha_5 + 1\cdot 0 + (-b)\cdot 0 + (-a)\cdot 0 + 0\cdot 0$$

it becomes clear that $\varpi_{\alpha\beta} = 0$. Thus, in this special case, $\alpha$ and $\beta$ are reciprocal to one another. The physical interpretation of reciprocity for a rigid body experiencing wrenches and twists along two reciprocal screws is an indication of the freedom of the rigid body. The rigid body is free to experience a twist along one of the screws while being constrained by a wrench along the other screw (Ohwovoriole, 1980; Ball, 1900). That is, the infinitesimal twist is not influenced by the constraining wrench, but if the twist were allowed to become finite, the geometry between the wrench in the twist would change, possibly altering the value of the virtual coefficient.

### 2.2.5 Classification of Screw Systems

In space there are, at most, six linearly independent screw axes. Accordingly, there are $\infty^5$ possible screws in space as there are $\infty^1$ possibilities for the pitch of a screw that may be defined along any of the $\infty^4$ lines in space (Hunt, 1978). If there exists any set of $k$ screws $(\$_{1\ldots k}, k = 1,2,\ldots)$, let them be expressed as the following $k\times 6$ matrix.

$$M = \begin{bmatrix} \$_{11} & \$_{12} & \$_{13} & \$_{14} & \$_{15} & \$_{16} \\ \$_{21} & \$_{22} & \$_{23} & \$_{24} & \$_{25} & \$_{26} \\ \vdots & \vdots & \vdots & \vdots & \vdots & \vdots \\ \$_{k1} & \$_{k2} & \$_{k3} & \$_{k4} & \$_{k5} & \$_{k6} \end{bmatrix} \qquad 2.6$$

The rank of $M$ indicates the number of linearly independent screws in the set as well as the order of the screw system defined by the set. To relate this to kinematic terms, a one system has one degree of freedom, that is, every member of the set is a multiple of a

single screw in space, while a six system has six degrees of freedom, defining all possible screws in space (Tsai and Lee, 1993). Although trivial, it bears mentioning that the matrix $M$ will never achieve rank greater than six, a limit that is determined by the largest possible column space of $M$ (Anton, 1977).

Now consider a body constrained by a wrench along each of these $k$ screws. If the rank of $M$ is $n$, then by the principle of virtual work, there are exactly 6-$n$ linearly independent lines in space along which an instantaneous twist of that body may be defined without affecting (reciprocal to) those wrenches (Hunt, 1978). It was shown by Ball and reiterated by many others including Hunt (Hunt, 1978), Gibson and Hunt (Gibson and Hunt, 1990a; 1990b), and Tsai and Lee (Tsai and Lee, 1993), that any screw system of order $n$ also defines a unique reciprocal screw system of order 6-$n$. That is, every one-system defines a unique five-system, every two-system, a unique four-system and every three-system, another unique three-system. Employing this characteristic, and recognizing the inherent complexity of characterizing four and five systems, it is both more efficient and meaningful to focus on one-, two-, and three-systems for the purposes of general characterization and classification of reciprocal screws.

The classification of screw systems by their order was included in Ball's treatise, however the most succinct identification of screw systems and special case sub-systems as they pertain to modern robotics can be found in Hunt's work (Hunt,1978). More recently Hunt's classifications have been rigorously verified by Gibson and Hunt (Gibson and Hunt,1990a; 1990b) through the implementation of projective geometry

while Tsai and Lee presented methods for determining principle bases for some of the special two- and three-systems (Tsai and Lee, 1993).

### 2.2.6 Extended Screw Theory

Ohwovoriole extended the implications of the virtual coefficient by investigating the systems that arise when the virtual work is nonzero. The motivation behind his analysis was with regard to automated industrial assembly. For the majority of cases, the assembly of parts was acted upon by wrenches emanating from contact constraints provided by mating parts or manipulator interaction. From this perspective, Ohwovoriole coined his terminology for the types of systems characterized by non-zero virtual coefficients.

In the circumstance that a wrench and infinitesimal twist produce a positive virtual coefficient, the pair was said to be repelling. Under general contact constraints, the wrench normally has a sense of pushing on the rigid body, indicating motion in the general direction of that wrench repels the rigid body from its contacting constraint. Hence, for a rigid body being acted upon by a wrench, an infinitesimal twist repelling to that wrench would be a motion oriented in the positive direction of the screw on which the constraining wrench is defined. In general, repelling twists will result in motions that reduce the intensity of a constraining wrench or eliminate its effects all together. As can be seen earlier in Figure 2.1 an infinitesimal twist of the sphere repelling to the normal force applied by the surface constraint would move the sphere away (positive z-direction) from the contact surface, in a sense repelling the sphere from the planar surface.

In the circumstance that a wrench and infinitesimal twist produce a negative virtual coefficient, the pair was said to be contrary. Again considering the presence of general contact constraints, a motion opposite of the constraining wrench would indicate geometric impossibilities for two true rigid bodies. For a rigid body being acted upon by a wrench, an infinitesimal twist, contrary to that wrench, would nominally produce a motion along the negative sense of the screw on which the constraining wrench was defined. Contrary twists are motions that inevitably will have the effect of increasing the intensity of the constraining screw or violating some other physical constraint if carried out. For the system described by Figure 2.1, an example of a twist contrary to the normal wrench would be the pure translation of the sphere into the constraining surface (Ohwovoriole, 1980; Ohwovoriole and Roth, 1981).

In the context of the model of the human knee, pushing wrenches emanating from contact constraints are present when the femur is in contact with the tibia, however, pulling wrenches are also affecting the system when any of the filaments representing the major ligaments or tendons become active. These constraining wrenches are provided by the limitation that the model links representing the ligaments cannot support a compressive load, only tension. With respect to the constraints in place due to ligament length limitations, the general wrench constraint will have a pulling effect on the rigid body, in a sense opposite of the perceived action of a contact wrench. As a result, twists repelling to ligament-induced constraints will nominally be decreasing the distance between ligament insertion sites, locally moving one rigid body closer to the other. Similarly, a twist contrary to ligament induced constraints will have the effect of increasing the distance between insertion sites, locally moving the rigid

bodies apart. As such the notions of repelling and contrary must be thought of in terms of positive and negative values rather than the more intuitive rigid body interactions from which their names originated.

### 2.3 Orthopedics

The etymology of the word "orthopedic" is the Greek *orthos pais*, which translates roughly to straight child. The first use of the term appears in the title of a 1741 work by a French doctor named Nicolas Andry. The title of Andry's book, Orthopaedia: Or the Art of Correcting and Preventing Deformities in Children: By such Means, as may easily be put in Practice by Parents themselves, and all such as are Employed in Educating Children, is the source that originated the term by which so many of today's physicians describe their medical specialty of correcting and preventing skeletal deformities. In addition to providing the verbal representation of orthopedics, Andry also introduced the visual symbol commonly associated with the specialty. The tree of Andry is a figure of a crooked tree, bound to a stake as an effort to straighten the plant (Dandy and Edwards, 1998). It is this area of medical expertise that has been assigned the task of dealing with skeletal conditions, including bone and joint traumas. Thus the study of the human knee from a clinical perspective naturally falls under the umbrella of orthopedics.

#### 2.3.1 Anatomy

The first step towards comprehending the biomechanical function of the knee joint is to understand the structural components of the joint. Along with the structural components, nonstructural anatomical bodies naturally reside within the region of the human body commonly associated with the knee. These include blood vessels, nervous

tissue, skin, and other fascia that primarily perform duties other than mechanical support or articulation about the human knee joint (Gray, 1995).

#### 2.3.1.1 Joints

Diarthrodial joints or movable joints are commonly organized by the clinical community into six categories based on the type of motion permitted. These include ginglymus, trochoides, condyloid, reciprocal reception, enarthrosis, and arthrodia (Gray, 1995). Ginglymus, more commonly known as hinge joints, are characterized by a perception that articulation occurs about a single axis throughout the range of motion of the joint. Orthopedic texts typically, and very disturbingly, classify the human knee as ginglymus, often erroneously concluding that the important motion occurs exclusively in one plane (Dandy and Edwards, 1998). Trochoides are described as pivot joints where motion is limited to rotation only, constrained by a structure exhibiting a pivoting-type motion within some ring. Condyloid are described as an ovoid head articulating within an elliptical recess, allowing all motions, save axial rotation, as in the wrist. Reciprocal reception joints, also known as saddle joints, allow all motions except axial rotation as well and are geometrically similar to two saddles rolling and sliding upon each other. Enarthrosis articulations are those joints that are more commonly described as ball and socket joints, typically allowing limited motion in all directions. The shoulder and hip are the principle examples for this category of joints. Arthrodia are those joints exhibiting gliding motions between two contacting surfaces as seen in the articulation of the vertebrae or the carpal joints (Gray, 1995).

#### 2.3.1.2 Bone

The typical human bone is composed of two types of tissue, compact or cortical bone and spongy or cancellous bone. Cortical tissue, which makes up the hard outer shell of all bones, is a dense and porous material. Cancellous tissue, while sharing the characteristic of porosity with compact bone, is somewhat less dense than cortical tissue. The advantage of this decrease in density is that it allows room in the lattice-type matrix of cancellous bone for the production and storage of bone marrow. It is in the cancellous bone, within the matrix, that the bone marrow performs its primary function of producing of blood cells. (Audesirk and Audesirk, 1996). The ratio of the amount of cortical tissue to the amount of cancellous tissue found in a bone varies from bone to bone as well as throughout the geometry of each individual bone. This provides each bone with the combination of physical properties most specialized toward a specific set of functions (Gray, 1995).

Three types of cells comprise the tissues of bone. They are the osteoblasts, bone forming cells, the osteocytes, mature bone cells, and the osteoclasts, bone dissolving cells. Together, these three types of cells contribute to the formation, growth, and maintenance of the bones of the human skeletal system (Audesirk and Audesirk, 1996). Bone modeling, the process by which mass is added to bone, occurs during the growth of mammals, while bone remodeling, the process by which bone mass is maintained or reduced, occurs throughout life in all bones.

The primary distinction between the processes of modeling and remodeling occurs in the relationship between osteoblastic and osteoclastic activities. There appears to be no interdependence between the activities of osteoblasts and osteoclasts

during bone modeling, however in remodeling, formation of new bone cells (osteoblastic activity) occurs slower than the resorption (osteoclastic activity) of existing bone cells, causing the weakening of bony structures with age (Nigg and Herzog, 1994).

Mechanical functions of bone in the human body include providing support for the carcass, protection for other systems and anatomical components, and linkage systems for the transmission and application of forces. Physiological functions of human bone include the production of blood cells and the storage of essential minerals. There are approximately 206 distinct bones in the "normal" adult human body and the size and shape of these bones varies considerably from person to person (Nigg and Herzog, 1994).

Four bones are present within the region of the body known as the human knee joint including the femur (thigh bone), tibia (larger bone of the shank), fibula (smaller bone of the shank), and patella (knee cap). They serve in concert as the framework of this vastly important and especially complex coupling within the human body. Fung reported ultimate tensile strengths for cortical bone in the human tibia to be 174 ± 1.2 MPa and for cortical bone in the human femur to be 124 ± 1.2 MPa (Fung, 1993), while Duck indicated femoral strength at 133 ± 14 MPa (Duck, 1990).

#### 2.3.1.3 Ligaments and Tendons

Ligaments and tendons are connective members, composed of collagen-based, white, fibrous tissue that perform the tasks of providing links between articulating structures and various entities within a joint. While tendons in general tend to exhibit a parallel structure of fibrous tissues, ligaments found in the human knee joint are

characterized by both parallel and oblique alignments of the fibrous tissues. This results in very strong, nearly inextensible links between the major structures of the human knee joint (Gray, 1995).

Ligaments and tendons are very similar in their structure and function with the major difference occurring in the types of structures that they connect. Tendons connect muscles to bone, providing an interface for the transmission of forces generated by muscular contraction. This results in active articulation constraints being applied to the connected structures. As individual muscles nominally contract along a single direction, the parallel alignment of fibers seen in tendons is arguably the most efficient design for the force transmission. When unloaded, the collagen fibers have a wavy appearance, however it has been shown that if a tendon is elongated by 10%, approximately 1% of this elongation is due to the alignment of the collagenous fibers (Fung, 1993).

The primary function of ligaments is connecting bone to bone, providing a nominally flexible link, often transmitting the reactive or passive forces resulting from the interaction between the connected structures and their environments. Some examples of reactive forces are fluid pressure within a joint capsule, gravity, contact with other structures, or the contribution of muscular force applied to a connected structure. The hierarchy and organization of the fibers within ligaments closely resembles that seen in tendons with the major differences of ligaments having smaller diameter fibers that may or may not be interwoven (Woo and Young, 1991).

Fung reported that the variance in the alignment structure of ligaments was most likely due to the altering stress modes seen throughout ranges of motion of joints (Fung,

1993). Calculated strength for a single collagen fascicle has been reported to be approximately 500 MPa (Duck, 1990). while Fung indicated the yield stress of tendons to be in the range of 50-100 MPa, rupturing "usually" at 10-15% elongation. Woo reported (Woo, et al., 1990) ligament tensile strengths of approximately 73 MPa, rupturing at just over 9% strain. Nigg and Herzog have reported similar values for strain at the onset of rupture (Nigg and Herzog, 1994).

Ligament graft length and placement have been shown to be important contributors to the mechanics of the human knee. Lewis, et al., studied these factors as they applied to anterior cruciate ligament reconstruction. They found that 3 mm variations in ligament "rest" lengths typically induced 50 % changes in the graft forces (Lewis, et al., 1990). In a similar study, Bylski-Austrow, et al., concluded that the force incurred by anterior cruciate ligament substitutes, and the limit of anterior translation of the tibia relative to the femur, were "extremely sensitive" to the placement of the femoral attachment location (Bylski-Austrow, et al., 1990).

#### 2.3.1.4 Cartilage and Menisci

Another collagen-based substance found throughout the human body is cartilage. In the early stages of development, all bone begins as cartilage consisting of chondrocytes that are progressively replaced by osteocytes as the body matures (Audesirk and Audesirk, 1996). Of interest when studying the human knee are articular cartilage and the menisci. Articular cartilage may be found on the contacting surfaces of bones within synovial joints (Nigg and Herzog, 1994). The menisci are two specialized C-shaped fibrocartilage objects found on the surface of the tibial plateau,

which appear geometrically as seating receptacles for the femoral condyles (Romanes, 1986).

The main biochemical components of articular cartilage are 50%-73% collagen (dry weight), 15%-30% proteoglycan (dry weight), and 58%-78% water (wet weight). In contrast, the menisci contain approximately 75%-80% collagen (dry weight), 2%-6% proteoglycan (dry weight), and 70% water (wet weight) (Mow, et al., 1990). Proteoglycans are a class of high molecular weight glycoproteins (compounds consisting of a protein and a carbohydrate) that are characteristically found in the extracellular matrix of connective tissues. It is this variation in composition, coupled with a marked difference in the structural arrangement of articular and meniscal cartilage that merit distinction between these two types of cartilaginous bodies. Articular cartilage is found on the surface of the tibial plateau, the posterior surface of the patella, and on the articulating surface of the femoral condyles, however the menisci are not as restrictively affixed, attaching mainly to the tibial plateau (Romanes, 1986).

Duck presents data for the elastic modulus of bovine articular cartilage in the range of 0.70-0.85 MPa while reporting a value of 0.45 MPa for bovine meniscal cartilage (Duck, 1990). Another study by Töyräs, et al., investigated the use of pulse-echo ultrasound techniques to measure cartilage thickness for meniscal elastic modulus determination. They reported values ranging from 0.1-1.6 MPa for the elastic modulus of bovine cartilage under varying compressive loads (Töyräs, et al., 2001).

Articular cartilage, which is found on the articulating surfaces of bone in joints, has the basic functions of providing lubrication, wear resistance, shock absorption, and limited load bearing duties. The coefficient of friction of articular cartilage is one of the

lowest known and despite limited regenerative ability, mature cartilage typically maintains superior wear resistance for many decades (Fung, 1993). The human knee joint is classified as a synovial joint, meaning it is enclosed by a capsule that is filled with synovial fluid, which plays a significant role in the lubrication, shock absorption, and the limited regenerative ability of cartilage.

All living tissue requires some type of nutrient supply and waste removal. With the lack of a vascular supply, the articular cartilage depends on synovial fluid to accomplish these tasks (Torzilli, et al., 1990). Healthy cartilage is also a low permeability microporous material, which prevents the rapid expulsion of fluid from the tissue under compressive loads. When the cartilage is subjected to a sudden compressive load, resistance to fluid movement away from the newly loaded volume, through and out of the microporous matrix of the cartilage, contributes to the dissipation and distribution of the load (Nigg and Herzog, 1994).

The medial meniscus covers approximately 50% of the contact area of the medial tibial plateau while the lateral meniscus covers approximately 70% of the contact area of the lateral tibial plateau. Meniscal tears accompany between 58% and 78% of traumatic ACL injuries, with the McMurray test and Apley's test the most popular diagnostic tools for detecting meniscal injuries. No significant difference was reported in the diagnostic accuracy of the use of clinical signs versus the use of magnetic resonance imaging techniques to predict meniscal injury (Rath and Richmond, 2000). From the attachment geometry, contact area coverage, and the indication of more compliant behavior, it appears the menisci function as the "shock absorbers" within the human knee joint.

#### 2.3.1.5 Other Components

##### 2.3.1.5.1 Synovia

The synovial fluid that bathes the contacting surfaces of the human knee joint plays a significant role in joint function. The fluid itself is a dialysate of the blood, meaning the larger blood molecules cannot pass through the synovial membrane into the joint capsule. Synovial fluid, secreted by the synovial membrane, is transparent, alkaline, and garners viscoelastic properties from the hyaluronic acid that is its main component (Ribitsch, 1990). It has been estimated that the thickness of the layer of synovial fluid between articulating surfaces in the knee is between 0.5 and 1.0 μm (Nigg and Herzog, 1994).

In addition to the cited functions of lubrication, nutrient transport, and hydrostatic contribution to shock absorption and load bearing, the viscoelastic properties also contribute to lubrication, load bearing and shock absorption duties (Ribitsch, 1990). As techniques are improved for the treatment of the injured knee joint, specifically total knee replacements, the importance of the contributions of synovial fluid to proper knee function cannot be discounted. It is necessary then, to devote attention to the search for a proper surrogate for the contributions of synovial fluid in such cases.

##### 2.3.1.5.2 Muscles

Approximately half of the mass of the average human is found within their muscles (Romanes, 1986). There are three basic classifications of muscle in the human body: striated, smooth, and cardiac. Striated muscles get their name from the striped appearance of their fibers and they have the function of providing the input force

necessary to both mobilize and stabilize the human body. Striated muscle, also known as skeletal muscle, is the variety that is most commonly associated with the nonspecific label of "muscle" (Audesirk and Audesirk, 1996) and usually operates in balanced groups to flex or extend skeletal joints (Dandy and Edwards, 1998). Striated muscles have a minimum of two insertions into skeletal members through tendonous structures and are usually controlled through voluntary stimulation provided by the nervous system (Romanes, 1986).

Skeletal muscles have the ability to contract at both rapid and slow rates, depending on the number and frequency of action potentials communicated through the neuron. Smooth muscles are so termed due to their lack of bands or striations associated with skeletal muscle and generally contract at much slower rates for sustained periods of time. The contraction of smooth muscle is generally not subjected to conscious control, initiated instead by the actions of hormones, stretching and spontaneity. Common locations of smooth muscle include the walls of the digestive tract the larger blood vessels, the bladder, the uterus, and most hollow organs.

Cardiac muscle is found only in the heart as it name suggests, and it has irregular striations similar to the regular stripes of skeletal muscle. However, unlike the skeletal variety, cardiac muscle has the properties of self-stimulation, is involuntary, and cyclically contracts at an intermediate speed, hopefully, for long periods of time (Audesirk and Audesirk, 1996).

### 2.3.2 Internal Derangement

The term internal derangement, originally coined by William Hey in 1784, has come to be associated with the disruption of proper function of the human knee joint.

Several conditions have become associated with internal derangement, including ligament sprains and tears and meniscus damage among the more common (Sisk, 1987). Injuries involving the patella and patellar tendon are also common injuries, particularly among collegiate athletic participants (Arendt and Dick, 1995). Proper diagnosis of an injury to the knee joint, or any other anatomical structure, is crucial to the most timely and complete return to health as possible for the injured party. The assessment of knee injuries is generally achieved through some combination of three common modalities, including clinical diagnostic examination, radiological examination, and surgical examination.

The primary method of determining the extent of a patient's injury is through clinical diagnostic examinations. All clinical examinations begin with an interview of the patient, including the history, severity, and location of the problem. This is followed by visual inspection of the troubled area, looking for any obvious deformities, inflammation, or other signs of trauma. Next is the palpation of the troubled area, again searching for swelling, temperature changes, sensitive areas, and differences between healthy structures. The movement of the problem area is the next step in the clinical diagnosis phase, beginning with the active motion of the affected areas followed by the investigation of the passive motion characteristics. Finally the stressing or straining of the problem areas is used to exhaust the information obtainable from this modality of the diagnostic process. The arrangement of the initial examination is deliberately structured such that the least painful data sources are investigated first, progressing to those maneuvers that have the potential to inflict the most discomfort last. It is also not

absolutely necessary to perform all of the stages of the clinical examination if the pain and invasiveness are sufficient to warrant other forms of diagnosis.

The secondary diagnostic technique orthopedists draw on to assess the extent of injury is the use of radiographic imaging to look inside the body for evidence of trauma. X-ray, Computed Tomography (CT), Magnetic Resonance Imaging (MRI), and ultrasound are all very common methods used to ascertain images of the internal structures of the human body in a minimally invasive manner (Sisk, 1987). X-rays are nothing more than maps of X-ray attenuation coefficient, with the classical form being that of a two-dimensional black and white semitransparent image formed by projecting X-rays through the region under investigation. Bone has high absorptivity compared to the surrounding tissue, casting a semitranslucent shadow on the X-ray film, effectively projecting a map of the geometry and structure of the bone for the clinician to interpret.

The inherent loss of data encountered when projecting three-dimensional information to a two-dimensional representation spurred the development of Computed Tomography. This type of imaging employs the attenuation coefficient of X-rays to capture two-dimensional slices from which three-dimensional images may be constructed by stacking successive slices. Magnetic Resonance Imaging takes advantage of phenomena associated with the nuclear properties of components within the human body to construct images. By subjecting the region of the body to a magnetic field and measuring the reactions to changes in that field, technicians are able to construct images with ever-improving resolution of important anatomical structures. Ultrasound methods take advantage of variances in the speed of sound in different materials to provide their contrast, however ultrasound signals exhibit appreciable

scattering through the cavities of cancellous bone, excluding it as one of the primary methods of obtaining visual representation of the internal structures of the human knee for diagnostic purposes (Barrett and Swindell, 1981).

Diagnoses are generally accomplished with the completion of clinical examination alone or the combination of clinical and radiological examination. If surgical intervention is warranted, clinicians will often choose to scope the knee joint before undertaking more invasive surgical techniques. The term scope refers to a surgical instrument known as an arthroscope that is inserted through a small incision into the joint cavity, availing a magnified visual inspection of the joint structures. Depending on the severity of the injury, surgery may continue using arthroscopic tools or it may require more open access to the joint structures to correct the problem. In either case, the surgeon is afforded the chance to visually confirm the diagnosis from the preliminary clinical and radiological examinations (Sisk, 1987).

**2.3.3 Diagnostic Tests**

There are several diagnostic tests, often called stress tests, to determine the nature and severity of ligament and meniscal injuries. Of those that test for ligament disruptions are the Abduction Test (TCL), Adduction Test (FCL), Anterior Drawer Test (ACL, PCL), Posterior Drawer Test (PCL), Lachman Test (ACL), Pivot Shift Test (ACL), and Reverse Pivot Shift Test (PCL, FCL). Common diagnostic tests for meniscal injuries include the McMurray Test, Apley's Grinding Test, and the Squat Test (Sisk, 1987). Each of these tests manipulates the human knee into a position that is believed to allow stressing of the targeted structures in order to assess damage. Generally, orthopedists initially perform the test(s) on the healthy limb, if one is

available, to gauge the patients "normal" joint laxity and to secure the confidence of the patient, encouraging them to relax as much as possible when it comes time to examine the injured limb (Dandy and Edwards, 1998).

While no test boasts 100% accuracy rates, a successful diagnosis depends largely on the skill and experience of the physician performing the examination. Donaldson, et al., presented a study of diagnostic examinations performed with the subject both conscious as well as under anesthesia. The results showed that while the patient was conscious, many of the tests produced false negative results, but under anesthetic, the number of these occurrences decreased significantly. The implication was that the conscious patient would naturally attempt to protect the injury, hampering the ability of the physician to accurately perform the examination (Donaldson, et al., 1985). The dependence on experience and skill, to some degree, may also be attributed to ambiguous and sometimes-conflicting descriptions of how each diagnostic test should be performed.

Taking the Lachman Test for ACL instability as an example, there is no uniformity in the manner in which current literature presents descriptions of this procedure. The basic instructions for performing the test are to place the knee in slight flexion, hold the thigh (femur) fixed, and attempt to translate the shank (tibia) anteriorly. The amount of translation relative to a healthy reference, such as the patient's uninjured limb if available, as well as the classification of the endpoint of that translation, indicates the severity of the ACL injury, as well as the possible presence of additional trauma.

Apparently to cover the inherent geometrical differences in human anatomy, there is the dissimilarity in the suggested orientations of the knee for the Lachman test. Katz and Fingeroth indicate the knee should be in 10° to 20° of flexion (Katz and Fingeroth, 1986), Dandy and Edwards specify the knee be only in a few degrees from full extension without quantifying this measure (Dandy and Edwards, 1998), and Sisk and Miller both instruct the knee be positioned from 0° to 15° of flexion with the affected extremity placed in "slight external rotation" (Sisk, 1987; Miller, 1997). Other sources are more specific, indicating a single value for the flexion angle of the knee during the test (Wheeless, 2001).

Next, the directives found in two versions of Campbell's Operative Orthopaedics, (Sisk, 1987) and (Miller, 1997), give rise to another concern about limb orientation. Their assertion of limb rotation in the absence of any such mandate by other authors raises the question of whether or not this plays a significant role in the execution of the examination. There is also the question of how each clinician estimates or ascertains what exactly constitutes $x$ degrees of flexion. It has been well documented in the literature that the human knee is a spatial joint, undergoing rotation in all three clinical planes during normal flexion (Murphy and Mann, 1990). Furthermore it has been shown that the estimation of bone movements simply by tracking the motion of the overlying skin does not produce valid results (Fuller, et al., 1997).

Finally there is the specification for the degree or severity of the sign. This is determined by the distance the tibia translates past that of a normal knee, which relies on the clinician's recollection of the health knee sign (if available), his ability to

estimate millimeter scale differences solely by palpation, and the classification of the termination of the subluxation as mushy or hard (Miller, 1997).

### 2.4 Knee Models

Throughout the study of human movement, many models of the various human musculoskeletal systems have been introduced to allow the application of developing mathematics and computing power to better describe the form and function of human motion. King presented a review of biomechanical models in 1984 that discussed musculo-skeletal models in four categories (King, 1984). These included models of bones, models of joints, models of individual body segments, and models of the entire human musculo-skeletal system. The undertaking of such an enormous task allowed only for the citation of examples of the majority of the models discussed and for coverage of only two human knee joint models.

Hefzy and Grood, seeking to expand on King's paper, presented a review of knee models in 1988 that remains a good reference to the various types and characteristics of human knee joint models (Hefzy and Grood, 1988). In 1996, Hefzy and Cooke authored an update to the 1988 discussion largely to describe advances made in dynamic models and those involving the patella and menisci (Hefzy and Cooke, 1996). The following discussion of the state-of-the-art knee models will follow the organization presented by Hefzy and Grood and Hefzy and Cooke.

#### 2.4.1 Physical Models

The first distinction to make between differing knee models regards what is being modeled. For the human knee, all models fall into two categories, those that attempt to model the physical environment by constructing a tangible model of the joint

and those that attempt to model a mathematical behavior of the joint through computation. Physical knee models consist of tangible objects that have been constructed to investigate some corporeal set of properties of the joint, while mathematical models rely on numeric analysis.

Hefzy and Grood reported (Hefzy and Grood, 1988) that Strasser (1917) was one of the first to develop a crossed four-bar type mechanism to model the behavior of the cruciate ligaments. This is an early example of representing the human knee as a physical model. In this model, the intersection of the two frame links appears to mimic the motion of the flexion-extension axis of the knee joint, however when compared to kinematic data, the mechanism geometry identifies the coupler link as the wrong bone. While the anterior cruciate and posterior cruciate ligaments have been identified as behaving similar to the links in the mechanism, it has been shown that there is no mathematical basis relating the linkage motion to cruciate ligament movements (Blacharski, et al., 1975). The crossed four-bar model was developed when it was realized that the flexion/extension motions of the knee closely resembled trajectories mapped out by coupler links of similar four-bars.

Other physical models constructed from plastic or wood have been utilized to investigate the contact behavior between the members of the joint. Some of these models were intended to reveal contact forces and stresses between the patella and femur as well as those between the tibia and femur. Models constructed of photoelastic materials have been used in a similar manner to investigate stress distributions throughout the components of a physical model of the joint.

### 2.4.2 Mathematical Models

Mathematical knee models are those that follow some constraint set forth by the approximation of an observed scientific behavior of the knee or mathematical relations developed from previous investigation of the joint and its components. Mathematical models are generally either anatomically-based or phenomenologically-based. Phenomenologically-based models attempt to replicate the mathematical response of the knee without considering the exact geometric or physical nature of joint components. Anatomically-based models attempt to represent the mathematical behavior of the knee based on the geometry and associated physics of the knee joint itself. Anatomical models can generally be subdivided into five categories: kinematic models, static models, dynamic models, patello-femoral models, and menisci models. Phenomenological models are generally categorized as simple hinge models, rheological models, or finite element models.

#### 2.4.2.1 Phenomenological

##### 2.4.2.1.1 Simple Hinge

The simple hinge model for the human knee has been proposed for many different applications. Hinge models have been used for the depiction of the motion of the thigh and shank in dynamic, full-body models as well as in the prediction of reaction forces in the joint or muscle load sharing during walking. Typically these models represent the bones as rigid bodies and do not consider the ligaments or the sliding contact between the joint members. Also, as the name implies these models tend to be limited to two-dimensional analyses of knee joint motion. Examples of studies that applied the simple hinge model include Smith and Kane (Smith and Kane, 1968), Kane

and Sher (Kane and Scher, 1970), Murray, et al. (Murray, et al., 1967), and Röhrle, et al. (Röhrle, et al., 1984).

#### 2.4.2.1.2 Rheological

Also falling into the phenomenological model category, rheological models typically model the knee as some type of viscoelastic hinge joint. These models commonly include the dissipative effects of muscles, ligaments, and cartilage but have little or no specific representations for these structures. Often these models represent the knee joint as a one or two-dimensional spring-mass-damper system. A study conducted by Moffatt employed a viscoelastic hinge model to analyze material properties of the knee and found that the data obeyed a Maxwell fluid model. In a similar study, Pope found that the behavior of their viscoelastic knee model closely resembled that of a Kelvin body or standard linear solid (Pope, et al., 1976). While definitions vary slightly for the term, a Kelvin body generally consists of a linear spring in parallel with a series combination of a linear spring and linear damper, grouping the model back into the category of a mass-spring-damper system.

#### 2.4.2.1.3 Finite Element

Another group of phenomenological type models that has gained in popularity are those that attempt to model the knee using finite elements (Hight, et al., 1979). While not true simple hinge models, nor categorizable as purely rheological models, finite element models share many properties with the simple hinge models and models representing the effects of the viscoelastic properties of the knee.

Improvements in computing power have allowed more accurate depiction of the structural components, permitting finer mesh representations of the modeled structures.

Bones are typically modeled using rigid beam elements with spring-type constraints defining their physics, while cartilage is often included as a porous matrix expelling and resorbing fluid. The models' depictions of the characteristics of cartilage within the human knee joint are improving, however very few address the role played by muscles and ligaments.

A study reported by Donahue, et al. used the finite element method to investigate the contact mechanics between the tibia and femur. In this study all materials were considered homogeneous, linear and elastic, however the representation of the bones as rigid bodies was shown to be valid when investigating the contact mechanics of the elastically modeled menisci and cartilage (Donahue, et al., 2000). There was no attempt in the model to include the load sharing characteristics of ligaments nor the force input contribution of the musculature surround the joint, as is typical for this type of model.

#### 2.4.2.2 Kinematic Methods

Kinematic methods have been employed to model the human knee joint, most noticeably to incorporate the relative rotation between the tibia and femur about varying axes. Those models generally fall into either Euler angle representations of these rotations or screw axis realizations.

##### 2.4.2.2.1 Euler Angles

The use of Euler angles has the advantage of representing the knee rotations about axes the clinician is "familiar" with such as flexion/extension, abduction/adduction, and internal/external. The problem with using Euler angles is that the resulting rotation given by a particular sequence of Euler parameters is directly

dependent on the order that the rotations are performed. This dependence allows for multiple distinct sets of Euler angles to be specified for varying series of orthogonal rotations that result in the same composite rotation (Goldstein, 1980). That is, the same motion can be described by distinctly different sets of Euler angles simply by changing the order that each of the rotations is applied, giving rise to multiple solutions for a single movement. This leads to ambiguity in study results as well as presenting difficulties in communication when rotation sequences are not uniquely specified.

Perhaps the most popular knee model based on Euler angles comes from Grood and Suntay (Grood and Suntay, 1983) who developed their coordinate system based on two body-fixed axes and one floating axis intersecting the two. Supported by Roth's work, Grood and Suntay attempt to eliminate the order dependence of the usual Euler angles by defining these special axes. The first body-fixed axis is the flexion/extension axis is located through the femoral condyles (medial to lateral), while the second body-fixed axis is located along the long axis of the tibia directed distal to proximal. The third floating axis is the common perpendicular of the two in the direction of their cross product. Descriptions of knee motion using this coordinate system are said to be employing Grood-Suntay angles. One particular difficulty associated with this type of coordinate designation is the inherent oppositeness between contralateral joints. In order to maintain a right-hand coordinate system, it is necessary for at least one axis to appear asymmetrical to the other coordinate system, disrupting any continuity during a comparison between the right and left systems.

Pennock and Clark propose a similar coordinate system based on bony landmarks requiring the specification of internal edifices such as the midpoint of the

transepicondylar line, the center of the femoral head, and the tip of the medial spine of the tibial eminence. Notwithstanding the difficulty of locating and tracking such landmarks *in vivo*, the study reported measured anterior/posterior drawer displacements depended on the selection of the coordinate system. When compared to similarly defined coordinate systems of Lafortune, Grood and Suntay, and Genucom, significant differences in displacement were noted throughout a typical gait cycle (Pennock and Clark, 1990).

**2.4.2.2.2 Instant Center/Screw Axis**

The instant centers method to describe rotation of the tibia relative to the femur is the two-dimensional equivalent of the instantaneous helical axis technique of three dimensions. Tracking the instant center of rotation throughout a range of motion for the knee has been used for the analysis of rolling-sliding contact and distraction-impingement conditions, however usually limited to planar analyses. Frankel, et al., used the method of Reuleaux to track instant centers or centrode in order to characterize joint surface motion. The authors found that the motion induced by healthy knees produced velocities tangential to the contacting surfaces, while knees with history of internal derangement produced instant center pathways different from those of the healthy knee cases (Frankel, et al., 1971).

McLeod and Cross extended the instant centers method to an instantaneous screw axis method by connecting the instant centers found in two parallel planes through the medial and lateral femoral condyles. They studied the motion of this "instant axis of rotation" through a series of X-ray images taken at 10° increments of flexion angle in an attempt to represent normal gait situations (McLeod and Cross,

1974). The benefit of these types of approximations was the attempt to extend instant centers to three-dimensional analysis, correct the uniqueness problem associated with Euler angles, and appease clinicians by fixing the descriptive coordinates to anatomical bodies.

Other, more classical definitions of the instantaneous screw axis were reported in studies by Lewis and Lew (Lewis and Lew, 1978) where an average or optimal screw axis was calculated for a given range of motion. The use of instantaneous screw axes alleviates the problem of uniqueness associated with Euler angles, however it is less intuitive than body fixed coordinate systems as the classical screw axis will typically have no continuous agreement with anatomically defined planes or landmarks. An added advantage to using screw axes to represent spatial motion is their invariance with respect to the choice of a coordinate system.

**2.4.2.2.3 Model Mathematics**

Kinematic models utilizing screw axis representations generally decribe knee motion by tracking the instantaneous helical axis of the tibia relative to the femur. Hefzy and Grood credit Strasser as the first to simulate the motion of the knee with a crossed four-bar mechanism. The intersection of the "cruciate" links was thought to define the relative instant center between the modeled tibia (coupler link) and femur (ground link), however, this method is limited to planar motion and the coupler link was shown to actually represent the femur. Hefzy and Cook noted this model as having the deficiencies of being two-dimensional and assuming that the cruciate ligaments were rigid bodies (Hefzy and Cooke, 1996). Freudenstein and Woo, as well as other authors,

have tracked the motion of the centrode, or path of the instant centers, for planar motion to study knee motions (Freudenstein and Woo, 1969).

The study of three-dimensional motion of the screw axis of the knee has been implemented using several different methods. Photographic and stereophotogrammetric methods have been used to compute the screw axis in order to investigate tibio-femoral separation during flexion as well as the effects of removing the cruciate ligaments (Blacharski, et al., 1975). The technique of tracking both fixed and moving axodes that fully describe the relative motion between the fixed and moving rigid bodies has also been attempted.

Mathematical models of kinematics either estimate or predict joint motion based on some mathematical relation prescribed for the motion of a moving coordinate frame relative to a fixed or global coordinate frame. Hefzy and Grood reported that many analytic functions have been used to attempt to mathematically describe kinematic knee models. Among these were a function involving the fifth root of the knee "flexion" angle by Crowninshield as well as quadric functions of the "flexion" angle by Walker. The review concludes models based on knee kinematics are useful only for motions with high repeatability such as those that may be modeled as one degree of freedom systems. For general knee motion, however, due to the variances between knee geometries, as well as dissimilarities in motions under different loading conditions, single parameter representations tended to break down.

**2.4.2.3 Static**

Static and quasistatic models have been developed in order to study forces that contribute to the stability of the knee particularly those from ligaments and surface

contact. Additionally, some of these models have been refined to study load distributions caused by active constraints on the joint. These constraints often take the form of various interpretations of muscular activity across the joint that are required to maintain stability. In either case, constraint equations, generally approximating equilibrium conditions were developed for various joint conditions in order to mathematically model the human knee joint.

Most models developed in this manner are statically indeterminate and solutions are arrived at by various means including the overgeneralization of the joint or simplifying the model until the number of unknowns matches the number of constraining equations. Another approach to solving the system is by increasing the complexity of the model by adding constraint equations until the system is fully determined. A general example of this approach is to represent ligament constraints with multiple linear equations, equivalently modeling the ligaments as some type of multiply banded structure.

**2.4.2.3.1 Load Sharing**

Hefzy and Grood report many models used to investigate the load distribution among muscles and ligaments for various activities. A two-dimensional study by Reilly and Martins was cited where only four input forces were considered and the location of the application of the joint contact force was incorrectly assumed to be constant. This study was a case where the model was oversimplified in order to obtain a fully-determined solution. Such models might have seen use in the early stages of prosthetic development, however, considering today's computational assets and the logging of more intricate sets of data, these are not suitable for human locomotion study.

Another more popular load sharing model that Hefzy and Grood cite as being used by authors such as Morrison, Harrington, and Nissan, attempts to model the forces shared by ligaments, tendons, and bones across the knee joint (Harrington, 1976; Morrison, 1970; Nissan, 1980). Data was collected for muscle activity using multichannel electromyographs. Data were also collected using a force plate to measure foot-to-ground reaction forces and limb segment acceleration data were collected using the questionable approach of tracking skin markers with an optical motion capture system. Values for individual ligament forces, contact pressures, and a number of forces corresponding to muscular groups were computed among disputed assumptions by employing different combinations of the collected data (Morrison, 1970).

Static or quasi-static load sharing models have also been analyzed using optimization approaches. Seireg and Arvikar modeled 29 muscles of the lower extremity as tensile forces along with reaction forces in ligaments and overall joint moments. Using the simplex optimization method with a variety of minimization criteria, the moments, loads, and reactions were computed for postures such as leaning, stooping, and standing (Seireg and Arvikar, 1973). Hardt performed a similar study, minimizing force and minimizing energy, in a model including 30 muscles represented by tensile forces throughout a gait cycle but reported poor agreement with electromyographic data (Hardt, 1978). Crowninshield used optimization methods to determine muscular forces in a planar model of the human elbow while maintaining limits on the maximum muscular forces (Crowninshield, 1978). Patriarco, et al., investigated muscle activity by optimizing mechano-chemical energy, both with and

without supplemental kinematic data, for human gait studies. Their results showed that improved kinematic data, such as joint angles and computed joint torques, were found to improve existing approaches more than selection of the optimization criteria (Patriarco, et al., 1981).

**2.4.2.3.2 Ligament Length**

In many of the knee models discussed, considerable effort has been given to determine the contributions the ligaments make to control knee motions, particularly to the study of the forces carried by ligaments. Models based on ligament length have addressed the issue of forces transmitted through ligaments by studying the relationship between joint motion and elongation of ligaments. Numerous techniques have been used to investigate this relationship such as the use of weight scales, Hall effect sensors, image capture devices, strain gauges, as well as comparisons with other types of elastic materials.

Ligament length based models have typically included two rigid bodies connected by ligaments models attached to the bodies at the ligament insertion sites. The movement of one body relative to the other is then mathematically investigated under the constraints placed on the ligament elongation based on previously studied ligament properties. Models for ligaments have ranged from the simple, single line between insertion sites to the complex, multiple line segment representations for a single ligament, accounting for the effects of segments wrapping around each other and the rigid bodies (Hefzy and Grood, 1988).

Crowninshield et al., studied the stiffness of the knee joint using a model based on ligament length. In the study, the ligaments were modeled with multiple segments

and the material properties for all ligaments were assumed to be equivalent to those determined from data collected for the medial collateral ligament. The constraint applied to the model was that no ligament was allowed to strain beyond 5% of its initial or "rest" length, effectively modeling the ligaments as linear springs. Using this model, Crowinshield, et al. were able to compute values for joint stiffness and study the relationship between that stiffness and simulated ligament absence or rupture (Crowninshield, et al., 1976).

**2.4.2.3.3 Femoral-Tibial Contact Stresses**

Models based on tibio-femoral contact were cited as studies primarily developed to determine the stresses in the bone due to contact and the resulting effect on bone structure and growth. Some of these models were cited as representing the contact forces as either a single force on the contacting surfaces or as two individual forces acting through the contacting surfaces of the medial and lateral tibial plateaus.

Minns (Minns, 1981) used the two-force representation to investigate the effects of anatomy on the forces affecting the medial and lateral plateaus. Hefzy and Grood cite several other researchers that used contact stress models. Some employed finite element methods or photoelastic techniques to study either or both healthy and abnormal knees. Many of these studies produced results not in agreement with similar research reported by other authors, however these variations were attributed to differences in loading conditions and other geometric parameters.

**2.4.2.3.4 Ligaments and Geometry**

The 1988 review of knee models credits Andriachi et al. (Andriacchi, et al., 1983), and Wismans et al. (Wismans, et al., 1980) with the "most comprehensive

anatomical quasistatic knee models available in literature" (Hefzy and Grood, 1988). There is no update for this category in the follow-up article that focused mainly on dynamic models and those that included either the patella or the menisci. Building on Wismans' model Blankevoort et al. (Blankevoort, et al., 1991a) investigated the recruitment of knee ligaments based on an assumption of the maximal strain and of stiffness values for the ligament bundles. The range of motion was from full extension to 95° of flexion, and recruitment under anterior posterior loadings along with internal external moments was also studied.

The leaps in the available computational power as well as the growth in biomechanics research since the publication of these articles suggests that such models have been surpassed. Donahue et al. (Donahue, et al., 2000) reported a study using a model of the human knee based on ligament and geometric constraints. The data for the geometry of the bones was obtained using spiral computed tomography (CT) scans. Soft tissue data was obtained using high accuracy laser digitization, and ligaments were modeled as nonlinear springs "similar to Wismans et al.". Another study reported by Gil et al. (Gil, et al., 1998), modeled the tibio-femoral joint using geometric and ligament constraints. Cadavaric data were collected using magnetic resonance imaging (MRI) to obtain the geometric structure of the bones and soft tissues, and ligaments were modeled as nonlinear springs. The model was validated through data attained by studying the cadaver knee in a robotic arm apparatus equipped with force sensors.

Another reconstruction of the human knee joint was carried out by Boisgard, et al., using data collected from thirteen magnetic resonance image sequences of a healthy knee at various degrees of flexion. With the goal of developing a method of studying

the three-dimensional kinematics of the human knee *in vivo*, the geometry and relative positions of the structural components of the human knee were interpreted from the scans and an animation through the thirteen positions was assembled (Boisgard, et al., 1994). With the continuing improvement of imaging resolution, sensing technology, and computational power and efficiency, static models based on ligament and bone geometry will continue to evolve into the realm of dynamic and kinematic models of the human knee joint.

**2.4.2.4 Dynamic**

The initial review of knee models included only one reported example of a dynamic model of the human knee. This model was two-dimensional, taking into account motion only in the sagittal plane. Dynamic models, by definition, describe the represented system incorporating the variable of time. Through the study of bodies, forces and motion, the constraining equations providing these time-based constraints usually take the form of differential equations. The representation of the knee in three dimensions with such equations presents an enormously complicated set of equations that must be solved simultaneously to maintain the validity of the model. The second review by Hefzy et al. discusses the evolution of solution techniques for such a set of constraining differential equations. First, the Method of Minimal Differential Equations (MDE) and the Method of Excess Differential Equations (EDE) used to solve the two dimensional cases are presented. Building on these techniques the Reverse EDE method and Modified Reverse EDE method are discussed which ultimately yielded a system of equations termed the Differential-Algebraic Equations (DAE) system.

In a recent contribution to a book, a three-dimensional dynamic model was cited that employed this method, authored by Hefzy and Abdel-Rahman. Several interesting conclusions were drawn in this work including the absence of evidence of a "screw home mechanism" and the absence of support for any "symmetrical femoral roll back" type motion (Hefzy and Abdel-Rahman, 2000).

#### 2.4.2.5 Patello-Femoral

Models of the patello-femoral joint are generally constructed to study the contact forces between the knee cap (patella) and the thigh bone (femur). Most models of this joint represent the femur and patella as rigid bodies, holding the femur fixed and constraining the patella with the quadriceps muscle, patellar tendon, and direct contact with the femur.

Early models included the assumption that the patella operates similar to a frictionless pulley, contributing only the alteration of the line of action of the force provided by the muscular inputs, but causing no discernable effect on its magnitude. This required that the resultant contact force between the femur and patella act along the line of the bisector of the angle formed by the quadriceps muscle force and the transmitted force in the patellar tendon. Hefzy and Grood (Hefzy and Grood, 1988) noted that this assumption has been proven incorrect through actual measurement of these forces. Similar studies were noted to model the patello-femoral joint as a lever with the fulcrum at the line of action of the patello-femoral reaction force, which was shown to pass through the center of pressure between the patella and femur.

In the update review of knee models, Hefzy and Cooke discuss more recent models of the patello-femoral joint, which used various methods to acquire the

geometry of the contacting surfaces. Some of the methods reported for data collection included X-ray photogrammetry, magnetic devices, introduction of dyes, pressure sensitive films, piezoresistive transducers, and micro-indentation sensors. Using the collected geometric data, various types of surface representations such as Coons' bicubic surface patches or third order asymptotic patches, were constructed to model the contacting areas. Finite element methods as well as other analysis techniques, some assuming two-point contact between the patella and femur and others employing more complex models of patellar constraint, were used to study the resulting model.

Studies that modeled the femur as a rigid body and allowed the patella to deform, were also reported, along with others that included components representing articular cartilage. Much of the value of the study patello-femoral models lies in the simulation and evaluation of various medical procedures involving the human knee joint (Hefzy and Cooke, 1996).

As technology evolves, the tendency in mathematical modeling is to increase the complexity of the analysis in the quest to more accurately represent the modeled phenomena. In the field of biomechanics, improvement of models is generally accomplished in one of two ways. The first is to enhance the accuracy of the representations for those items already included in the model, accomplished by taking more precise data, using more exact mathematical representations, or using more realistic input conditions. The second way biomechanical models are enhanced is to include additional components not considered in previous models. In the case of the study of the human knee joint, an example of this could be a passive tibio-femoral joint model expanded to include the patella and its constraints.

Models including both the tibio-femoral joint and the patello-femoral joint insist more significance be placed on the analysis of the contacting surfaces, leading to the inclusion of deformable bodies in the representation. While the computational power to deal with rigid body models including the patella, femur and tibia is at hand, some simplification of model parameters is required for analysis using deformable bodies or surfaces. This simplification is often accomplished by representing the bone structures as combinations of geometric primitives or some other compact mathematical entity such as polynomial functions or parametric patches. For passive motions, however, Blankevoort showed the use of a thin, linear, elastic layer on a rigid surface to be a valid approach of modeling articular contact and that the differences between models using nonlinear and linear deformable layers were small (Blankevoort, et al., 1991b).

Hefzy and Cooke reported on four studies of that include models of this type. Models including both the patello-femoral and tibio-femoral joint understandably include additional simplifications to allow for timely analysis. The simplifications include modeling the tibio-femoral joint as a four bar, as discussed previously, representing the joints as two dimensional, and limiting the valid range of joint positions due to geometric deficiencies. Two of the studies were reported to represent these joints in two dimensions while two were cited as modeling the joints in three dimensions (Hefzy and Cooke, 1996).

#### 2.4.2.6 Menisci

The medial and lateral menisci of the human knee rest on the tibial plateau and are composed of fibrous cartilage. The function of these structures is not fully understood and until the recent evolution of finite element methods, little modeling was

feasible due to the geometric complexity of the structures and nonlinear behavior of their mechanics. Accurate representation of the deformation of the flexible matrix in the presence of expulsion and resorption of capsular fluid is difficult at best and when coupled with the varying geometry and physical condition of test specimens, validation of adopted representations is extremely challenging. While the confirmation of the functions of the menisci remains, it is generally asserted that these structures provide some measure of stability and load bearing at the joint as well as afford both cushioning and lubricating effects during tibio-femoral contact.

Hefzy and Cooke reported several studies that investigated the various functions of the menisci that included the determination of material properties and load bearing characteristics. Results for both of these types of studies are necessary to accurately model the menisci with finite element methods. A study by Bendjaballah et al. (Bendjaballah, et al., 1997) was singled out as the most inclusive of knee models containing structures representing the menisci. The resounding limitation of this model is that it is solvable only at the position of full extension.

**2.5 Radiological Imaging**

Crowninshield, et al., developed a model of the human knee, discussed earlier in the review of knee models, employing 13 elements based on the major ligament insertion sites and lengths. During the experimental validation of the model the authors noted that specimen-to-specimen variation dictated a need for the collection of a significant number of samples to validate the model. The authors further cited a study where 32 specimens were used to evaluate the function of a single ligamentous structure

and projected that a similar scale validation for each of their 13 elements was not feasible due to the required number of specimens (Crowninshield, et al., 1976).

During a study of the posterior cruciate ligament, Grood, et al., reported values with standard deviations between one sixth and one third of the measured parameter meant to describe the average size of six test specimens (Grood, et al., 1989). Variations of this magnitude have the potential to occur in every constraint defining a workspace model, and the number of possible combinations of dissimilarities is only somewhat limited by measurement resolution. A further, more basic measurement that relates directly to the displacement workspace is that of ligament length. In a study of functional anatomy of the anterior cruciate ligament (ACL), Amis and Dawkins cited five papers reporting ACL lengths ranging from 22 mm to 39 mm with a mean value of 32 mm, (Amis and Dawkins, 1991) while a study by Lanzendorf reported values from 21.8 mm to 25.1 mm for the length of the ACL (Lanzendorf, 1988).

The anatomic deviations among the population with regard to the effect on function can be readily seen in the erroneous results obtained with standard diagnostic tests. As Brand noted, most clinicians have experienced cases where a patient had indeed ruptured ligaments but showed no indication of such from the accepted diagnostic examination. Also, patients have exhibited evidence of ligament damage that was predicted by diagnostic examinations but under radiological imaging or surgery, this was observed not to be the case (Brand, 1986).

At this time there is no publicly available database that is representative of the geometric variability of general human anatomy and study-by-study construction of such a data set is not practical considering the extreme shortage of "healthy" cadaveric

specimens. The computation of workspaces for a "general" knee would be essentially fruitless due to the considerable variation in human anatomy, thus, in order to demonstrate the construction and use of the workspace concepts, it is necessary to develop a test case from "real" data. Construction from real data will also begin the validation process by showing the workspace does exist for at least one human anatomic specimen. From an application standpoint, until a data set is available which spans the variations seen in a population, the clinical usefulness of workspaces in that population will remain dependent on the ability to construct workspaces on case-by-case bases. The development of radiological imaging methods and the progression of computational efficiency and power provide possible avenues for accomplishing this task.

The most commonly used radiographic imaging techniques can be divided into three categories based on the type of radiation each employs. The first category of radiation, X-rays, is used for many applications and typically relies on the absorption, scattering, and transmission of X-rays to render image features. Bone readily absorbs X-rays, making this technique well suited to detecting skeletal trauma, while pneumonia can be detected due to the differences in X-ray attenuation between normal and fluid filled lungs. Often patients will be subjected to some form of an indicator element with a high X-ray absorption coefficient in order to render tissues of lower absorption coefficients visible, such as blood vessels, digestive tracts, or the ventricles of the brain. The typical X-ray imaging system will include an X-ray source, the object of interest, and some type of detector (Barrett and Swindell, 1981).

An early limitation of the use of X-rays for anatomical imaging was that a three-dimensional object was exposed but represented by a two-dimensional projection of that image. Surrounding materials or geometric dissimilarities also hindered differentiation between materials of similar absorption characteristics. These problems lead to the development of an alternative method of using X-rays that has called computed tomography or CT imaging. The basic idea behind the process was to rotate the source and detector around an object in order to obtain a slice or two-dimensional image of the object at the area of interest (Barrett and Swindell, 1981). Using this technique, an object could be three-dimensionally reconstructed by "stacking" subsequent slices, and materials of differing absorption coefficients can more readily be distinguished. Improvements in technology have allowed the development of spiral CT scanning techniques, fine-tuning resolution to the point of the detection of lesions of the liver and lung nodules (Calhoun, et al., 1999). The result of this technological advancement is a method of data collection that is well suited to the task of, among other things, obtaining geometric descriptions of the bones associated with the human knee joint.

While the detection of other, less absorptive structures in the human knee is possible using CT imaging techniques, the presence of higher absorptivity materials such as bone limits the effectiveness of this process. This is especially true if the structures in question is located between bony masses, as is the case for the cruciate ligament insertions in the intercondylar notch. This problem introduces the need for, and a widely used application of, the next category of radiological imaging that uses gamma rays to accumulate data.

Nuclear magnetic resonance (NMR) imaging is based on the detection of gamma radiation emitted from a radionuclide within a patient's body (Barrett and Swindell, 1981). The stimulation of gamma ray emission is due to the phenomenon of nuclei possessing a magnetic moment, and, when exposed to a radio wave of a specific frequency in the presence of a strong magnetic field, will resonate at the input radio wave frequency (Bradley and Tosteson, 1982). The frequency is known as the resonant frequency for the nuclei, giving the process its name, Nuclear Magnetic Resonance. Negative public connotation of the word "nuclear" caused the omission of this term from its presently accepted name of Magnetic Resonance Imaging or MRI.

The following is a highly simplified discussion of the phenomena exploited by MRI scanning techniques. Magnetic moments can arise in nuclei containing odd numbers of protons, neutrons or both, as is the case with hydrogen atoms. When such nuclei are placed within a magnetic field, the net magnetization (average of all the nuclear magnetic moments) is in the same direction as the magnetic field at an equilibrium state. This equilibrium magnetic state is called the longitudinal magnetization, $M_L$. Should this equilibrium be disturbed, as is the case when the proper radio frequency is applied to the nuclei, the net magnetization will begin to shift alignment toward that of the combined magnetic field called the transverse magnetization, $M_T$. At the initial equilibrium state, $M_T$ is zero and as the secondary magnetic field is introduced, $M_L$ decreases while $M_T$ increases and precesses about the longitudinal axis. When the secondary magnetic field is removed, $M_T$ decays to zero while $M_L$ gains in strength, returning to the equilibrium state.

The process is characterized by two time constants, one associated with how long the nuclei take to realign after the disturbance, $T_1$, and one associated with how long the nuclei can maintain a transverse magnetization, $T_2$. In general $T_2$ is shorter than $T_1$ in the same material, however $T_1$ is generally shorter in liquids than in solids, while $T_2$ is normally shorter in solids than in liquids (Bradley and Tosteson, 1982). Table 2.1 contains a list of approximate relaxation time constants for some common biological tissues.

From the values of $T_1$ and $T_2$, suitable TR, "time between repetitions", and TE, "time 'til echo", settings can be selected to best contrast the targeted tissues. For the case of resolving the ligaments and cartilage associated with the human knee, the $T_1$ value for connective tissue is significantly larger than that of the surrounding tissues such as bone, fat, and muscle. It is also evident that the $T_2$ values for connective tissue are again larger than that for bone, fat, and muscle, however this difference is not as

Table 2.1 Approximate longitudinal ($T_1$) and transverse ($T_2$) relaxation time constants for various biological tissues (Taxt and Lundervold, 1994).

| Biological Tissue | $T_1$ (msec) | $T_2$ (msec) |
|---|---|---|
| cerebrospinal fluid | 2500 | 150 |
| connective tissue | 840 | 58 |
| white matter | 1000 | 66 |
| air, bone | 390 | 180 |
| gray matter | 1600 | 80 |
| striated muscle | 1100 | 46 |
| blood | 5500 | 170 |
| fat | 480 | 50 |
| parotid gland | 780 | 49 |
| tumor | 1600 | 110 |

pronounced as in the case of the $T_1$ time constant. As a result, in order to provide themost significant contrast between these structures, a moderately short TR and TE, which is referred to as a $T_1$ weighted scan, is predicted to produce the best results.

Figures 2.2, 2.3, and 2.4 depict the relative contrast levels expected between connective tissue and fat as well as connective tissue and striated muscle for varying TR and TE times. The surfaces are based on the relationship given by Equation 2.5.1,

$$I = C\left(1 - e^{\frac{TR}{T_1}}\right) \cdot e^{\frac{TE}{T_2}} \qquad 2.5.1$$

where $C$ is a constant based on machine and environment properties.

Taking advantage of the different intensity values by adjusting the TR and TE times, radiologists can fine-tune their scan sequences to provide sharp contrasts between selected tissues. Commercially available software can reconstruct three-dimensional models from the resulting MRI scans of the objects that have been targeted by this

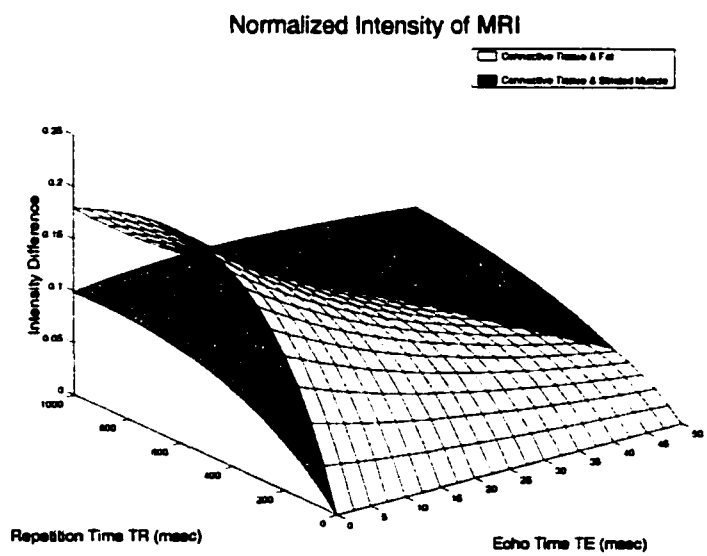


Figure 2.2 Intensity differences between materials surrounding the human knee joint for varying TR and TE

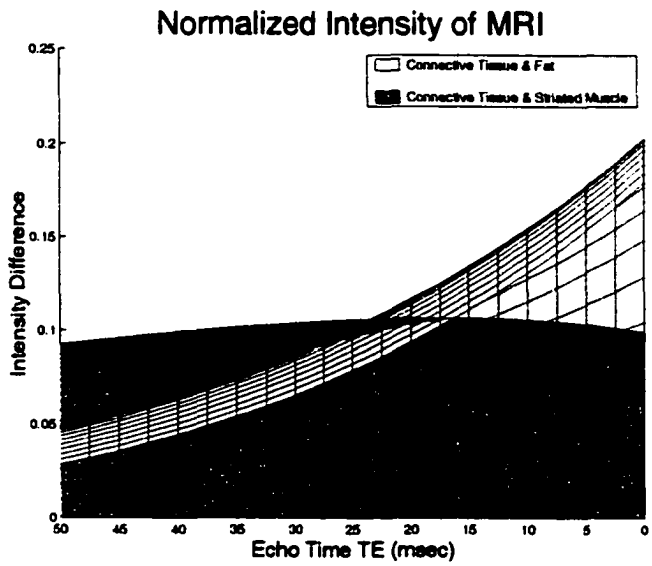


Figure 2.3 Intensity differences between materials surrounding the human knee joint (TE projection)

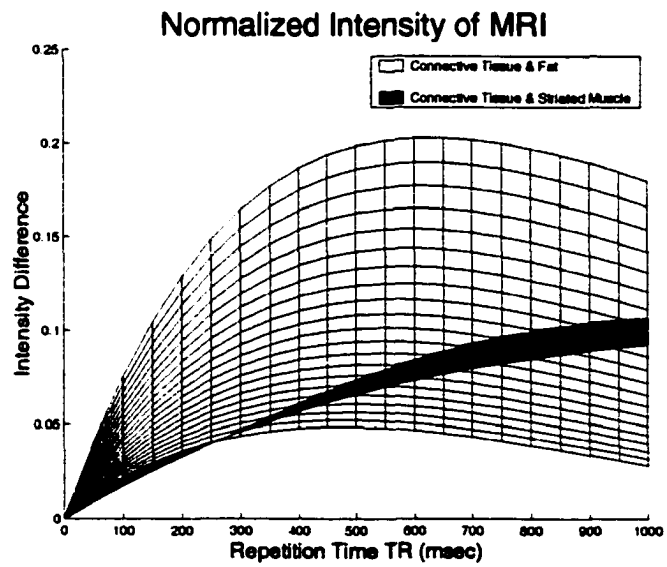


Figure 2.4 Intensity differences between materials surrounding the human knee joint (TR projection)

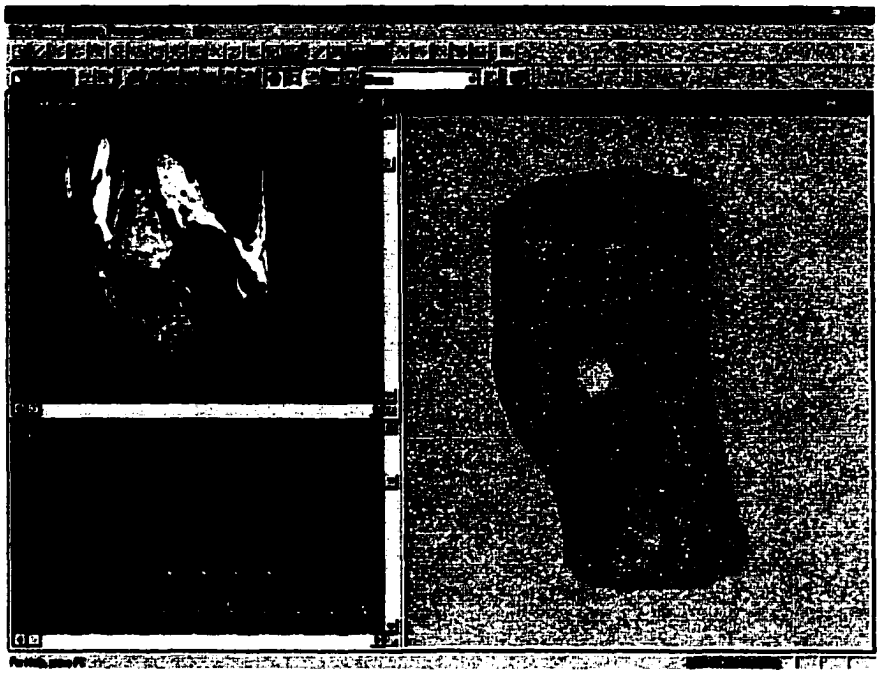

Figure 2.5 Screenshot of Able Software's 3D-Doctor software package recognizing the bones of the knee joint from MRI data.

contrasting to obtain geometric data describing the structures of the human knee joint. Many of these codes have the ability to reconstruct images from a myriad of imaging modalities. 3D-Doctor (Able Software Corporation, Lexington, MA) is one package that can be used to generate surfaces and volumes from MRI, CT, ultrasound, and other volumetric imaging techniques. These three-dimensional objects can be exported in standard formats for use with many engineering and computer aided design packages. Figure 2.5 shows a sample image taken from the company's web site[1] of a reconstruction of the bones in the human knee joint, demonstrating the software's ability to recognize and reconstruct objects.

As technology improves and resolutions become sharper, the use of medical imaging techniques to generate very accurate models of structures in the human body *in*

[1](October, 2001) http://www.ablesw.com/3d-doctor/

*vivo* could provide enough patient specific data to personally model anyone seeking care. Interactive technologies such as fluoroscopy, when combined with the three-dimensional reconstruction software, may also prove to be a reliable method of human skeletal kinematic data collection and processing.

# CHAPTER 3. METHODS AND MODELING

## 3.1 Clinical Data

In order to build a meaningful model of the human knee, it was necessary to collect data from bona fide human sources. Due to the inherent complexities of bone surface geometry and the variances of ligament insertion locations, ligament rest lengths, and surface geometry, no representative set of parameters has been established that accurately characterizes the human knee joint for the general population. This fact does not preclude, however, the possibility that the human knee joint may be characterized by the geometry of the workspaces it generates. One of the primary questions raised by the application of workspace analysis to the human knee is whether or not there are commonalities shared between seemingly different knee geometries.

*In vitro* studies have been reported where exact surface geometries were employed to examine human knee kinematics by analyzing motion between actual knee components, either from total knee replacement prostheses or cadaver specimens. (Godest, et al., 2000), (Chan and Seedhom, 1999) Executing such a study *in vivo* requires the accurate representation of skeletal components of a healthy living subject. It has been shown that the use of skin-mounted markers for this purpose is unreliable, (Fuller, et al., 1997) however, the rigid attachment of markers directly to bone causes both pain and a need for anesthetics, potentially compromising or retarding the normal movement. As a result, *in vivo* analysis of healthy human knee joint kinematics commonly included geometry obtained through some radiological imaging technique or geometric approximation (Boisgard, et al., 1994), (Tewes, et al., 1997), (Donahue, et al., 2000). Methods of medical imaging exploiting radiological phenomena include

Magnetic Resonance Imaging (MRI), Computed Tomography (CT) scans, X-ray imaging, and fluoroscopy. Methods of approximating knee geometry have relied on the detection of bony landmarks and the use of geometric primitives to construct a representation of knee components.

For the purposes of developing the workspaces in this study, three basic parameter sets were necessary. They included the surface geometry of the tibia and femur, the ligament insertions into the tibia and femur, and the "rest" lengths of the modeled ligaments. It should be noted that the specification of a rest length is not intended to indicate any information concerning the stress condition of a ligament. It has been noted that definition of zero strain or zero stress positions of connective tissue is extremely important when studying physical properties (Nigg and Herzog, 1994). For the purposes of this geometric investigation, ligaments will be considered inextensible, qualifying the rest length as the ligament length under the auspices of a passively constrained knee. Several different methods and types of data sets were explored for workspace development including data sets collected through previous research, data sets from donated or public sources, and data sets collected specifically for this research.

### 3.1.1 Data Collection

#### 3.1.1.1 MIT/MGH

A matched pair of cadaver knees was obtained from Harvard Medical School for study at the Newman Laboratory for Biomechanics and Human Rehabilitation at the Massachusetts Institute of Technology (Cambridge, MA). Data were collected from the pair for various studies, including the investigation of possible relationships between

ligament insertion sites and Hounsfield units generated during CT imaging (Morgan and Murphy, 1997) as well as the determination of ligament "rest" lengths and mechanical properties through video scanning techniques (Lanzendorf, 1988).

The right knee was dissected, removing all extraneous soft tissue as well as the patella and its attachments. The four major ligaments (anterior cruciate, posterior cruciate, tibial or medial collateral, and fibular or lateral collateral) were then sectioned mid substance, disarticulating the tibia and fibula from the femur. The unmarked bones were mounted individually in a water bath, and scanned by an EMI 7070 CT scanner (EMI Ltd., England) at the Massachusetts General Hospital Radiation Medicine Department. The scans covered approximately 12 cm from the joint centerline with a nominal spacing of 2 mm between scan slices. The specimens were then removed from the bath in order to proceed with the marking of the ligament insertion sites.

Computed tomography utilizes differences in X-ray attenuation values caused by, among other things, density variations to produce a visual representation of the scanned objects composition. Large density variations within an object produce higher contrast images signifying the need for significant departure between the ligament insertion site environment density and the ligament insertion site maker density to

Table 3.1 Number of ligament insertion site markers used by Murphy, (Murphy, 1990) (* indicates a broken drill bit was visible in addition to the number of markers listed).

| Ligament | Number of Balls (Femur) | Number of Balls (Tibia) |
|---|---|---|
| Anterior Cruciate | 9 | 10 |
| Posterior Cruciate | 10* | 10 |
| Tibial Collateral | 9 | 8* |
| Fibular Collateral | 9 | 6 |

facilitate marker detection. Each of the four ligaments was resected down to its insertion site on the femur and tibia or fibula, whichever was appropriate, to identify and expose the intended marker locations.

One millimeter diameter, 316 series, stainless steel balls (New England Miniature Ball) were chosen to serve as markers for the ligament insertion sites. Holes in the cortical shell, distributed evenly (as determined by visual inspection) along the bone/ligament interface, were predrilled with a 0.97 mm (#62) drill bit, and one steel ball was press fit into each cavity. Table 3.1 shows the number of markers used to identify the boundary of each ligament insertion site. The bones were then remounted in the water bath and scanned again from the joint centerline to approximately 12 cm, above or below, with a nominal spacing of 2 mm between scan slices.

The CT data were supplied as one bitmap image per data file each covering 320 by 320 pixels with each pixel 0.47 mm on a side. Data files were labeled numerically to identify the sequential order in which slices were obtained. The pixel values as supplied were scaled such that air and water had values of 256 and 1256, respectively (Morgan and Murphy, 1997).

The left knee was included as one of four specimens investigated in a study of the material properties of the ligament tissues of the human knee. Harvesting was the same as with the matching right knee. The specimen was obtained fresh, sealed in plastic bags and frozen at –20 °C until dissection. Prior to dissection, the knee was thawed in room temperature water and the bone-ligament-bone complexes were cut out for the four major ligaments, including the anterior cruciate, posterior cruciate, tibial collateral, and fibular collateral. The ligaments were potted and cast to provide

duplicate geometry for various measurements. After potting and casting were complete, the ligaments were removed from the potting media, wrapped in saline-soaked gauze, sealed in plastic bags, and frozen at –20 °C.

Prior to measurement, the ligaments were thawed in room temperature water while remaining in the sealed plastic bags. Each ligament was placed in the potting apparatus for measurement. One end of the ligament was clamped in the frame and oriented vertically by suspending a 48 g weight from the free end. Images of the ligament were obtained using a high resolution, black and white video camera (378 lines x 483 lines) input and displayed on a 768 x 480 pixel monitor. The insertions of the ligaments were stained with a thin line of 0.1% solution of toluidine blue, and three images of the ligament were obtained, rotating the apparatus 90° between successive images. To determine the ligament rest lengths, the number of pixels each ligament spanned in the images was counted and converted from pixels to standard units of length. Pixel sizes were determined by imaging standards of known length. Table 3.2 shows the mean length and variation in length of the three images (Lanzendorf, 1988).

#### 3.1.1.2 Visible Human Project (VHP)

The National Library of Medicine (NLM) recognized that the growth of technology and the internet would lead to a time when its traditional reference databases

Table 3.2 Ligament rest lengths as measured by Lanzendorf (Lanzendorf, 1988).

| Ligament | Mean length (mm) | Variation in length |
|---|---|---|
| ACL | 23.6 | 3.2 % |
| PCL | 17.1 | 11.2 % |
| TCL (MCL) | 103.6 | 5.7 % |
| FCL (LCL) | 50.4 | 3.1 % |

and information services could be complimented by electronically-based services. NLM also understood the growth potential of the application of medical imaging techniques to research. These ideas and observations fostered the development of what is known today as the Visible Human Project (VHP).

In 1991, the University of Colorado (Denver, CO) was awarded the initial contract to acquire CT scans, MR images, and cryosection images in the transverse plane of one representative male subject and one representative female subject with a nominal spacing of 1 mm between image slices. The principle investigators on the award were Victor M. Spitzer, Ph.D. and David G. Whitlock, M.D., Ph.D. The resulting VHP image set for the male includes axial MR images of the head and neck, and longitudinal MR images of the remainder of the body with approximately 4 mm of spacing between images. The MR images have a resolution of 256 x 256, with 12 bit grayscale pixels. Also in the male data set are coincident CT and anatomical images of the entire body taken axially at 1 mm slice intervals. The CT images have a resolution of 512 x 512, 12 bit grayscale pixels, while the anatomical images have a resolution of 2048 x 1216, 24 bit color pixels. There are a total of 1871 images each for both the CT and the anatomical data sets. The male data set was made available in November of 1994 and in August of 2000, higher resolution axial anatomical images of the male specimen were released. The female data sets had the same characteristics as the male set with the exception of 0.33 mm spacing for the axial anatomical images.

Both the male and female full data sets are available for download through the NLM web site[1] subsequent to the completion of the required licensing agreement. Complete data sets on DAT media are also available for purchase on the NLM web site

[1] http://www.nlm.nih.gov/research/visible/visible_human.html

either by body region or as one complete set. Further information concerning the Visible Human Project can be obtained through their page on the NLM web site (Ackerman, 2000).

#### 3.1.1.3 HealthSouth

Inquiry into potential data sources led to discussions with Dr. Charles Greeson of the HealthSouth Diagnostic Center (Baton Rouge, LA) concerning the content of MR images. Permission was obtained to investigate the collection of data in the form of MRI scans from the HealthSouth Diagnostic Center of consenting patients under a condition of anonymity, however no scans of this nature were performed at the center in a timely manner. As a result, the head technician (Mr. David Frye) performed a typical set of knee scans on a healthy co-worker at the diagnostic center fitted with a contrast enhancing knee coil. Using the Center's GE Signa Series MRI scanner (GE Medical Systems, Milwaukee, WI), seven sets of scans were obtained of a 28-year-old male subject of varying excitation and relaxation times with a resolution of 256 x 256, 16 bit grayscale pixels. Table 3.3 gives a brief description of some of the characteristics of the MR images obtained from HealthSouth Diagnostic Center.

Table 3.3 Distribution of HealthSouth Diagnostic Center data sets.

| Scan Number | Anatomical Plane | Number of Slices | Slice Thickness |
|---|---|---|---|
| Series 1 | Sagittal | 10 | 5 mm |
| Series 2 | Axial | 32 | 4 mm |
| Series 3 | Coronal | 18 | 4 mm |
| Series 4 | Coronal | 16 | 4 mm |
| Series 5 | Sagittal | 20 | 4 mm |
| Series 7 | Sagittal | 60 | 1.6 mm |
| Series 8 | Sagittal | 48 | 4 mm |

### 3.1.1.4 University of Minnesota and Regions Hospital

A matched pair of fresh frozen cadaver knees was obtained from the University of Texas Medical Center, through the Biomechanics Department at the University of Minnesota (Minneapolis, MN). The knees were thawed and immediately implanted with the reference marker coordinate systems. Prospective data collection included the use of CT scanning in conjunction with MRI scanning, making it necessary to employ a marker system compatible with both data collection methods. After consultation with two medical doctors specializing in orthopedics (Dr. Greeson and Dr. Gregory A. Brown), a technician experienced with radiological imaging (David Frye), and professional literature, it was decided that titanium was the most desirable material from which a marker system could be constructed. Titanium has been reported to yield minimal artifacts in both MRI and CT scanning environments, exhibit minimal paramagnetic behavior, and it has been observed by those familiar with clinical imaging techniques, to produce significant contrast with respect to biological matter (Fiala, et al., 1993; Sutherland and Gayou, 1996).

Titanium screws with a diameter of 1.3 mm and of various lengths, donated by Synthes Corporation (Paoli, PA), were used as reference markers and ligament insertion site markers during the data collection process. The screws were originally designed for maxillofacial applications and, depending on the length of each screw, were packaged either individually or as a kit that included two 1 mm diameter pre-drilling bits and three customized hand screwdrivers. A single incision was made anteriorly on each specimen to expose the anterior surfaces of the femur and tibia for coordinate system marker implantation. Care was taken not to disturb any tissue unnecessarily in order to

capture, as accurately as possible, the natural, intact, relative geometry between the tibia and femur. The locations of the screws in the coordinate system were predrilled using the supplied drill bits and a commercially available Black and Decker (Towson, MD) electric hand drill. The screws chosen to serve as reference markers, 14 mm long, 1.3 mm diameter, were manually implanted into the bone, each in a predrilled pilot hole, using the screwdrivers included in the Synthes kit.

The shafts of the tibia and femur were reamed with a $\frac{7}{16}$ in. drill bit powered by the electric hand drill. The left knee was mounted on wooden dowels inside a custom built container constructed of a 36 in. length of $\frac{1}{4}$ in. wall thickness cylindrical acrylic tubing, two $\frac{1}{4}$ in. acrylic plates and two six in. diameter polyvinyl chloride (PVC) pipe access fittings. The housing was then transferred to the Regions Hospital Nuclear Medicine Department (St. Paul, MN) and scanned with a GE HiSpeed CT/i scanner (GE Medical Systems, Milwaukee, WI), capturing approximately 3 cm beyond each set of coordinate system markers. The container was removed from the CT conveyor and the specimen was removed from the container. The procedure was repeated for the right knee, again capturing approximately 3 cm beyond each set of coordinate system markers. These first two sets of scans were performed in order to provide reference geometries for an intact human knee before any disruption or dissection of the capsular elements.

With the reference scans complete the left knee specimen was further dissected and the femur was disarticulated from the tibia and fibula. As each ligament was exposed and severed, markers were placed at the apparent location of the insertion into the cortical shell. Soft tissue was dissected away leaving only the screw markers, bone,

and cartilage, however the patella and patellar tendon were left attached to the tibia. Four, equal length, 1.3 mm diameter titanium screws were used to mark each ligament insertion site, spacing them uniformly along the ligament-bone interface. The same length screws were used to mark the insertions on both the tibia and the femur, however different length screws were used to distinguish the markers used for each ligament. Table 3.4 lists the length of the screws used to mark each ligament insertion site both on the femur and tibia or fibula.

With the markers in place, the left femur was remounted on a wooden dowel and placed in the acrylic container. Similarly, the tibia/fibula/patella cluster was mounted on the other wooden dowel and placed in the container as well. The bones were arranged in a near normal extended knee configuration within the container while maintaining approximately 1 cm of separation between the tibia and femur so they would not appear on the same slice in the resulting set of scans. The container was returned to the Regions Hospital Nuclear Medicine Department and placed back in the GE HiSpeed CT/i scanner. The specimen was scanned from approximately 3 cm "above" the femoral reference markers to approximately 3 cm "below" the tibial reference markers. The specimens were then removed from the container, packaged, and returned to the University of Minnesota Biomechanics Department for storage.

Table 3.4 Ligament insertions with assigned titanium screw marker lengths.

| Ligament | Screw Length |
|---|---|
| Anterior Cruciate | 12 mm |
| Posterior Cruciate | 8 mm |
| Fibular Collateral | 6 mm |
| Tibial Collateral | 10 mm |

### 3.1.2 Data Retrieval

The primary tool used for the visualization and extraction of data from the various image files was a C program originally developed by Morgan (Morgan and Murphy, 1997) that was adapted to interpret the data of each image set as necessary. The program employs OpenGL and Motif routines to read and visualize an ASCII formatted version of the image file that is simply a bitmap of the image with any file headers removed. All data files were originally stored on tape or disk in binary format. A C program was written to read the binary data into a buffer and write the information out to separate files in ASCII format. This was all the manipulation that was necessary to convert the MIT and VHP data into the ASCII bitmaps described above. The HealthSouth and UMN data proved to be slightly more difficult to extract.

The HealthSouth MRI data was acquired on DAT tape media from an unknown UNIX operating system on a Sun Solaris workstation. The tape was dumped from an external DAT drive to a DEC ALPHAStation 500 running Digital UNIX 4.0f (Compaq Computer Corporation, Houston, TX) in the Biomechanics Research Lab in the Department of Mechanical Engineering at Louisiana State University (Baton Rouge, LA). With the aid of the Remote Sensing and Image Processing Lab in the College of Engineering at Louisiana State University (Baton Rouge, LA) a C program was written to interpret the dumped data and extract the header files and image bitmaps as separate entities for each image slice record. The resulting bitmaps were left in binary form to allow visualization on PCs running Windows NT operating systems through the use of image processing software obtained as freeware from the web. These imaging visualization products included Scion Image (Scion Corporation, 2000) and ImageJ

(Rasband, 2000), which allow visualization and provide some file conversion utilities for general medical image files.

The data obtained through the University of Minnesota and Regions Hospital was originally saved in the standard DICOM format (N.E.M.A., 2000) using proprietary General Electric Medical Systems software, Advantage Windows™, the operating system for the Regions Hospital CT machines. The MO cartridge containing the data was loaded into a Pinnacle Micro Vertex magneto optical drive (Pinnacle Micro, Rancho Santa Margarita, CA) and mounted on a Silicon Graphics O2 workstation (SGI, Mountain View, CA). Data were copied to the workstation and the more accessible CD media for future access under the same directory structure found on the original MO cartridge.

The software package eFilm Workstation 1.5.3 (eFilm Medical, Inc., Department of Medical Imaging at the University Health Network and Mount Sinai Hospital, Toronto, Canada) was used to view, manipulate and convert the CT images from the standard DICOM format into generic grayscale bitmap files. The eFilm software far exceeded the capabilities and performance of any previously tested CT or MR image manipulation package. Some of the capabilities Workstation allowed were full accessibility to toggle overlays, measure distances and Hounsfield units, contrast variation based on Hounsfield units, and batch generation of standard image formatted files. Using these features, the CT images were displayed for the highest possible contrast between the bone and the surrounding media, including air, soft tissue, and biological fluids. Image overlays were included with initial studies to assure proper orientation when displayed with the modified Morgan code. Later, these overlays were

omitted to eliminate any possible interference during contour determination. The eFilm software was employed again to adjust the image contrast to best isolate the titanium screws from their surrounding media. All resulting images were saved to 512 x 512 Windows bitmap images, transferred to an SGI workstation, and converted to PGM (portable gray map) for display and contouring. "Bone" isolation images were obtained for the disarticulated left knee scans while "Screw" isolation images were obtained for both intact and disarticulated left knee scans.

### 3.1.3 Contour Determination

The UMN data set was the only complete data set, including ligament insertion sites, ligament length, bone geometry, and at least one known orientation. Other data were employed to develop and validate operation of the code as well as investigate the application of such a construction to clinical practice. The MIT data set did not include a reference position for the intact joint while the VHP and HealthSouth data were deficient in resolution and lacked markers for ligament insertions. For these reasons, the remainder of this section, unless otherwise indicated, will be concerned with the extraction, manipulation, and analysis of the UMN data sets.

One of the main motivations behind the adaptation of Morgan's C program was its ability to determine the boundaries of objects by thresholding on those pixels that are found at the junction of the imaged object and the surrounding medium. The program allowed for the display of the image file on screen along with the display of zoomed areas of the image on a predetermined scale. Detection of the boundaries of an object within the displayed image was facilitated by locating pixel grayscale values above a user-defined threshold and stepping to the adjacent pixels (also above the threshold

value) until the starting pixel was reached and the contour was closed. As the contour of the boundary was determined, the second window, used to display the zoom image, displayed the detected boundary for comparison to the original image. The program allowed the adjustment of the thresholding values as well as initial starting points to refine the image until the proper contour (as determined by the user) was found. After a suitable representation of the boundary was located, the coordinates were written to a file in Cartesian ($x$,$y$,$z$) coordinates. The next file in the sequence of slices was opened and the process was repeated until all contours were found and recorded.

Obtaining the brightest possible value for bone in order to isolate it from surrounding tissues was not compatible with obtaining the maximum contrast between bone and the titanium screws. As a result, there were several instances in the "bone" images, where it was clearly evident that the screws had shown up both in the scan image as well as the determined contour. The contours were corrected by replacing the points corresponding to the screw contributions with the appropriate pixel coordinates representing the bone geometry. An example of a section of a contour file before and after the removal of a screw head is shown in Figure 3.1. In general, the inclusion or

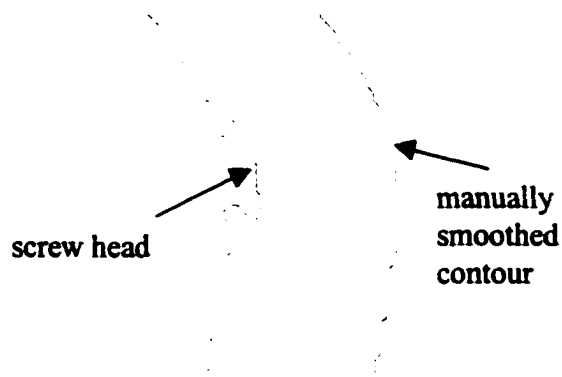


Figure 3.1 Example titanium screw removal from bone contour.

exclusion of these artifacts would have no effect on the interactions of the bones of the knee joint as most were at the periphery of ligament insertions, locations which do not typically contact the opposing bone surfaces. The smoothing was necessary in order to reduce the complexities of fitting surfaces between successive, discrete contours.

Two other manual operations were performed on some of the contour data files in order to prepare them for facet generation. First was the elimination of duplicate data points, typically found with the inspection of the beginning and ending points for each contour data file. This bug in the contouring algorithm was not noticed until after contours were obtained and was easier to remedy by manual methods rather than coding methods. Finally, the addition of capping points was necessary in order to provide the necessary elements to fit facets to the final contour. These points were located approximately one tenth of the span between slices beyond the final contour to maintain the natural contour of the bone. This distance was chosen to prevent the introduction of geometry that would contradict the resolution of the data, yet maintain the general integrity of the bone shape.

### 3.1.4 Surface Representation

A C program was written to fit flat triangular facets between the contour slices in order to estimate a surface for the bone geometry. The nominal pixel spacing in the $x$-$y$ plane was approximately 0.3125 mm for both dimensions. The nominal spacing between slices, the $z$-axis of a Cartesian frame, was approximately 1.0 mm. Mathematical definition of the surface geometries allows geometric transformations of the joint model through multiple relative orientations without resampling or rescanning. After the surface geometry was placed in the desired orientation, a regular grid in the

tibial or moving $x$-$y$ plane was projected to intersection with the surface to generate corresponding $z$-components. The result was uniformly spaced grids of $z$ values representing the tibia/fibula and femur surfaces that could be directly compared to determine the fixed orientation displacement workspace. The projection with respect to the tibial coordinate system was chosen because in normal human knee motion, the femur tends to roll and slide relative to the tibial plateau as is exemplified by the geometry of the surfaces. Simply put, the contact surface of the tibia remains relatively constant when compared to the behavior of the contact areas of the femur. In order to maintain the fixed coordinate system coinciding with the femoral origin, it is necessary to transform to the tibial coordinate system, apply the orientation transformation for the joint position and projections, and transfer back to the femoral (or world) coordinate system. In addition to the projected $z$ values themselves, the normals to the facets for each data point on the tibial surface grid were computed for later use.

Close inspection of the triangular facet surfaces resulting from this process showed a marked crystalline or blocky appearance of the bone geometry. While more complex and smoother surfaces could be used to visualize and streamline data manipulation, the faceted appearances gave good indication of the quality of the data collected. The facets also gave an indication of the resolution of the data as well as suggesting where the model could most benefit from revision or increased accuracy. When the uniformly spaced $x$-$y$ grids are projected onto the surface of the bone representations, this blocky appearance all but disappears. The programs written for the projection operations allow for the variation of the grid increment values, however the time to execute the code is inversely proportional to the square of the increment value.

For example, cutting the increment value in half, quadruples the number of points that define the surface grids. Two concerns that were addressed when choosing the grid spacing for the tibia and femur were the resolution of the input data, and the resulting computational time.

### 3.1.5 Ligament Realization

Contours were generated for each titanium screw in images that were adjusted to maximize the contrast between the screws and all other surrounding media. Sets of contours representing the reference coordinate systems embedded in the tibia and femur were generated twice. One set came from the initial scan of the specimen with the members of the joint capsule left intact, while the second set was obtained from the second scan of the specimen, performed after the disarticulation of the knee and marking of ligament insertions. These contours were collected for their respective scan series and plotted using the Rhinoceros software package (Robert McNeel & Associates, Seattle, WA). A model of a cylinder with a diameter of 1.3 mm was generated and oriented to each titanium screw in the set of contours. The length of the cylinder was chosen to correspond to the length of the titanium screws represented by the each set of contours and each cylinder was positioned to cover the largest portion of the area enveloped by the contours. The three-dimensional coordinates relating the marked ligament insertion sites to locations along the CT series showed possible correlations between the bone density, manifested in the scan pixel intensity or Hounsfield units, and ligament insertions. Figure 3.2 shows a single CT image with modified window and leveling parameters to show the possible correlation between the density of the bone and the ligament insertion site.

The geometric transformations of the reference screw array from the disarticulated joint scans to the intact joint scans were computed for both the tibia and femur. With these transformations, the locations of the screws marking the ligament insertion sites were transferred from the disarticulated reference system to the intact reference system, allowing for the computation of the ligament lengths as well as visual inspection of the intact bone orientations. This procedure guarantees at least one feasible position and orientation of the tibia relative to the femur that does not violate the ligament constraints.

### 3.1.6 Displacement Workspace Generation

The fixed orientation displacement workspace of the human knee represents the volume that is swept out by a point on the tibia as the modeled bone is maneuvered through all possible translations relative to the femur. For simplicity, this point on the tibia is chosen to coincide with the moving coordinate system origin attached to the rigid body representing the tibia. As this is a fixed orientation workspace, the selection of a different point on the rigid body modeling the tibia would result only in translating the workspace along a vector from the origin of the moving coordinate system to the new workspace sweeping point. The shape of the fixed orientation displacement workspace is invariant with respect to the target point on the moving reference frame that is selected for tracking through the range of relative displacements.

#### 3.1.6.1 Surface Constraints

With the tibia and femur represented by grids with common spacing between points, generation of the surface constrained displacement workspace for a given

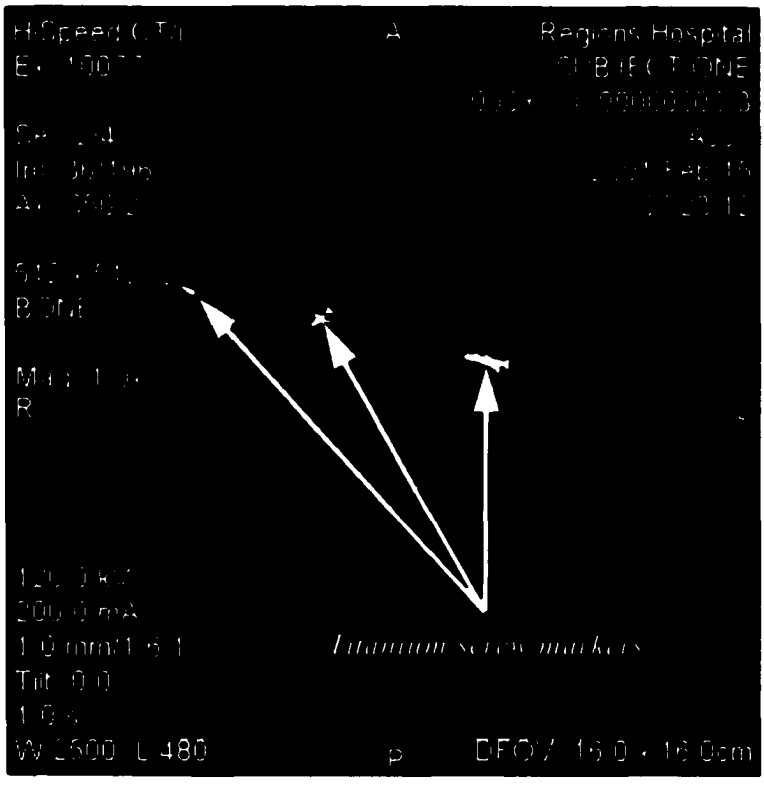

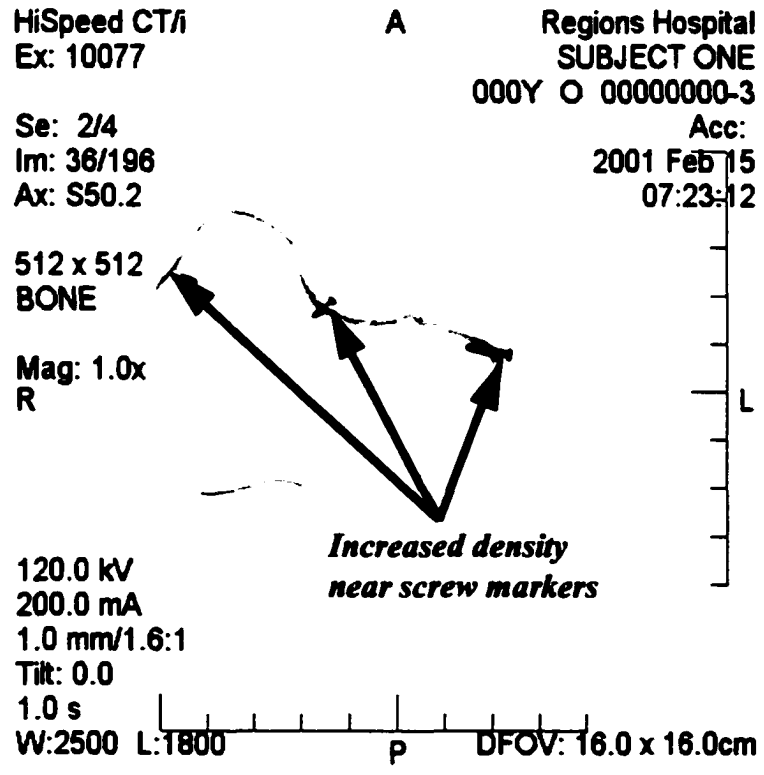


Figure 3.2 Example CT showing possible correlation between density and ligament insertion.

orientation is an easy task. The origin of the tibial (or moving) coordinate axis is initially positioned such that the maximum $x$ and $y$ values of the tibial grid coincide with the minimum $x$ and $y$ values of the femoral grid. The minimum distance between tibial grid points and femoral grid points having the same world $x$ and $y$ coordinates at that moment is determined and a displacement of the tibial origin by the negative of that value (along the $z$-axis) yields a point on the workspace. The tibial grid is translated in single increment values across the entire femoral grid, marking points on the workspace as it travels. Figure 3.3 shows an example traversal of a tibial grid across a femoral grid. The viewing direction is along the negative $z$-axis.

As each point of the surface constrained displacement workspace is found, a computation to determine whether it is interior or exterior to the workspace constrained by each of the ligaments is performed. In order for a point on the surface constrained displacement workspace to be valid, it must lie wholly within or on the surface of all the workspaces defined by individual ligament constraints. More succinctly stated, every point on the surface constrained displacement workspace must be within or on the combined intersection of all ligament workspaces.

#### 3.1.6.2 Ligament Constraints

The displacement workspace for a single ligament constraint has the geometric shape of a sphere in Cartesian three-dimensional space. This can be visualized by thinking first of the ligament as a string with one end attached to the world coordinate system origin. The other end is attached to the moving coordinate system origin. The set of all possible displacements of the moving coordinate system without breaking the

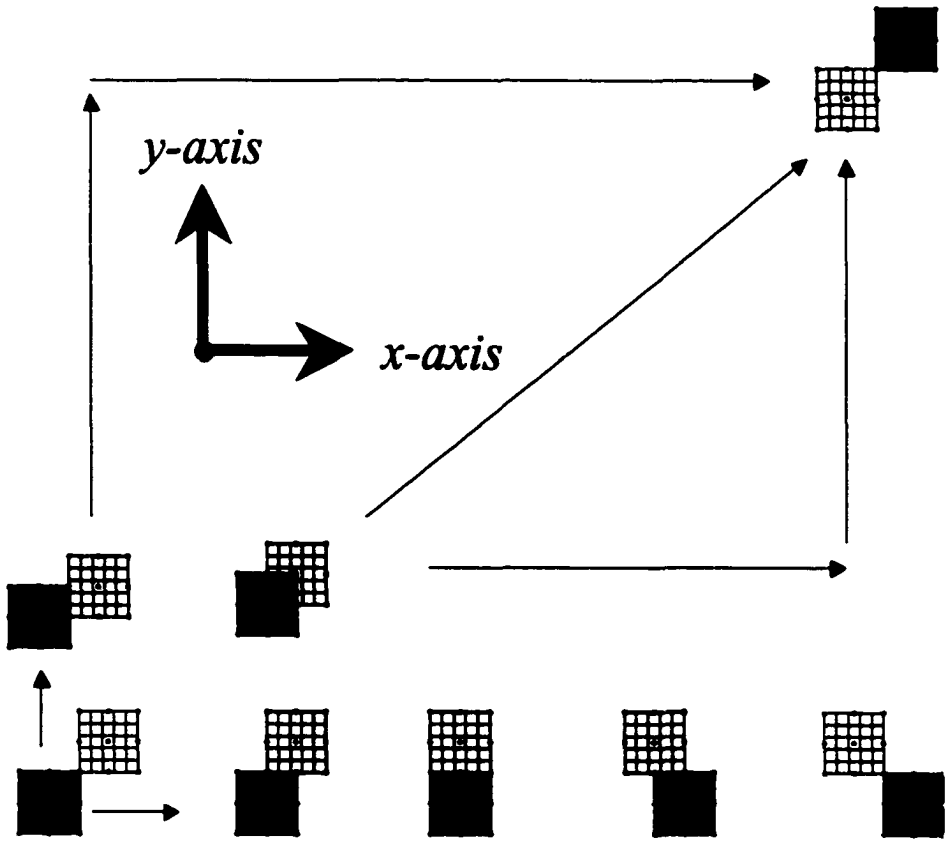


Figure 3.3 Example traversal of tibial grid (black) over femoral grid (white).

string produces a sphere with a radius equal to the length of the string. Now assume the attachment of the string to the fixed coordinate frame is not at the origin of the fixed coordinate system, but at some other point on the (rigid) fixed reference frame. The center of the sphere simply translates from the origin of the fixed coordinate system to the other point on the reference frame. This point on the reference frame is analogous to the representation of the femoral insertion site of the ligament in this model of the human knee joint. Under the constraint that the orientation of the moving coordinate system relative to the fixed coordinate system is constant, consider the attachment of the moving end of the ligament to the moving reference frame at a point other than the origin. This would affect the workspace again by a simple translation of the sphere along a vector directed from the attachment point to the moving (tibial) coordinate

system origin. This attachment point is analogous to the representation of the tibial insertion site of the ligament. Figure 3.4 shows a simplified two-dimensional version of the construction of a ligament workspace. The origin of the tibial coordinate system is chosen as the point to represent the workspace because it is the most intuitive reference for the tibial insertions sites. It should be noted that for the fixed orientation workspace, any point on the (rigid) moving coordinate frame produces identical geometry for the workspace description to any other point. The difference is simply the translation of the volume that is the workspace.

Combining multiple ligament constraints between two rigid bodies to produce a constant orientation workspace is simply a matter of taking the Boolean intersection of the spheres that define the single ligament fixed orientation workspaces. This is readily apparent when one considers a string anchored at both ends with some slack in the string itself. Consider a string with a length of five meters with each end anchored to the ground three meters apart. The anchor points are again analogous to the femoral insertion sites and let the midpoint of the string represent the common tibial insertion

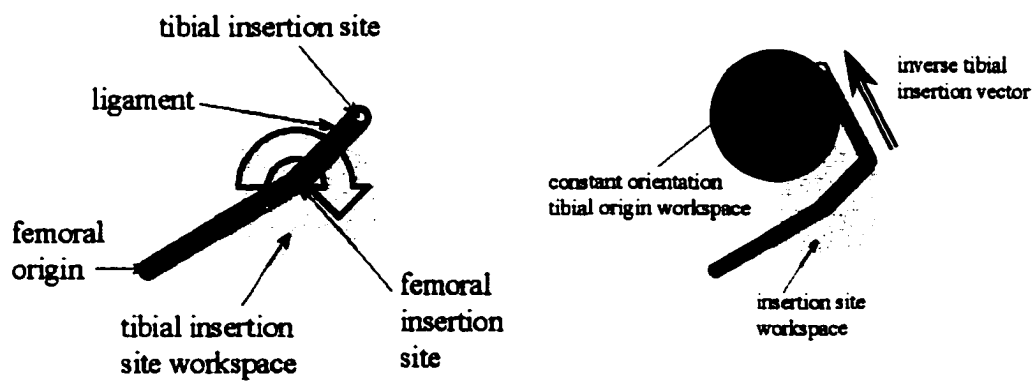


Figure 3.4 Two-dimensional, fixed orientation, single ligament workspace construction example.

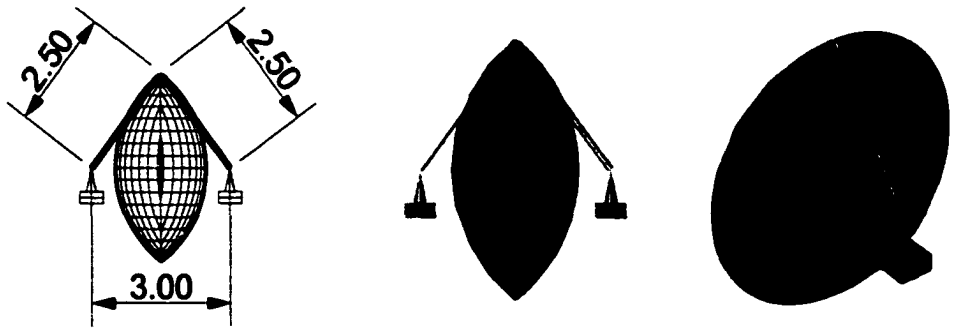


Figure 3.5 Resulting workspace from two ligament constraints.

site. Grasping the midpoint and moving it through all possible positions, traces out the intersection of two spheres of 2.5 m radii whose centers are three meters apart. Figure 3.5 shows this construction graphically.

Similarly, for higher numbers of ligament constraints, the fixed orientation displacement workspace reduces to the total intersection of the spheres generated from each individual ligament constraint. Finally, the intersection of the workspace defined by the contact between bone surfaces with the workspace defined by ligament constraints is the total fixed orientation displacement workspace of the human knee.

## 3.2 Knee Model

### 3.2.1 Primary Responsibilities

The basic structure of the model investigated in this research was proposed by Murphy in his Ph.D. dissertation (Murphy, 1990). Several others have taken Murphy's initial model and fine-tuned it for the development and discussion of various displacement workspace concepts for the human knee (Zhang, 1995; Omeltchenko, 1997; Schreiber, 1997). In one form or another, this model has been employed to investigate the kinematics of the human knee based on the relative motion of the tibia to the femur, subject only to the constraints of the four major ligaments. The included

ligaments, consisting of the two cruciate ligaments (ACL, PCL) and the two collateral ligaments (TCL, FCL), have been modeled both as inextensible links as well as marginally extensible links. The notion of the displacement workspace is a relatively straightforward idea. Simply stated, a displacement workspace is a set of positions that a moving coordinate system may occupy with respect to a fixed coordinate system. Thus to model a generic mechanism, it is necessary to include at least one specification to anchor the fixed coordinate system, one identifier as the moving coordinate system, and the inclusion of the constraints relating the fixed and moving coordinate systems to one another. This is the basis for the model presented here to investigate the kinematics of the passively constrained human knee joint.

### 3.2.2 Fixed Coordinate System

The fixed coordinate system for the displacement workspace knee model is chosen to coincide with some point within or on the femur. The femur is assumed to be a rigid body, which can be defined kinematically as an object with the property that the relative distances between all points attached to the body remain constant (Seely and Ensign, 1933). An exact specification for the origin of the fixed reference frame attached to the femur is not formally given as one choice will produce no distinct effect on the resulting workspace, save a linear translation, when compared to another choice. However, for purposes of visualization, the approximate location of the fixed coordinate system chosen for this evaluation is now briefly described. In order to facilitate simple registration with the data obtained from the University of Minnesota CT scans, the $z$-axis was chosen to be normal to the plane of the image slices oriented distal to proximal. The $x$-axis was chosen in the plane of the scan, oriented medial to lateral

while the *y*-axis completed the right hand coordinate system, oriented anterior to posterior. The origin of the fixed coordinate system was chosen to lie at the visually perceived base of the intercondylar notch approximately 1.2 cm below the bone surface.

### 3.2.3 Moving Coordinate System

The moving coordinate system of the displacement workspace knee model was chosen to coincide with some point within or on the tibia. As with the femur, the tibia was modeled as a rigid body and the (fixed orientation displacement) workspace was defined by the volume swept out by the point rigidly connected to the tibia as it was taken through all translations relative to the fixed coordinate system that were possible without violating model constraints. Different choices for the point on the tibia assigned to locate the workspace have no effect on the resulting workspace volume beyond a simple linear translation between the different points. For simplicity, the moving coordinate system, or tibial coordinate system, was chosen to agree with the fixed coordinate system, or femoral coordinate system, during the primary scan with the joint capsule intact. That is with the *z*-axis normal to the plane of the scans oriented from distal to proximal. The *x*-axis was oriented medial to lateral while the *y*-axis completed the right hand coordinate system oriented anterior to posterior. The origin of the tibial coordinate system was chosen, visually, approximately 2.4 cm below the bone surface at the midpoint between the tubercles of intercondylar eminence.

### 3.2.4 Constraints of the System

#### 3.2.4.1 Ligament Length

The ligaments in the model of the human knee were considered virtually inextensible as studies have indicated that isometric fibers were present in ligaments

throughout the range of motion of the human knee. Ortiz, et al. in a study of the location of isometric regions of the femoral attachment of the posterior cruciate ligament reported variations with the loading condition of the knee joint, yet for each loading condition, isometries were identified (Ortiz, et al., 1998). Fuss presented data that supported the presence of "guiding bundles" within each of the cruciate ligaments of the human knee that were under constant tension throughout the range of motion of the knee. Citing the recruitment of additional bundles through normal motion, Fuss concluded that collagenous fibers have "practically invariable length" (Fuss, 1989). In their study of human anterior cruciate ligament strain using photoelasticity methods, Yamamoto, et al., reported the presence of a "zero strain area" in the anterior cruciate ligament during knee motion (Yamamoto, et al., 1998).

The boundary of the ligament constrained displacement workspace was characterized as the threshold for exceeding the ligament length maximums. That is, the displacement of the moving coordinate system relative to the femoral coordinate system was limited such that the distance between ligament insertion sites did not exceed the values for the ligament length estimates. Traversal of the moving coordinate system beyond these limitations was assumed to represent the onset of ligament damage. The wrench associated with the active ligament was taken to lie along the screw axis between tibial and femoral insertion sites, directed away from the rigid body representing the tibia. Based on model constraints, this constraint was interpreted as a pure force wrench, characterized by inducing a pulling effect on the tibia.

The modeling of the ligament constraints as inextensible links was in line with studies that have shown relatively small strains associated with ligament failure. Nigg

and Herzog reported that 8% strains were sufficient to cause rupture in rabbit ligaments, however, the authors pointed out that ascertaining a zero strain reference condition depended largely on the boundary conditions, testing environment, and loading history (Nigg and Herzog, 1994). Flemming, et al., in a study of strains in the anteromedial band of the anterior cruciate ligament, measured strains of 3.0 ± 1.4 % under 150 N of anterior shear load at 30° of flexion *in vivo*. The study was designed to mimic the execution of a typical Lachman test, which is a clinical diagnostic test designed to characterize the anterior cruciate ligament's ability to limit anterior translation of the tibia relative to the femur. (Fleming, et al., 1993) In his review of methods used to model skeletal loads, van den Bogert reported that physiological ligament strains are typically less than 10%, underscoring the need for accurate data should an attempt be made to simulate ligament strain. He also noted that the use of the same rest length for all kinematic analysis was a necessity in order to minimize the scaling error encountered when studying such small percentages of discrete data (van den Bogert, 1994).

Each major ligament of the human knee was modeled as a single inextensible fiber that inserted into the femur and tibia through the center of the marked ligament insertion sites. The primary scan of the specimen was performed with the joint capsule fully intact and positioned such that the four major ligaments would be near full extension. From the disarticulated scans, the ligament insertion geometry was measured and transferred to the scans of the intact capsule using the titanium screw reference system included in both scan operations. Many authors have investigated the ligaments of the human knee as sets of multiple, independent bundles. Blankevoort, et

al., investigated the behavior of the cruciate ligaments as two distinct bundles per ligament and the collateral ligaments as three distinct bundles per ligament. Investigating the ligament activity as the joint was flexed, the authors noted fiber bundles were activated or deactivated throughout the range of motion of the joint studied (Blankevoort, et al., 1991). Furia, et al., looked for and located isometric relationships within various bundles of the anterior cruciate ligament (Furia, et al., 1997), and Race and Amis looked at the loading of the posterior cruciate ligament as a double bundle structure (Race and Amis, 1996). Sidles, et al., investigated nearly isometric relationships between insertion sites as criteria for selecting potential reattachment sites for anterior cruciate and posterior cruciate ligament reconstruction (Sidles, et al., 1988), and Martelli, et al, developed a model for the anterior cruciate ligament based on nine independent, curvilinear fibers (Martelli, et al., 1996). Expanding the ligament constraint criteria to incorporate multiple bundle representations is a simple task, given accurate data for the bundle insertions. With such information, the displacement workspace based on ligament constraints would be based on fiber or bundle length limitations rather than whole ligament length limitations.

#### 3.2.4.2 Surface Contact

The surfaces of the tibia and femur, obtained from the CT scans, were considered to be rigid bodies. Discrete, regularly spaced grids, in the $x$- and $y$-directions, were interpolated to the $z$-coordinate of the bone surfaces, as explained in Section 3.1.6.1, and the surface-constrained displacement workspace, based on contact between the tibia and femur, was constructed by stepping one grid over the other,

intermittently computing the minimum distance between the overlapping grid points. The wrench associated with surface contact is aligned with the surface normal to the tibia through the contact point. Again, model constraints dictate that the surface contact wrench be a pure force wrench, however surface contact wrenches have the effect of pushing on the rigid body representing the tibia.

Structures not represented in this model of the human knee joint included the articular cartilage, the menisci, synovial fluid, and capsular components. Lord presented a method for estimating articular cartilage thickness based on bone geometry and kinematics, showing articular cartilage on the femoral head varied from 1 to 2.5 mm (Lord, 1994). Buckwalter presented similar estimates for the articular cartilage thickness on the human femoral condyle of just over 2 mm (Buckwalter, 1999). Shrive and Frank discussed the various properties of articular cartilage including tensile properties, compressive properties, viscoelasticity, etc. They surmised that the surface of articular cartilage did not play a significant role resisting compression however high proteoglycan content cartilage (deeper articular cartilage) might (Shrive and Frank, 1994). Due to the size and only partial, possible contribution to compressive tolerances, representations for articular cartilage were left out of the preliminary knee joint model.

Brown investigated the role of the meniscus of the human knee with emphasis placed on load-bearing capabilities. His research showed deformations near 1 mm for both medial and lateral menisci thickness under loading. In his conclusion, Brown underscored the need for further research into the mechanical properties of the menisci citing limitations with macroscopic sampling methods (Brown, 1990). Frank and Shrive estimated that the menisci keep the articular cartilage of the human knee from

contact up to loads of approximately half a body weight (Frank and Shrive, 1994). Kelly, et al., surmised that the meniscus was a significant load-bearing member of the human knee joint that was best suited for shock absorption and load distribution (Kelly et al., 1990).

Bylski-Austrow, et al. studied the movement of the menisci under load and concluded the structures move to accommodate the changing positions of the articulating surfaces. This finding seemed to indicate that the menisci function to distribute load across the joint rather than dissipate it (Bylski-Austrow, et al., 1994). To what extent the cartilage and menisci contribute to load bearing, load transmission, and contact surface enhancement continues to be debated among researchers. What is evident from the literature is that these structures should be included in kinematic models of the passive constraint system of the human knee joint as omitting them leads to significantly different geometries and loading conditions (Bylski-Austrow, et al., 1993).

Unfortunately the menisci and articular cartilage did not appear in CT scans and without information regarding their geometry and their material properties, their contributions were neglected for this initial development of workspace analysis of the human knee joint. Titanium was chosen as the marker material based on its reported performance in multiple imaging modalities. The MRI instrumentation was not available during data collection and was to be the source of the soft tissue, surface contact constraint geometries. However, the test specimens were refrozen for the possibility of future use. Incorporation of cartilage and miniscal geometry into the knee

model remains a possibility should the opportunity to obtain MRI scans of the joint be made available.

# CHAPTER 4. RESULTS AND ANALYSIS

## 4.1 Displacement Workspaces

For the purposes of studying the kinematics of the human knee model, there are two main categories of position, or displacement, workspaces that are of interest. These are the fixed-orientation displacement workspaces (FODW) and variable-orientation displacement workspaces (VODW). The FODW consist of all possible translations of the tibia while maintaining a constant orientation relative to the femur. The VODW remove the constraint of constant relative orientation, allowing the tibia to assume any orientation that does not violate the model constraints. For the same constraint geometry, the FODW, by definition, will always be contained within the VODW. If a VODW for a given set of geometric constraints is allowed to include all possible orientations of the tibia relative to the femur, then the union of all FODW corresponding to the same set of constraints defines the contents of the VODW.

### 4.1.1 Variable-Orientation Displacement Workspaces

The basic idea behind determining a VODW for the human knee is to locate the extreme relative positions and orientations that the joint components may attain without violating model constraints. As this construction envelopes a tremendous amount of kinematic data, communicating that information clearly and efficiently poses a major challenge in the establishment of its role in biomechanical applications. Position and orientation data for every natural (not damaging to joint structures) task of the human knee joint model is contained in the definition of the general VODW. Load configurations for every position and orientation of the tibia relative to the femur as predicted by the joint model may be addressed by the construction of the VODW. Even

the progression through constraint activations during failure or other simulations is not beyond the realm of information that may be gained through VODW analysis. Simply plotting out the position and orientation of the tibia relative to the femur in the model does not begin to represent all information obtained in a VODW analysis. For example, consider the case of a point on the boundary of a VODW that is reachable in multiple, distinct orientations. Which, if either of these orientations should be taken as the true boundary of the displacement workspace and displayed as such? Is any one orientation more significant than another? If not, how are multiple possibilities represented for that one point on the workspace succinctly? If so, have inaccuracies in data collection had an effect on the conditions that led to the choice of one orientation over the others?

Omeltchenko's development of the VODW for the human knee based on ligament constraints presents the workspace as a color coded set of discrete points representing the extreme position and orientation of a tibial coordinate system relative to a femoral coordinate system (Omeltchenko, 1997). Application of these algorithms to the MIT/MGH data set collected by Murphy (Murphy, 1990) and Lanzendorf (Lanzendorf, 1988) showed some instability in the computations and raised some concerns about previous assumptions regarding the MIT/MGH data.

The computation of the VODW was noted to produce markedly different results for the same input data, while varying workspace computation parameters such as the number and the spacing of contours. Some of the contours appeared smooth and regular, however some contours exhibited sudden, often erratic behavior that was not consistent with previous displacement workspace computations. It is believed that the model of the knee joint for the given input data, reached kinematically redundant

configurations where the small perturbations used to progress the moving coordinate system around a contour, were not sufficient to cause the minimum energy criteria to shift the position and orientation from the previous point to a new location on the contour. The problem appears to be algorithmic or computational in nature, rather than conceptual, as the previous implementations have produced reasonable results and other authors, such as Chen, et al, have used similar methods to map out displacement information for the human knee joint (Chen, et al., 2000).

Concerns were also raised regarding the MIT/MGH input data that consisted of ligament insertion sites obtained from one specimen of a matched pair of cadaver knees and of ligament "rest" lengths obtained from the contralateral specimen. The assumption concerning the data was that bilateral symmetry of the human body would allow the combination of the ligament length data with the insertion site data to form a clinically accurate model of the human knee. Workspace analysis was unable to confirm this assumption by locating a position and orientation for the model that did not violate the either ligament or surface contact constraints. In fact, valid positions and orientations were not obtained until the ligament lengths were effectively doubled, demanding data be collected from a single joint to eliminate the need for the base assumption. Figure 4.1 shows an example of this shortcoming. The tibia and femur were oriented near full extension, as interpreted visually through reconstructed bone surfaces, and the FODW was computed for the ligaments and surfaces. The permissible volume for the surface constrained displacement workspace is the space on the positive $z$-direction side of the surface workspace. The permissible volume for the ligament workspace is the space interior to the intersected spheres. For the model of the human

knee to assemble, there must be some intersection between these two volumes, however, as Figure 4.1 shows, there is considerable separation (approximately 25 mm) between the two workspaces. This means that this particular orientation is not valid for the data set defining the knee model. Numerous attempts were made to find valid orientations by altering the relative angles between the tibia and femur with no appreciable decrease in the distance separating the surface and ligament constrained FODWs.

An especially beneficial feature of Omeltchenko's implementation was the inclusion of a graphical user interface that allowed representations for the positions and orientations of the tibia and femur to be displayed with a corresponding location on the VODW.

The system allowed the user to see a visual interpretation of the joint geometry simultaneously beside the workspace geometry, complete with graphical representations

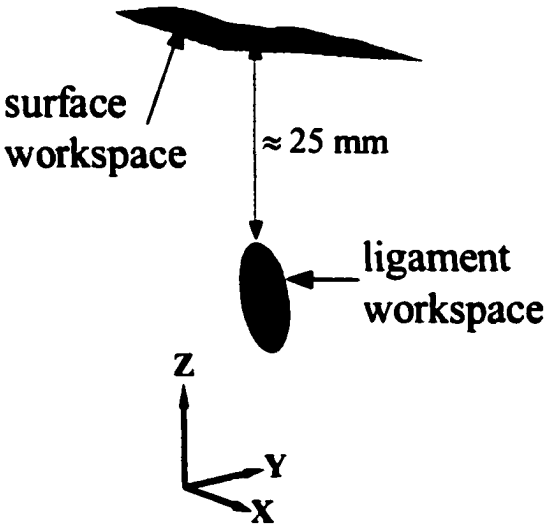


Figure 4.1 Example showing invalid knee model data from MIT/MGH specimens.

of ligament activation as well as numerical coordinate system location and orientation information. It was noted through this interface, for the majority of the cases of the VODW, that points defining the volume representing the tibia seemed to penetrate the volume representing the femur. This was a clear violation of contact constraints between the tibia and femur, which were not included in the workspace generation, indicating that much of the information represented in the workspace computation was not realizable in a physical sense. That is, the axes of the constraining forces contributed by the ligaments would never be realizable in the majority of positions and orientations represented by the VODW. This meant that information necessary to predict valid constraint wrenches that would operate on the tibia could not be obtained from this particular construction of displacement workspaces of the knee joint model.

In order to use extended screw theory to develop the concept of velocity workspaces of the human knee, some type of technique for obtaining authentic constraints on the joint model was necessary. Lessons of Omeltchenko's VODW construction indicated that surface interactions between the tibia and femur must be considered in the constraint development and kinematic ambiguity should be avoided if possible. As this was a first attempt to construct and characterize the velocity workspaces of the human knee, constraint generation was designed to be the most direct and simple process possible. For these reasons, the fixed orientation displacement workspace was chosen to serve as the limiting geometry for the constraint generating process. Its selection allowed the elimination of the possibility of orientation ambiguity, many simplifications for the inclusion of bone surface constraints, and efficient validation of the space using geometric primitives.

### 4.1.2 Fixed-Orientation Displacement Workspaces

By specifying a constant orientation, the determination of a displacement workspace simplified dramatically. One of the most desirable results of fixing the orientation was the (obvious) elimination of multiple orientation configurations occurring at the same point on the workspace boundary. Imprecision in data collection did not have the potential to undermine the validity of the workspace itself. That is, the construction of a fixed orientation workspace was accomplished by simple geometric intersections of individual, easily determined constraint boundaries. Transition along the surface of the FODW was also nicely defined with intersections between individual constraint boundaries marking multiply constrained positions. Finally, the problem of defining when and where "contact" occured was reduced to a minimum distance computation.

FODWs exhibited another characteristic, stemming from their relative simplicity, which enhanced their usefulness. The interior of the FODW under the knee model parameters was free of any constraint. Only on the surface of the FODW was there at least one constraining force acting on the tibia from ligaments or surface contact with the femur. Interior to the FODW, the tibia had total freedom. This feature allowed the FODW to communicate a definite status concerning the constraint level for specific orientations of the joint. Using the VODW, the interior did not necessarily correspond to a totally unconstrained configuration. That is, a single point within, as well as on the surface of, the VODW may have corresponded to many distinct joint orientations whereas the points of the FODW, both interior and surface, represented definite, unique geometries of the tibia relative to the femur.

Kinematic data involving the human knee is useless if recorded without some type of relative orientation information regarding the tibia and femur. Data must also be discrete. If some method for obtaining geometry of the joint constraints is used, there is enough information to construct and track the FODW throughout movement represented by the kinematic data.

Two of the most popular forms of medical imaging (MRI and CT) were looked at as possibilities of minimally invasive methods of obtaining joint structure information in a clinical setting to numerically define the model of the human knee. The HealthSouth data set was generously provided as representatives of typical MRI scans taken in the clinical setting using a knee coil, while the VHP MR images were transverse slices spaced 4 mm apart. Figures 4.2 and 4.3 include two representative MR images from the HealthSouth data set. Figure 4.2 shows a sagittal view of a patient's knee revealing geometry data on the articular cartilage of the bone surfaces. Figure 4.3 is a coronal view of the same patient's knee where the anterior cruciate ligament is visible, revealing striations that correspond to bundles of ligament fibers.

Figure 4.3 does not represent the striations well until the image is inverted. Figure 4.4 is the negative of the image in Figure 4.3 revealing clearly discernable striations. The spacing of the coronal slices, however, could have significant effects on the extracted geometry. The figures show promise toward clinical, *in vivo* usage for the extraction of geometric data necessary to specify parameters of the human knee model, including articular cartilage, and the underlying bone, ligament insertion sites, and ligament lengths. Additional information concerning the strain condition of the

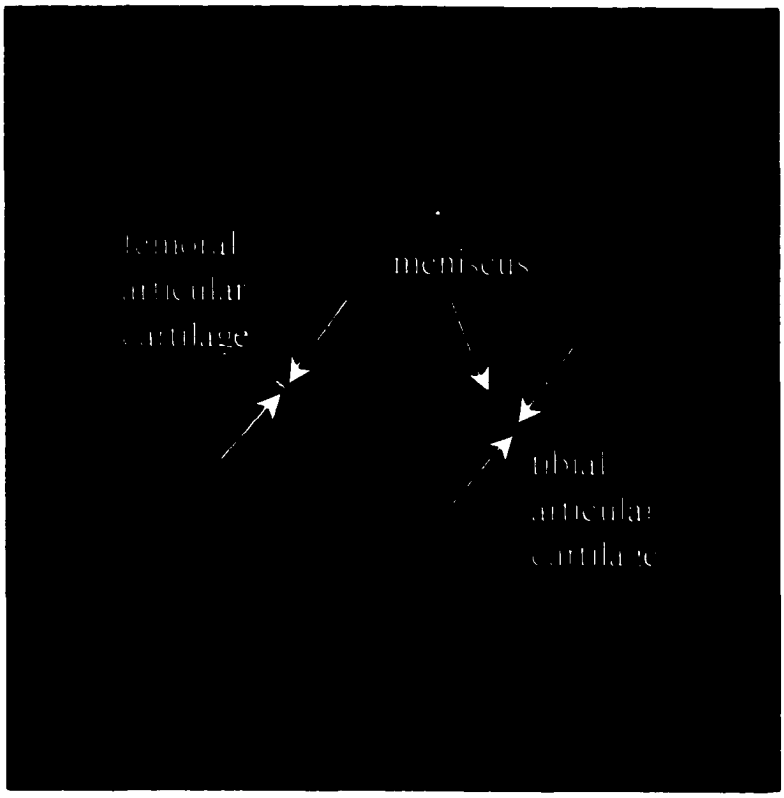


Figure 4.2 Sagittal MR view of the human knee joint (1.6 mm slice thickness).

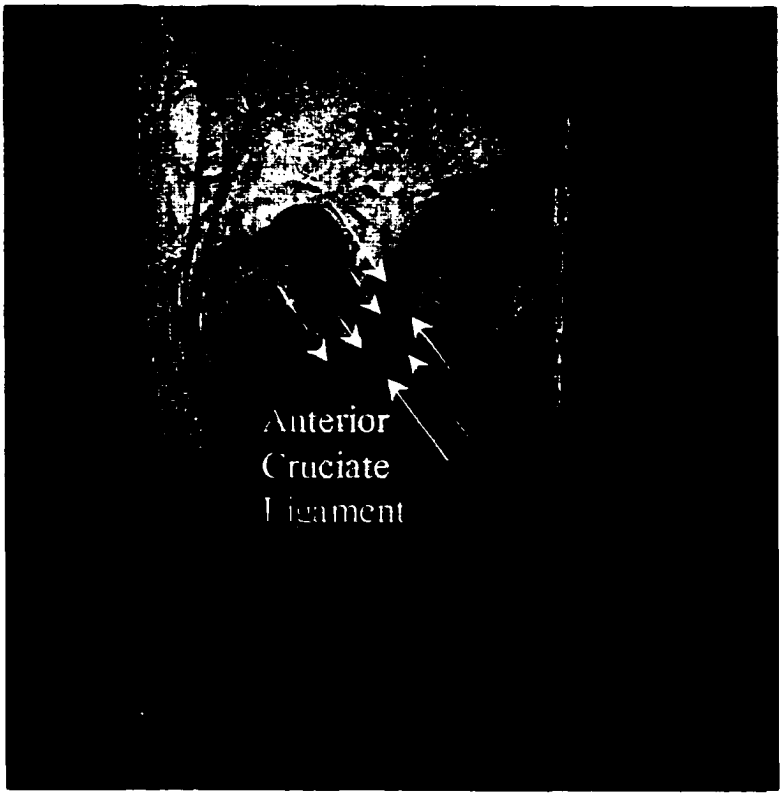


Figure 4.3 Coronal MR view of the human knee joint (4 mm slice thickness).

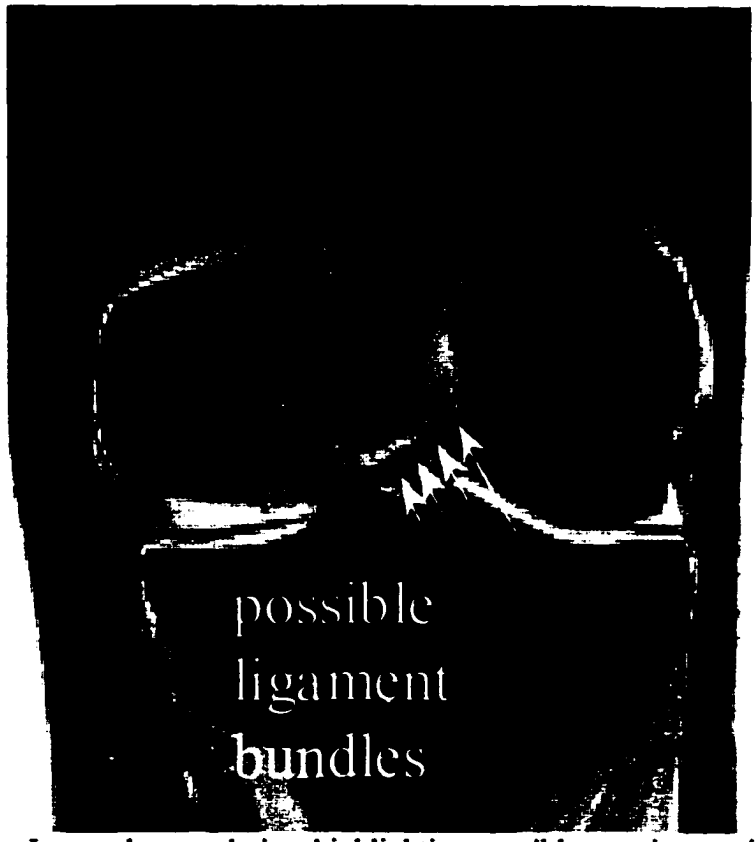


Figure 4.4 Inverted coronal view highlighting possible anterior cruciate ligament bundles.

ligament fibers in the scanned configuration may also be attainable using this imaging technique. Promise, however, requires validation, before the resulting data may be used with confidence, which is beyond the scope of this investigation.

CT images were obtained in the MIT/MGH, VHP, and UMN/Regions Hospital data sets. When the FODW was constructed using the MIT/MGH data, no orientation was found where at least one constraint was not violated. That is, no FODW was constructed using the raw MIT/MGH data. Ligament lengths were lengthened until workspaces were found, however, other than verifying construction and visualization methods, these findings hold no worth as real workspaces. The VHP CT scans served much the same purpose, providing example CT files to develop and verify the surface

geometry construction techniques. The CT images were whole body slices with spacing between slices of 1 mm. No ligament insertions were marked on the scans and the resolution in the scan plane, due to whole body cross sections being captured in each 512 x 512 image, was greater than 1 mm per pixel. The MRI scans were taken in the transverse plane with 4 mm nominal spacing between slices, so the accurate detection of ligaments, most of which ran nearly parallel to the imaging plane, was only possible in two or three images per ligament. As a result, the VHP data set proved to be insufficient for the extraction of knee parameters of the precision necessary for model construction.

In order to resolve the issues encountered during the investigation of data sets collected for other studies, the UMN/Regions Hospital data collection was designed specifically for workspace development. The marking of insertion sites, and scanning before disarticulation were steps taken to ensure that the data would yield at least one valid orientation for the FODW. The data were collected from one of a matched pair of cadaver knees, leaving the possibility of investigating some of the questions that arose from previous data sets.

A typical CT image of the tibia is shown in Figure 4.5(a). After processing that image, a contour was determined and is shown overlaid in Figure 4.5(b), filled in green to provide contrast. The raw contours obtained from the disarticulated scans of the femur and tibia/fibula complex are included in Figure 4.6(a) and 4.6(b). After manually smoothing the protrusions from the contours corresponding to the titanium marker screws, the contours were put through the faceting algorithms to construct representations for bone surfaces.

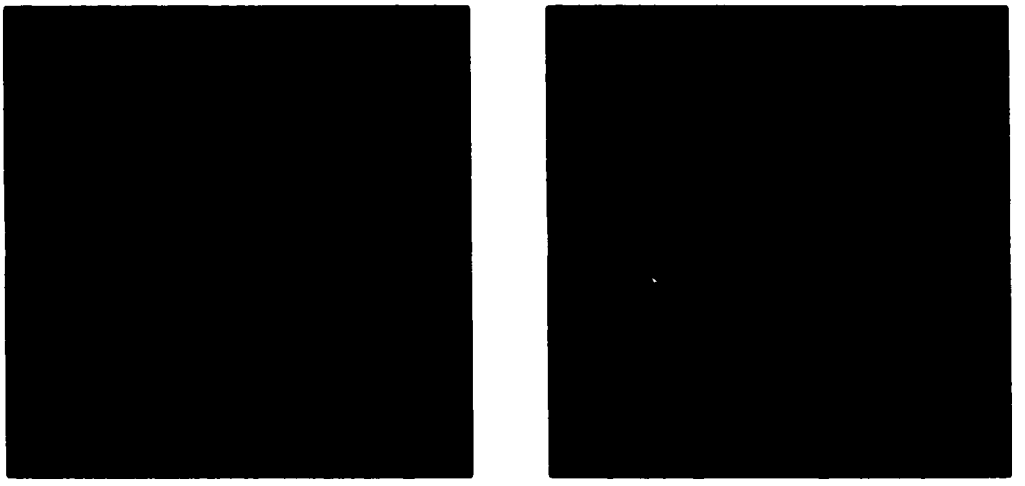

(a) (b)

Figure 4.5 (a) Representative CT slice of disarticulated femur, (b) Contour overlaid on representative CT slice of disarticulated femur.

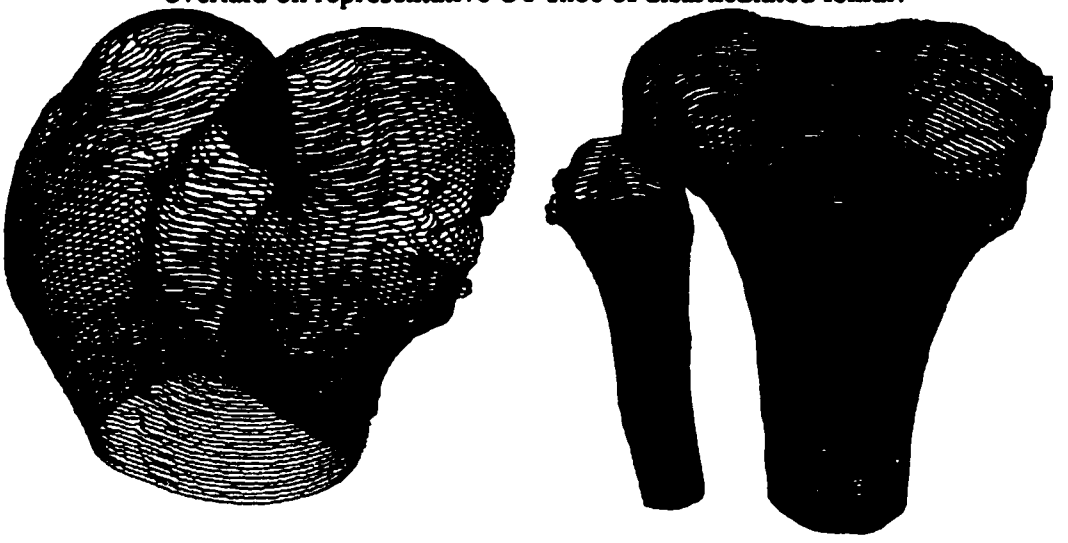

(a) (b)

Figure 4.6 (a) Raw femoral contours from disarticulated UMN/Regions Hospital CT scans. (b) Raw tibial contours from disarticulated UMN/Regions Hospital CT scans.

A uniform grid was projected along the z-axis (normal to the contour planes) until intersection with the resulting surfaces, creating a discrete set of points representing the bone surfaces. Figures 4.7 and 4.8 show these point representations for

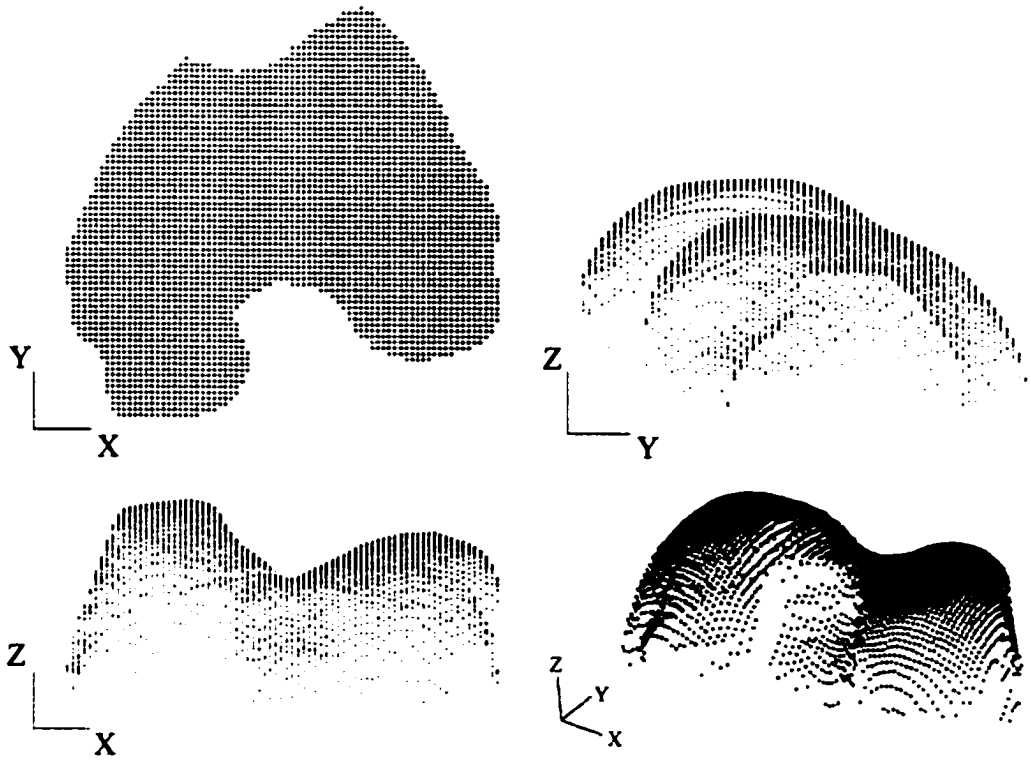


Figure 4.7 Regularly spaced point representation of Femoral Surface.

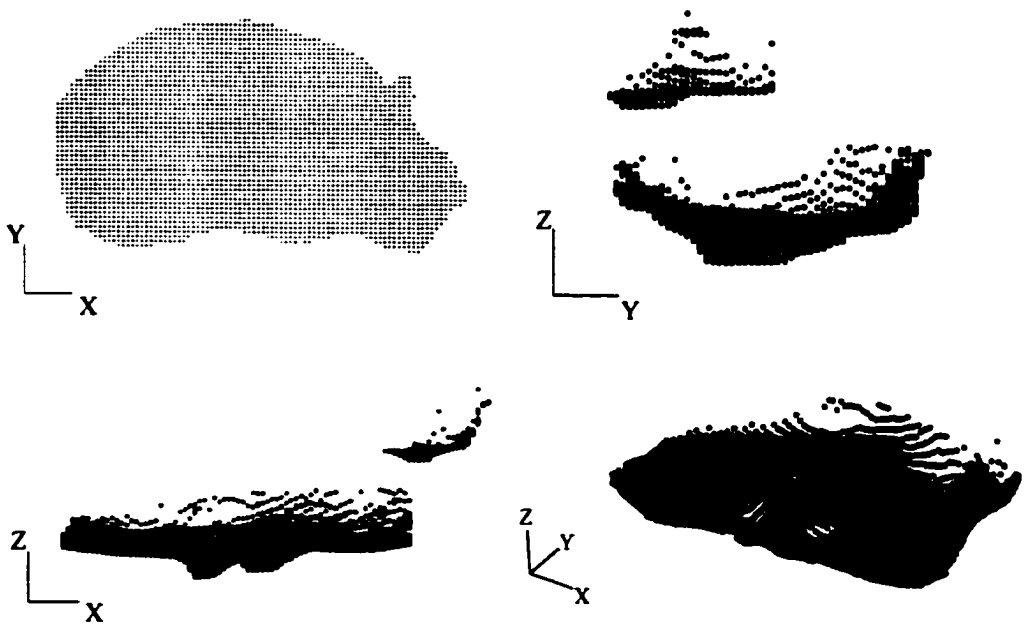


Figure 4.8 Regularly spaced point representation of Tibial and Fibular Surface.

the intact scan orientations of the femur and tibia, respectively. The coordinate system axes indicate the orientation of the world coordinate system origin with each coordinate axis scaled to 1 cm in length.

Adjusting the windowing and leveling settings of the eFilm display software, the titanium screws were isolated in their corresponding scan slices. Figure 4.9(a) shows the default setting for one of the CT slice images, while Figure 4.9(b) is the same slice adjusted to isolate the screw markers. Using the same algorithm that located the bone contours, the outlines of the titanium marker screws in each slice were extracted. Using the ligament marker screw coordinates relative to the reference screws present in both sets of scans, the ligament insertion sites were transferred from the disarticulated scans to the intact joint scan. For each of the four major ligaments, ligament lengths were modeled as the distance between the femoral and tibial ligament insertion sites in the

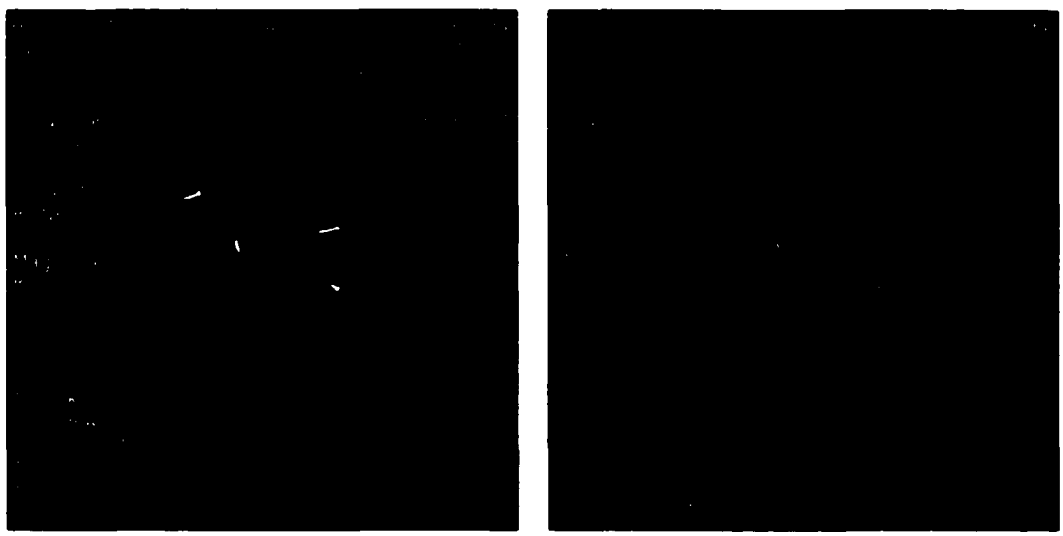

(a) (b)

Figure 4.9 (a) Default eFilm display of Femoral CT image (settings W:6095 L:23) (b) Adjusted eFilm display of Femoral CT image isolating titanium screws (settings W:2500 L:2000)

intact scan. With corresponding surface geometries and ligament lengths and insertion coordinates, the data was analyzed to obtain a FODW of the human knee model.

Figure 4.10 shows several views of the FODW generated for the relative orientation of the intact set of scans. The surfaces of the FODW represent the extreme displacements of the moving coordinate system origin with respect to the femoral coordinate system origin. The representations of the ligament-constrained surfaces are true surfaces, defined mathematically by spheres with radii equal to the ligament lengths. The surface contact area, however, consists of discrete point data that a surface has been interpolated through in order to facilitate visualization.

The axes plotted with each view of the FODW correspond to the principle directions of the femoral, or fixed, coordinate system axes. As the shape and size of the FODW is invariant with respect to the location of the fixed coordinate system, the

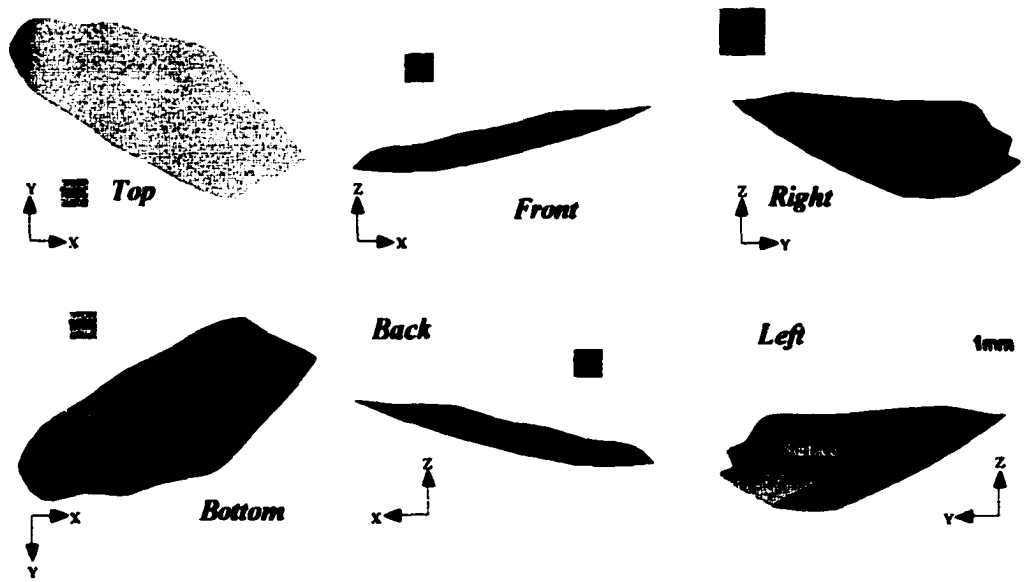


Figure 4.10 FODW of the human knee (UMN/Regions Hospital data set). Intact joint scan orientation (near full extension).

geometric location of the femoral coordinate system origin was not included. Accompanying each view of the FODW is a (1 mm x 1 mm x 1 mm) cube to provide a reference for the general scale of the volume.

Many expected details are included in the FODW. The ACL appears to limit anterior translation while the PCL apparently does the same for posterior translation. The TCL claims the role of the limiting constraint for medial translation while the FODW implies that surface contact limits lateral translation in this particular orientation.

**4.2 Velocity Workspaces**

The constraining wrenches imposed on the tibia by the femoral surfaces and ligament attachments consist of pure force wrenches in our model. The ligaments are modeled as single filament inextensible elements, connected to the rigid bodies representing the tibia and femur through spherical joints. Spherical joints allow three degrees of rotational freedom, meaning that the individual filaments are incapable of transmitting a torsional load to the tibia or femur. The use of multiple filaments to model individual ligaments may be incorporated into future constructions to simulate constraint activity distributed across a ligament insertion site, essentially allowing torsional loads to be imposed by ligament constraints. The lack of any significant friction between the articulating surfaces of the tibia and femur as well as the inability of the individual filament insertions to transmit torque, prohibits the constraining wrenches from containing couple components. As a result, the constraining wrenches generated within the model are pure force constraints, which are zero pitch wrenches in their screw representations. As such, the mathematical description of the constraining

wrenches, when placed in the form of screw coordinates, degenerates into the line or Plücker coordinates of the wrench axes.

Unlike most engineering materials, the physical properties of human tissues including modulus of elasticity, yield strength, and Poisson's ratio have not been well established in literature. The lack of significant numbers of test specimens, the inability to reliably test properties *in vivo*, and the variations (including age, weather, gender, physique, etc.) between actual test cases produces estimates with wide variations in studies of these various properties (Duck, 1990; Fung, 1993; Viidik, 1990; Woo, et al., 1990). As a result, the estimation of the intensities of the constraining wrenches in the model would be inappropriate and produce widely varying results, detracting from kinematic implications of the velocity workspace concept. This omission of finite magnitudes treats the contribution of all ligament and surface wrenches equally, looking only at their geometric contributions. However, due to the lack of couples in the set of constraining wrenches, this has no mathematical effect on the resulting space defined by the reciprocal and repelling conditions. That is, a wrench of a significantly large force is simply the wrench of unit force multiplied by some scalar, and as will be seen in Equation 4.2.1, positive scalar multiplication does not change the solution space of the inequalities defining the velocity workspace. The violation of a constraining wrench does not depend on the magnitude of the wrench or virtual coefficient, only the presence of negative virtual work.

With these considerations in mind, the velocity workspace of the human knee may now be defined. The set of all instantaneous twists reciprocal and/or repelling to the complete set of wrenches constraining the rigid body representing the tibia

constitutes a velocity workspace of the human knee for the given position and orientation of the joint. The boundary of the velocity workspace consists of all instantaneous twists reciprocal to the set of constraining wrenches at a point in the displacement workspaces. The interior of the velocity workspace consists of all instantaneous twists repelling to the set of constraining wrenches, while the exterior of the velocity workspace is entirely composed of those instantaneous twists contrary to at least one of the wrenches in the constraining set. Physically, the velocity workspace represents the set of all possible instantaneous twists the tibia may follow without violating (causing an increase in) the active ligament or surface constraints as defined by the model of the human knee. Essentially the tibia is at some point within the displacement workspace and the velocity workspace represents all possible motions the tibia might undertake without leaving the volume of the displacement workspace. Mathematically, the velocity workspace must satisfy the following set of linear inequalities:

$$\begin{bmatrix} \beta_{11}\alpha_4 + \beta_{12}\alpha_5 + \beta_{13}\alpha_6 + \beta_{14}\alpha_1 + \beta_{15}\alpha_2 + \beta_{16}\alpha_3 \\ \beta_{21}\alpha_4 + \beta_{22}\alpha_5 + \beta_{23}\alpha_6 + \beta_{24}\alpha_1 + \beta_{25}\alpha_2 + \beta_{26}\alpha_3 \\ \vdots \\ \beta_{m1}\alpha_4 + \beta_{m2}\alpha_5 + \beta_{m3}\alpha_6 + \beta_{m4}\alpha_1 + \beta_{m5}\alpha_2 + \beta_{m6}\alpha_3 \end{bmatrix} \geq \begin{bmatrix} 0 \\ 0 \\ \vdots \\ 0 \end{bmatrix} \qquad 4.2.1$$

Where $\alpha_i, (i = 1,2,\ldots,6)$ are the twist coordinates of residents of the velocity workspace

$\beta_{ji}, (j = 1,2,\ldots,m;\ i = 1,2,\ldots,6)$ are the wrench coordinates of the $m$ members of the constraint set

These inequalities are the result of imposing both the reciprocal and repelling limitations on the potential members of the velocity workspace. There is no member of

the velocity workspace contrary to **any** member of the set of original constraining wrenches. That is, these equations define the set of instantaneous twists that are either reciprocal or repelling to the constraining wrenches imposed on the tibia. Interchanging the first three components of the twists with the last three components allows the velocity workspace to be defined as follows:

$$VWS = \{\tilde{\alpha} \mid [\beta]_{m\times 6}[\tilde{\alpha}]_{6\times 1} \geq [0]_{m\times 1}\} \qquad 4.2.2a$$

where

$$[\tilde{\alpha}] = \begin{bmatrix} 0 & 0 & 0 & 1 & 0 & 0 \\ 0 & 0 & 0 & 0 & 1 & 0 \\ 0 & 0 & 0 & 0 & 0 & 1 \\ 1 & 0 & 0 & 0 & 0 & 0 \\ 0 & 1 & 0 & 0 & 0 & 0 \\ 0 & 0 & 1 & 0 & 0 & 0 \end{bmatrix} \begin{bmatrix} \alpha_1 \\ \alpha_2 \\ \alpha_3 \\ \alpha_4 \\ \alpha_5 \\ \alpha_6 \end{bmatrix} \qquad 4.2.2b$$

It is important to note that any member of the velocity workspace cannot be a member of the set of twists contrary to the original, unsimplified set of constraining wrenches. The reciprocal space of the constraining wrenches, when written in the form of $\tilde{\alpha}$, is by definition, the null space $(N(\beta))$ of the matrix $\beta$. This space is closed under the operations of scalar multiplication and vector addition, meaning the linear combination of any elements in $N(\beta)$ is also an element of $N(\beta)$. Thus, elementary row operations employed to arrive at a basis set for $N(\beta)$ have no effect on the reciprocity condition with the original set of constraints. All elements of $N(\beta)$ represent infinitesimal twists that are rearranged as shown in Equation 4.2.2b for $\tilde{\alpha}$ and reciprocal to $\beta$ by definition. The repelling space of the constraining wrenches $(P(\beta))$ is a halfspace that is closed under the operation of positive scalar multiplication only. The simple operation of multiplying a member, $\tilde{\alpha}$, of $P(\beta)$ by any negative scalar produces some

vector that represents a twist contrary to a member of the set of constraining wrenches. As a result, general elementary row operations, such as those used in commercial mathematics package functions, could affect the repelling categorization of an instantaneous twist. This requires the repelling constraints to be satisfied with respect to the original, unmodified $\beta$ to assure some type of inversion has not occurred while obtaining reduced representations of $\beta$.

### 4.2.1 Algorithmic Construction

The solution to a set of $m$ simultaneous linear inequalities is covered by an area of mathematics known as convex analysis and is commonly encountered in the discussion of linear programming and optimization problems. In his dissertation, Ohwovoriole presented an algorithm for determining this solution set based on theorems and definitions explored by Goldman and Tucker as well as other authors. What follows here is the implementation of that discussion by Ohwovoriole, absent of proof, which may be found in Goldman and Tucker's paper (Ohwovoriole, 1980; Goldman and Tucker, 1956).

Given a set of $m$ simultaneous linear inequalities in $n$ unknowns, the solution space can be determined as follows. Arranging the inequalities so they may be written in matrix form as in Equation 4.2.2a results in the matrix Inequality 4.2.3.

$$\begin{bmatrix} \beta_{11} & \beta_{12} & \cdots & \beta_{1n} \\ \beta_{21} & \beta_{22} & \cdots & \beta_{2n} \\ \vdots & \vdots & \ddots & \vdots \\ \beta_{m1} & \beta_{m2} & \cdots & \beta_{mn} \end{bmatrix} \begin{bmatrix} \tilde{\alpha}_1 \\ \tilde{\alpha}_2 \\ \vdots \\ \tilde{\alpha}_n \end{bmatrix} \geq \begin{bmatrix} 0 \\ 0 \\ \vdots \\ 0 \end{bmatrix} \qquad 4.2.3$$

The system may be separated into a homogeneous expression and inhomogeneous expression by replacing the greater than or equal to condition ($\geq$) with

an equality condition (=) and a strictly greater than condition (>), respectively. The rank $r$ of the matrix defined by $[\beta]$ is the number of linearly independent equations included in the homogeneous expression. The solution space of the homogeneous expression $[X_H]_i$, $i = \{1,2,\cdots,d\}$ is, by definition, the Null space of the matrix $[\beta]$ and has dimension $d = n - r$. $[X_H]$ is said to be the $d$-face or $d$-dimensional face of the solution to Inequality 4.2.3.

To construct all possible ($d$+1)-faces or ($d$+1)-dimensional faces, $m - r + 1$ rows of $[\beta]$ are selected simultaneously. This can be done in $q$ distinct ways where

$$q = \frac{m!}{(m-r+1)!(r-1)!} \qquad 4.2.4$$

For each of these $q$ occurrences, form the submatrix $M$ from the selected $m - r + 1$ rows and the submatrix $N$ for the remaining $r - 1$ rows, and determine any nontrivial solution $[X_p]$ to inequality 4.2.5a and Equation 4.2.5b.

$$[M][X_p]_j > 0, \quad j = \{1,2,\cdots,q\} \qquad 4.2.5a$$

$$[N][X_p]_j = 0, \quad j = \{1,2,\cdots,q\} \qquad 4.2.5b$$

The solution space of the matrix inequality may then be represented by

$$[\tilde{X}] = \sum_{i=1}^{r} \lambda_i [X_H]_i + \sum_{j=1}^{q} \gamma_j [X_p]_j \qquad 4.2.6$$

where $\lambda$ can be any real scalar
$\gamma$ can be any real positive scalar

The construction of the (d+1)-faces is very similar to classic optimization problems in linear programming (Hildebrand and Johnson, 1970). The general minimization problem of Inequality 4.2.7 seeks the coefficients that will minimize the

value of the function $f(x)$, (assuming the vector components, $x_i \geq 0$) while satisfying the inequality relationship.

$$[A][\vec{x}] \leq [\vec{b}] \qquad 4.2.7a$$

$$\min(f(\vec{x})) \quad \text{subject to } [A][\vec{x}] \leq [\vec{b}] \qquad 4.2.7b$$

Equations 4.2.5a and 4.2.5b may be adapted to this problem by determining the null space basis of the matrix $N$ and using the sum of those elements as the function $f$ to minimize. Inequality 4.2.5a is satisfied by multiplying $M$ by –1, setting $b$ to some negative value, and solving the minimization problem in Inequalities 4.2.7a and 4.2.7b.

**4.2.2 Visualization**

Screw axes, twist axes, and wrench axes are six-dimensional objects, five of which are independent. Representation of these objects in three dimensions and promptly projecting that representation to two dimensions inherently results in some information being lost. For that reason, the structure of the visualization scheme for the twists and wrenches discussed in the following sections bears mentioning. The pure force wrenches of the constraint sets are presented as three-dimensional arrows, constructed by placing a cone at the end of a cylinder as shown in Figure 4.11(a). Pure rotation twists are constructed as three-dimensional arrows projected along a circular arc about the axis of rotation for approximately 90° as shown in Figure 4.11(b). Translations are depicted as flat, two-dimensional arrows in the direction of the translation as shown in Figure 4.11(c). Finally, general twists with nonzero, finite pitches are shown as a helical shaped surface, capped by a three-dimensional cone as shown in Figure 4.11(d).

Whenever possible, a rendered projection view is supplied with a Cartesian coordinate system gnomon and some form of a planar surface to aid in perspective interpretation. No visual cues are used to differentiate between repelling, contrary and reciprocal screws beyond the text description accompanying figures.

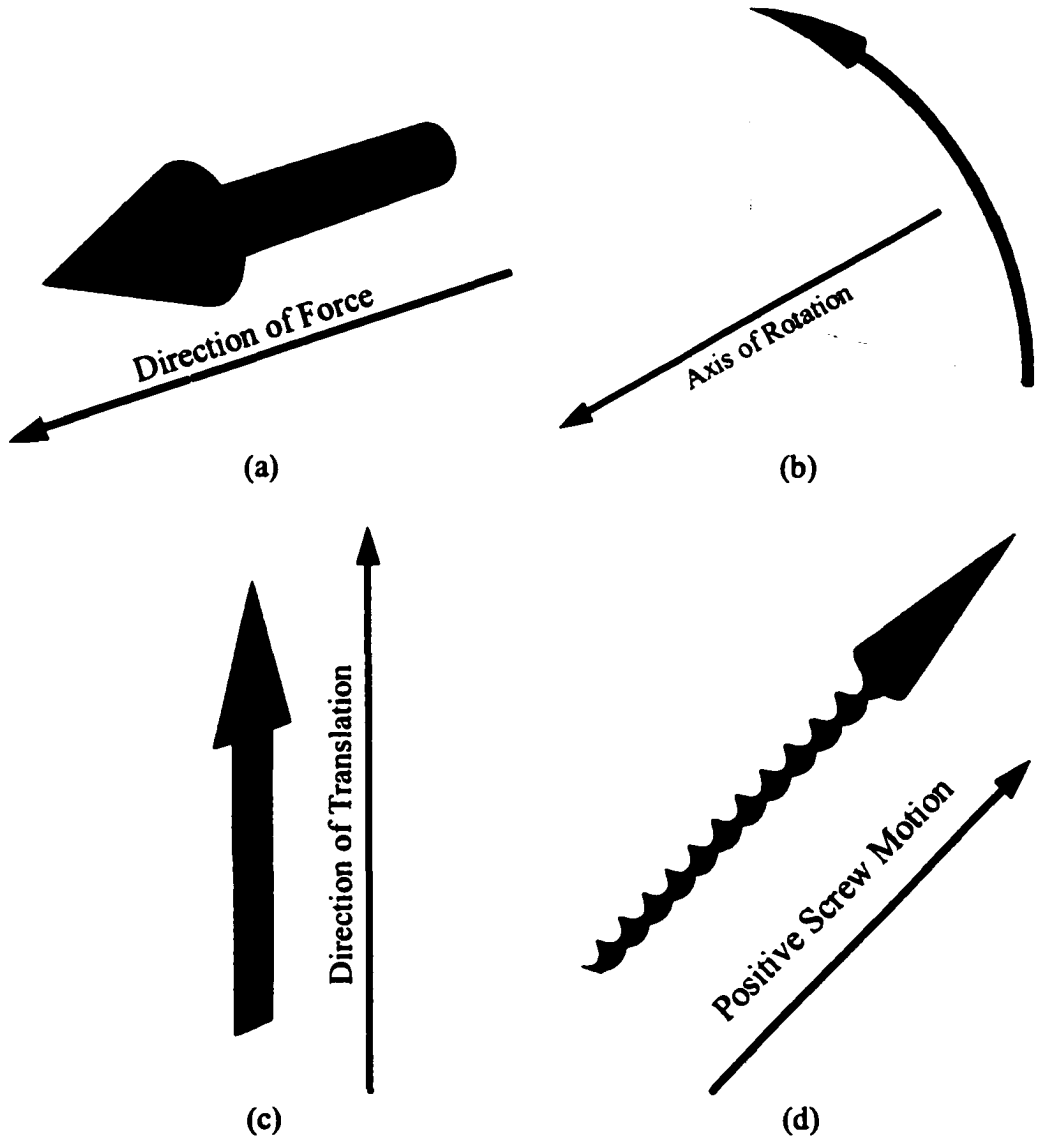


Figure 4.11 Visualization Key (a) Pure force wrench (b) Pure rotation twist (c) Pure translation twist (d) General twist-finite, nonzero rotation and translation.

### 4.2.3 Velocity Workspace Boundaries

#### 4.2.3.1 The One-System

In the case of the set of constraining wrenches reducing to one linearly independent screw, there is one distinct configuration for the corresponding velocity workspace boundary basis. This constraint set, containing one linearly independent pure force wrench, is said to form a one-system, dictating that the corresponding reciprocal space is a five-system. This five-system is the boundary of the velocity workspace corresponding to the one-system of constraints. The typical constraining one-system will have the effect of limiting or influencing motion along one screw axis. The one system is completely characterized by its one linearly independent screw. As the wrenches generated in our model of the human knee are all pure force wrenches, the limited motion is necessarily the instantaneous twist along and in the opposite direction of the screw axis of the wrench constraint. Figure 4.12(a) shows a visual representation of the components of the constraining set of the one-system with the screw coordinates of the wrench given with respect to the $X_lY_lZ_l$ coordinate reference frame. Figure 4.12(b) represents a basis for the reciprocal space (velocity workspace boundary) corresponding to the one-system of constraints depicted in Figure 4.12(a). In this representation planar arrows have been used to represent pure translations (infinite pitch twists), while pure rotations (zero pitch twists) take the form of arcing, double-headed arrows. Again the screw coordinates for the twists are relative to the moving coordinate reference frame $X_lY_lZ_l$. It is readily apparent that the computation of the virtual work done by the wrench in Figure 4.12(a) along each of the twists of 4.12(b) will be zero.

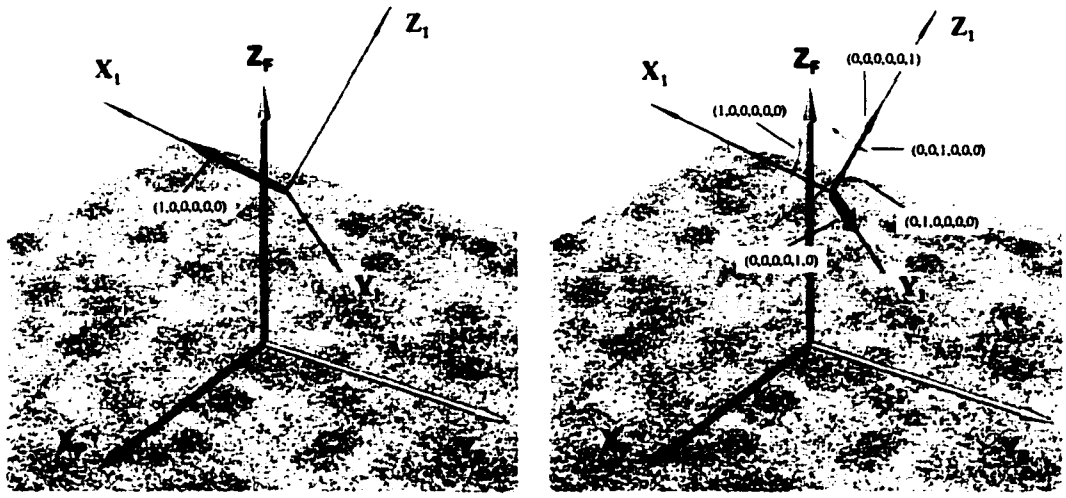


Figure 4.12 (a) Constraining wrench set composed of one linearly independent screw (b) Velocity workspace boundary basis twist representation for general one-system of constraining wrenches.

The sphere resting on the horizontal surface in Figure 2.1 is in a constraint condition identical to that of Figure 4.12(a), given the proper coordinate transformation. Taking that physical sense into account, it is apparent that the sphere is free to move instantaneously along any of the twists presented in Figure 4.12(b) without breaking or violating the constraint of the surface contact.

The general one-system of constraining wrenches, resulting in the general five-system of possible twists, occurs when the tibia is at a point on the displacement workspace corresponding to a single active constraint or, in a somewhat less likely scenario, when multiple constraints become coincident. This system is (geometrically) the most common encountered as it arises at all points of the ligament constrained displacement workspace boundary that lie on exactly one sphere. The same characterization cannot be applied to the surface contact constrained displacement workspace boundary as the orientation between and geometry of the surfaces may allow

multiple points of contact resulting in a linearly independent (or possibly dependent) constraining wrench for each point of contact.

#### 4.2.3.2 Two-Systems

When the set of constraining wrenches reduces to two linearly independent, pure force wrenches, the resulting constraint system takes the form of a two-system. Hunt gives a general description of a two-system as a set of twists (wrenches) composed of members belonging to one of two distinct one-systems (Hunt, 1978). The character of the resulting two-system is dependent on the relationship between of these underlying one-systems. To simplify the visualization of the constraining two-system, the $x$-axis of the moving coordinate system is taken to be coincident with one of the screw axes. The $z$-axis is then oriented to be coincident with the common perpendicular between the two screw axes and the origin located at the intersection of the $x$-axis screw and the common perpendicular. The $y$-axis is determined by the right hand rule. Figure 4.13(a) shows this coordinate system alignment for a general two-system.

Two special cases arise in the event that the screw axes of the independent wrenches in the two-system intersect, either finitely or at infinity. In the case where the two screw axes intersect at a finite point, the resulting plane containing both screws is mapped to the $x$-$y$ plane with the normal through the point of intersection corresponding to the $z$-axis. Parallel screw axes (intersecting at infinity) have infinitely many common perpendiculars, which in this case will be used to define the $x$-$z$ plane when considered with the screw axes of the wrenches. The origin in this case is located at any point on either of the screw axes. In both of these cases, the entire two-system of constraining

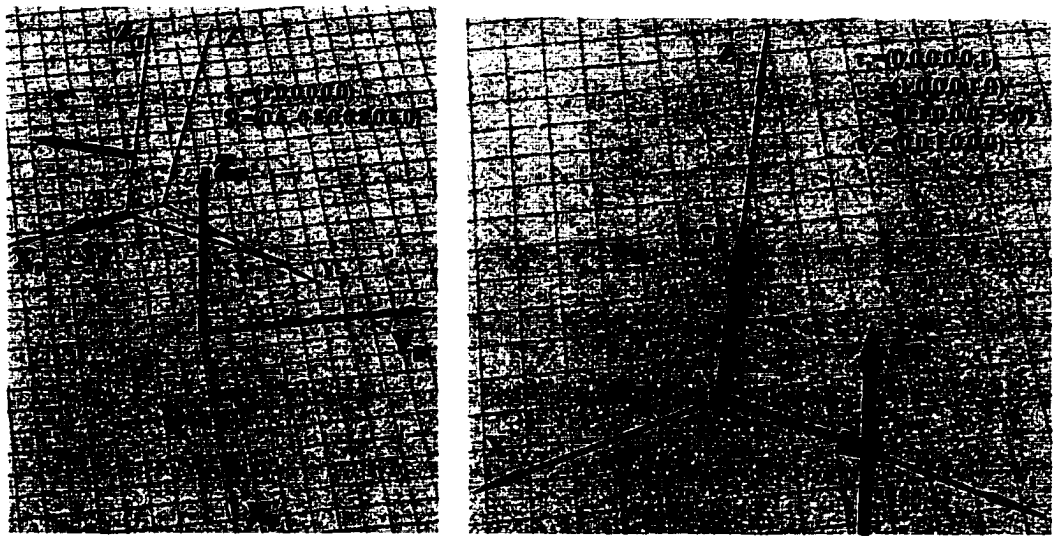

Figure 4.13 (a) Example constraining wrench set composed of two linearly independent screws. (b) Velocity workspace boundary basis twist representation for general example of a two-system of constraining wrenches.

wrenches reside in the plane of the independent screws allowing rotations about screw axes and translations along screw axes that are perpendicular to the defining members of the two-system. When two ligaments define one of these special cases for the constraining two-system, the moving coordinate system origin, attached to the tibia, is on the intersection of two of the spheres of the displacement workspace and all four of the ligament insertion sites (two tibial, two femoral) must be coplanar. When only surface constraints define one of these special two-systems, the surface normals of the tibia at the contact points must also be coplanar, and for the mixed ligament-surface contact constrained conditions, the ligament must be coplanar with the surface normal of the tibia at the contact point. The occurrence of these special two-systems in the joint model will become more prevalent if the effect of ligaments wrapping around bone and other ligaments or multi-bundle ligament representations are incorporated into the generation of the displacement workspace. That is, the occurrence of two ligaments interfering with one another, depending on the method used to model this situation, will

cause the constraining wrenches to intersect at the point of interference. Also, the presence of more possible constraints in the model definition heightens the possibility of intersection between members of the constraining set. These interference phenomena were not considered in this initial development of displacement and velocity workspaces, however the effects should be addressed in future evolutions of this research as the workspace concepts are expanded and refined.

The corresponding velocity workspace boundary is a four-system in the case of the constraining set generating a two-system. For the general case of two wrenches acting on screw axes that do not intersect, if the coordinate system is aligned as outlined above, the velocity workspace boundary will take on the following general characteristics as shown in Figure 4.13(b). The velocity workspace boundary will contain pure rotations and pure translations about the z-axis for two of its bases elements ($\tau_1$ and $\tau_4$). There will be one twist basis element ($\tau_2$) on a screw parallel to the x-axis, through the intersection of the z-axis with the off-axis wrench ($\$_2$) screw axis. The final twist basis ($\tau_3$) will lie on a screw parallel to the y-axis through the origin with a pitch corresponding to the cotangent of the angle between the two wrenches when projected to the *x-y* plane. When the cotangent is infinite, the twist basis, $\tau_3$ is a pure translation in the y-axis and when the cotangent is zero, $\tau_3$ is a pure rotation about the y-axis through the origin (also the intersection of the wrench screw axis $\$_2$ with the z-axis, similar to $\tau_2$).

#### 4.2.3.3 Three-Systems

When the set of constraining wrenches consists of three linearly independent pure force wrenches, the condition is classified as a three-system. Hunt presents the

general three-system as any three screws that do not belong to the same two-system (Hunt, 1978). That is, any of the three linearly independent screws, taken two at a time, form a distinct two-system. The properties of the underlying two-systems that are formed from the linearly independent members of a three-system determine the organization of the three-system. The most general three-system occurs when an arbitrary, linearly independent wrench is added to a general two-system, forming a total of three distinct, general two-systems between the independent members of the constraining set. Having the coordinate system fully specified by the "base" two-system, the representation of the third wrench is projected along its axes until it intersects one of the principle planes chosen by the proximity of the intersection point to the origin. This compacts the visualization and delivers some rudimentary information on the effect of the third wrench on the rigid body relative to the other system wrenches. Figure 4.14(a) shows an example three-system with the third screw axis projected to its intersection with a principle plane that is closest to the origin, namely the *y-z* plane.

The velocity workspace boundary corresponding to the constraint set described by a general three-system will itself be a three-system. Figure 4.14(b) shows the basis set for the boundary of the velocity workspace generated when the constraint set is that of the example in Figure 4.14(a). Note that while the dimension of the velocity workspace boundary has decreased with respect to the constraining two- and one-systems, the complexity of the basis elements seems to have increased. The workspace boundary is no longer spanned by disjoint translations and rotations. These motions must occur in concert at specified ratios (pitches) in order to be members of the

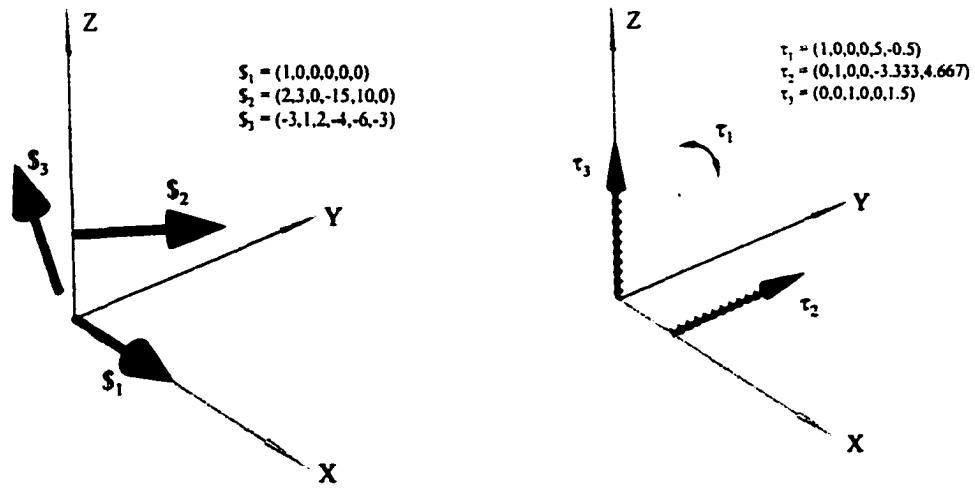


Figure 4.14 (a) Example constraint set composed of three linearly independent wrenches. (b) Velocity workspace boundary elements for example of three linearly independent constraint wrenches.

reciprocal system. Another perspective on this assertion is that the constraints are more thoroughly defined resulting in the reciprocal motions being more specifically defined as well. For a general three system to be produced by ligament constraints alone, the position of the tibia must correspond to a point on the displacement workspace where at least three spheres defining individual filament workspaces intersect. Surface constraints alone can give rise to a constraint set that is a general three-system, and combinations of surface constraints with one or more ligament constraints may also be responsible for this configuration.

There are special cases when the boundary of the velocity workspace behaves in an easily characterized manner. Consider the case where the constraining set is composed of three, noncoplanar, parallel wrenches. When the boundary of the velocity workspace is computed it is readily seen that the behavior of the underlying two-systems that are compatible with each other readily define the basis of the velocity workspace boundary for the overall three-system. For this situation, there will always

be one plane normal to the principle planes defined in the underlying two-systems. This is readily apparent by the specification that the constraints be parallel. The ramifications of this are that a pure rotation (zero pitch twist) about any axis normal to this plane and that any pure translation (infinite pitch twist) parallel to this plane will lie on the boundary of the velocity workspace. Figures 4.15(a), 4.15(b), 4.15(c), and 4.15(d) graphically depict the construction of an example of this special case three-system from the underlying two-systems. Table 4.1 shows the wrench and twist coordinates for numerical and computational comparison.

In the analysis of the velocity workspace construction from the underlying two-systems, the intersection of the basis elements of the three reciprocal spaces form the velocity workspace boundary of the overall three-system. Figures 4.15(a), 4.15(b), and 4.15(c) show the velocity workspace boundary four-systems generated by the underlying two-systems composed of $\$_1$ and $\$_2$, $\$_1$ and $\$_3$, and $\$_2$ and $\$_3$, respectively.

Figure 4.15(d) shows the velocity workspace boundary three-system resulting from the presence of all three constraining wrenches. The twists $\tau_1$, $\tau_2$, and $\tau_3$ are present in all velocity workspaces generated from each underlying two-system, but the twist $\tau_4$ is not. That is, as the two-systems are parallel wrenches, each velocity workspace boundary for these two-systems consists of translations in the plane normal to the two wrenches ($\tau_1$ and $\tau_3$), rotation about axes parallel to the two wrenches ($\tau_2$), and rotation about axes intersecting the two wrenches ($\tau_4$). Intersecting the three velocity workspace boundaries in the same coordinate system finds the $\tau_1$ and $\tau_3$ translations forming the same plane and the $\tau_2$ rotations coincident. As the constraining

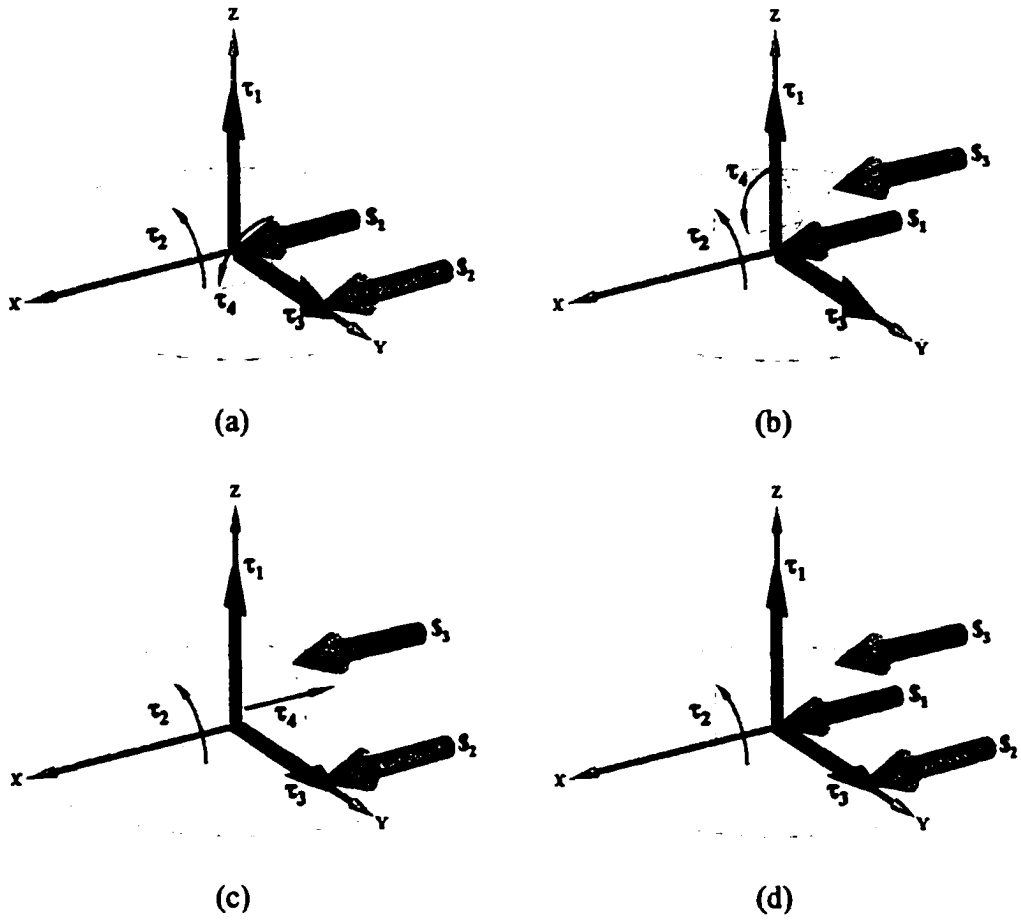


Figure 4.15 (a) Velocity workspace boundary from $\$_1$ and $\$_2$ constraints. (b) Velocity workspace boundary from $\$_1$ and $\$_3$ constraints. (c) Velocity workspace boundary from $\$_2$ and $\$_3$ constraints. (d) Velocity workspace formed by intersecting those formed by underlying two systems.

wrenches are noncoplanar and parallel, there is no line that intersects all three wrench axes resulting in the removal of the freedom expressed by the $\tau_4$ twists.

Extending these notions to the general three-system does not lead to succinct reductions to pure translations or rotations since the planes defined by underlying two-systems assume more complicated relative geometries. The pure translations and pure rotations combine into general twists in order to satisfy the reciprocity condition for all constraining wrenches, yielding basis twists about distinct screws.

Table 4.1 Wrench and twist coordinates for construction of example three-system.

| Figure number | Wrench coordinates | Twist coordinates |
|---|---|---|
| 4.15(a) | $\$_1 = (1,0,0,0,0,0)$<br>$\$_2 = (1,0,0,0,0,-15)$ | $\tau_1 = (0,1,0,0,0,0)$<br>$\tau_2 = (0,0,1,0,0,0)$<br>$\tau_3 = (0,0,0,1,0,0)$<br>$\tau_4 = (0,0,0,0,1,0)$ |
| 4.15(b) | $\$_1 = (1,0,0,0,0,0)$<br>$\$_3 = (1,0,0,0,10,-10)$ | $\tau_1 = (0,1,0,0,0,0)$<br>$\tau_2 = (0,0,1,0,0,0)$<br>$\tau_3 = (0,0,0,1,0,0)$<br>$\tau_4 = (0,0,0,0,1,1)$ |
| 4.15(c) | $\$_2 = (1,0,0,0,0,-15)$<br>$\$_3 = (1,0,0,0,10,-10)$ | $\tau_1 = (0,1,0,0,0,0)$<br>$\tau_2 = (0,0,1,0,0,0)$<br>$\tau_3 = (0,0,0,1,0,0)$<br>$\tau_4 = (15,0,0,0,-0.5,1)$ |
| 4.15(d) | $\$_1 = (1,0,0,0,0,0)$<br>$\$_2 = (1,0,0,0,0,-15)$<br>$\$_3 = (1,0,0,0,10,-10)$ | $\tau_1 = (0,1,0,0,0,0)$<br>$\tau_2 = (0,0,1,0,0,0)$<br>$\tau_3 = (0,0,0,1,0,0)$ |

#### 4.2.3.4 Four-Systems

If the set of constraining wrenches is spanned by four linearly independent wrenches, the constraining set is said to form a four-system. The boundary of the corresponding velocity workspace then forms a two-system, consisting of two linearly independent basis twists. As was the case with three-systems the coordinate axes are fully defined after the consideration of two of the wrenches in the system. The third and fourth wrenches are projected along their respective screw axes to an intersection with one of the principle planes in order to compact the visual representation. Continuing in the spirit of his previous descriptions, Hunt describes the general four-system as any four screws not all belonging to the same three-system (Hunt, 1978). Indeed the nuances of the four-system may be described by the coordination of the behavior of the (four) underlying three-systems, however it has previously been noted

that the behavior of three-systems depends in the interactions of the underlying two-systems. As such, a less nebulous approach to characterizing the general four-system is to look at the interactions of the (six) underlying two-systems.

Upon consideration of six distinct two systems, describing two linearly independent screws that lie in the intersection of their reciprocal spaces becomes very difficult to generalize. In one of the more exhaustive discussions on the classification of screw systems, Gibson and Hunt limit their discussion to one-, two- and three-systems due to the difficulties associated with describing the general cases of a four-system. They argued that it is sufficient to discuss the reciprocal systems of higher order screw systems in order to bring about some understanding of the more complex system (Gibson and Hunt, 1990a; 1990b). Many authors have commented on the general two system including, Gibson and Hunt, Phillips, and Rimon and Burdick, exhaustively covering them from multiple perspectives (Gibson and Hunt, 1990a; 1990b; Phillips, 1984; 1990; Rimon and Burdick, 1995a; 1995b). The difficulty with the application of this methodology to describe velocity workspace boundaries resulting from four-systems is that a true, general two-system of twists must include wrenches in its reciprocal space with nonzero pitches, otherwise there is a loss of generality. Given the components in the model these wrenches are not plausible constraints and any attempt to characterize the velocity workspace boundary in this manner will provide no model specific information and likely describe fictional characteristics of the general boundary.

In the current configuration, each of the four major ligaments is modeled as a single filament. The only way a four-system of constraining wrenches can be the result

of only ligament limitations is if all four filaments are taut. The spheres representing the displacement workspaces of each of the individual ligament constraints must have at least one point in common on the valid workspace boundary. It is also possible that a constraining four-system be generated from surface contact alone, or as a combination of both ligament and surface constraints. As a result the locations on the current fixed orientation displacement workspace that might have a two-system as its velocity workspace boundary include the intersection of all four ligament constrained surfaces and the whole of the surface defined by the contact constraints.

#### 4.2.3.5 Five-Systems

Many of the arguments for avoiding a discussion of the general five-system coincide with those listed for the four-system. If the set of constraining wrenches has five linearly independent members, then the set is said to form a five-system, and the corresponding velocity workspace boundary forms a one-system. The interesting aspect about the condition when the constraining wrenches constitute a five-system is that a single screw and its scalar multiples span the reciprocal space. The current state of the knee model requires that at least one surface constraint be active for this situation to arise. In all likelihood, unless the displacement workspace reduces to a single point, more than one linearly independent surface contact wrench (and not all four ligament constraint wrenches) will be present when a five-system arises. It is possible for the surface contact constraints alone to generate a constraining five system, along with varying combinations of ligament and surface constraints.

Extreme range-of-motion positions have a higher likelihood of instigating the onset of a five-system from passive constraints alone. Even though only one or two

ligament constraints may be active, the joint contact surfaces have the potential to increase in their order of contact as the knee approaches a limiting position and orientation. Similar to robotic mechanisms with joints having limited ranges of motion, the human knee does not reach every configuration possible in three-dimensional space. At some point, the knee must become fully constrained, normally with the addition of external or active inputs. That is, if the femur is rigidly fixed, a single twist may be applied to the tibia until it reaches a state of full constraint. The normal knee, however, allows motion between its constituents, meaning for some configurations it is not fully constrained. It is during this transition from unconstrained to fully constrained configurations that the joint model is more likely to encounter higher order constraint systems such as the five-system.

Figures 4.16(a) and 4.16(b) show a simple example of a five-system and the corresponding velocity workspace boundary one-system. The example intentionally

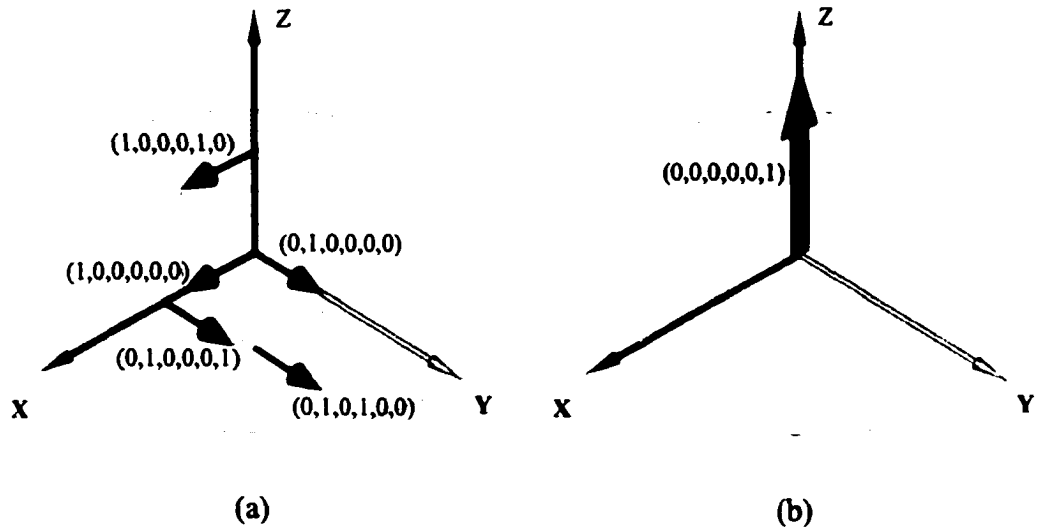


Figure 4.16 (a) Example constraint set composed of five linearly independent wrenches. (b) Velocity workspace boundary elements for example of five linearly independent constraint wrenches.

includes an underlying three-system of the same form as the special case example in the discussion of three-systems to simplify this discussion. If the underlying two-systems of the five-system in Figure 4.2.3.5(a) are considered one at a time, it is readily apparent that the one-system in Figure 4.2.3.5(b) is a member of the reciprocal space for each of the underlying two-systems. Mathematically, it is also apparent that the one-system velocity workspace boundary satisfies the reciprocal condition given in Inequality 4.2.2 for each of the wrench constraints.

#### 4.2.3.6 Six-Systems

If the set of constraining wrenches contains six linearly independent wrenches, the constraining set is said to be a six-system. For this situation, the corresponding velocity workspace boundary space is empty and there are no possible infinitesimal twists the rigid body representing the tibia may pursue that produce zero virtual work. That is not to say that the tibia in our model cannot move. The rigid body representing the tibia may indeed be fully constrained such that there are no motions possible, however a constraint set that spans the entirety of three-dimensional space does not rigidly fix the tibia relative to the femur. There may or may not exist a repelling space where the tibia may proceed along twists that produce positive virtual work with respect to the model constraints.

This type of situation may be physically interpreted as the condition obtained when any motion of the tibia will change at least one or more constraint wrenches. This is a significant point to velocity workspace analyses. There is no limitation in the model of the human knee that dictates contact between the tibia and femur cannot be

broken. There is no limitation that proclaims a ligament may not relax and relinquish its contribution to the mobility condition of the tibia relative to the femur.

Looking at these realizations from a robotics perspective, this type of behavior is to be expected when a mechanism is considered that has constraints that operate in only one sense or direction. Indeed the defining characteristic of a passive constraint system is that it reacts to limit or control the effects of active inputs to the system. Herein lies an argument for the necessity of co-contraction to fully control a joint such as the human knee. It is possible for the joint model to reach a state of full constraint with the addition of a single active input. However, with the ligaments and surfaces modeled as they are, reaching a position and orientation where the entire space of twists is contrary to at least one wrench imposed by the passive constraint system is not possible. If it were, then the model would have exactly one valid position from which it could never escape without violating a model constraint.

A specific example of a six-system is not included as there is no corresponding velocity workspace boundary and the six-system would present itself simply as a basis of the six dimensional screw space. From the standpoint of reciprocity, six-systems are relatively uninteresting, however the repelling space, or interior of the velocity workspace of a six-system can present some interesting situations. For that matter, constraint sets with significant numbers of wrenches, linearly independent or not, present some intriguing situations when the interior of the corresponding velocity workspace is explored.

Figure 4.17(a) includes the discrete point set representing the femur and tibia from the UMN data set in the scanned orientation. Surface patches are included to

show the approximate coverage of the ligament insertion sites on the bones. Figure 4.17(b) shows the same ligament insertion sites rendered with the modeled constraint wrenches (shown in gray arrows) and the Cartesian reference frame attached to the tibia. Mathematical analysis finds all four constraint wrenches to be linearly independent indicating that the reciprocal set of twists corresponding to this constraint condition will be a two system. Figure 4.18(a) shows the results of the computation of the reciprocal twist basis plotted along side the constraint set. Figure 4.18(b) provides the most interesting view of the $\$_1$ twist, which seems to intersect all four constraining wrench axes. The axis of $\$_1$ appears to be the nominal flexion/extension axis of the human knee in the given position and orientation. From no more than the ligament insertion locations near full extension, the workspace approach determined the physically relevant approximate axis of normal motion, illustrating the potential of this type of analysis.

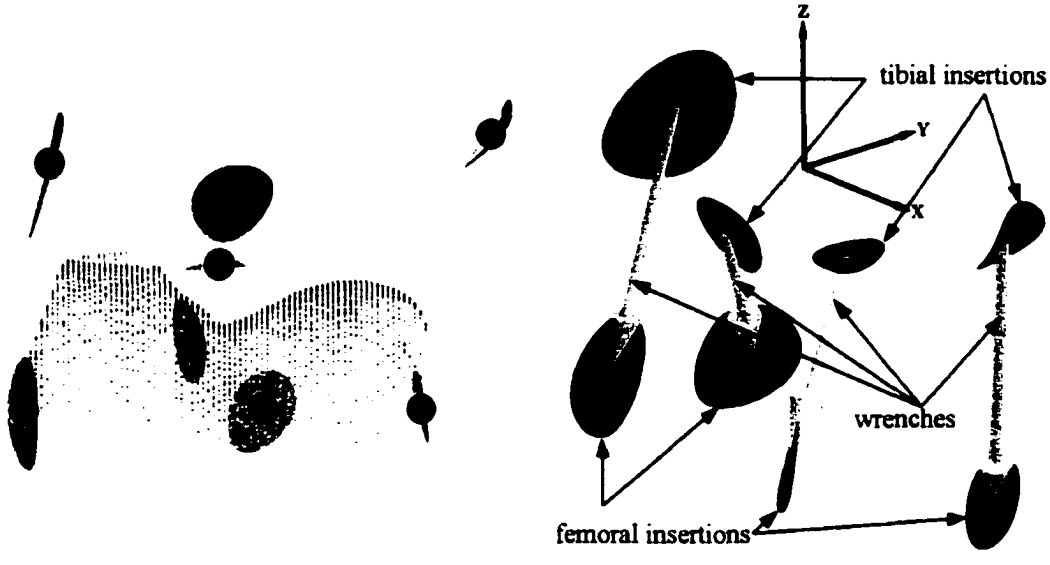


Figure 4.17 (a) Schematic of the knee components near full extension. (b) Rendered ligament insertion sites and modeled constraint wrenches.

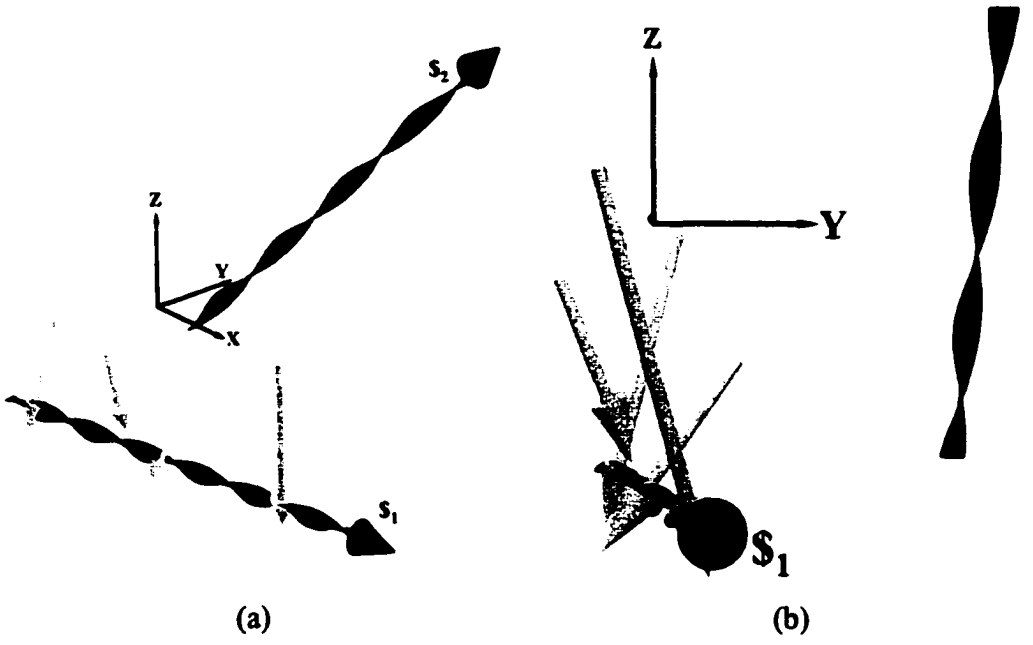


(a) (b)

Figure 4.18 (a) Reciprocal twist plotted with corresponding constraining wrenches. (b) View along $\$_1$ axis showing an intuitive "flexion/ extension" axis of the knee.

### 4.2.4 Velocity Workspace Interiors

The interior of the velocity workspace for any set of constraint wrenches is highly dependent on the geometric relationship between the members of the constraining set. For example, a one-system consisting of two oppositely directed, coaxial wrenches has no interior points in its velocity workspace, yet the velocity workspace boundary is a five-system. That is, there exists no twist that produces positive work when evaluated with all constraining wrenches, yet the boundary of the corresponding velocity workspace has five independent basis twists available for reciprocal motions. In contrast, for a system with $m$ constraining wrenches (with $n$ dimensions and $r$ linearly independent wrenches), by Equation 4.2.4 there is a maximum of $q$ distinct twists that will produce positive virtual work with respect to at

least one member of the constraint set and non-negative virtual work with respect to the remaining members of the constraining set.

Considering the general case of a single constraint wrench imposed by the model of the human knee joint, a twist having positive intensity along the screw axis of the constraining wrench will produce positive virtual work while a twist having negative intensity along the screw axis of the constraining wrench will produce negative virtual work. The repelling space of the lone constraining wrench is spanned by any linear combination of the twists of the reciprocal space with a positive definite scalar multiple of the twist producing positive virtual work. Likewise, the contrary space is spanned by any linear combination of the twists of the reciprocal space with a positive definite scalar multiple of the twist producing negative virtual work. When considered individually, every wrench constraint in the model has this relatively simple repelling and contrary twist halfspace structure. It is the combination of all individual contrary and repelling halfspaces that determines the ultimate parsing of screw space into the repelling, reciprocal, and contrary subspaces under the entire constraint set. The intersection of all individual repelling twist halfspaces defines the interior of the velocity workspace for the given constraint configuration of the knee joint model. In contrast, the union of all individual contrary twist halfspaces defines the exterior of the velocity workspace for the given constraint configuration.

Recalling the one-system described previously, the repelling space for either of the wrenches is exactly the contrary space of the other. When the intersection of the two repelling spaces is evaluated, the result is an empty space as there are no twists repelling to both wrenches. Stated in another manner, every twist not in a reciprocal

space for this example will be contrary to one of the constraining wrenches and repelling to the other. The evaluation of the intersection of all twist spaces that are repelling can be seen to be empty while the union of all twist spaces that are contrary span all non-reciprocal screws in space. In such a case the velocity workspace consists of the velocity workspace boundary alone, defined as simply the reciprocal space of the constraining wrench set.

One of the more interesting cases to look at when constructing velocity workspaces for the model of the human knee is the case of the constraining wrench set being full rank. That is, the constraint set must contain at least six linearly independent wrenches. At first glance, the constraint configuration would imply that the rigid body representing the tibia is fully constrained. However, upon construction of the velocity workspace it is discovered that this is far from being true. Murray, et al. and Latombe provide some insight into the notion of force closure, which is the analogous to full constraint of a rigid body (Latombe, 1991; Murray, et al., 1994). From a wrench-oriented perspective, force closure is defined as a rigid body having the capability to resist the effects of any wrench applied to it. That is, there are constraining wrenches acting on the rigid body that can form a linear combination to cancel any new wrenches encountered by the rigid body (Murray, et al., 1994). Adapting this notion to workspace terms, force closure is the condition that every twist in space is contrary to at least one wrench in the constraining set. As a consequence, the reciprocal and repelling twist spaces must be empty. When a constraint set reaches full rank, the reciprocal twist space is empty, however the repelling twist space may or may not be, depending on the relationship between the constraints.

The model of the human knee includes constraints interpreted as zero pitch wrenches acting either normal to the tibial surface or along the axis between ligament insertion sites. The concept of force closure is popular in the design and motion planning of robotic grippers, and, continuing the obvious hand analogy, the forces imposed by grippers and grasps are termed fingertips. The wrenches found in the human knee model are equivalent to frictionless fingertips, characterized as frictionless point contacts. This assertion is obvious with respect to surface contact constraint wrenches. However, with respect to ligament induced constraint wrenches, some clarification is warranted. By Latombe's description, frictionless fingertips may exert a force normal to the rigid body at the point of contact, and hardcontact fingertips may exert a force in any direction into a surface at the point of contact (Latombe, 1991). Ligament induced wrenches do not typically occur with normal orientations relative to the tibial surface and would appear to be analogous to hardcontact fingertip configuration. The implication of a hardcontact fingertip is that it may counter forces in any direction, whereas the frictionless fingertip may provide countering forces in only one direction. Ligaments behave more like a frictionless fingertip in the sense that they may counter (tension) loads in one direction only. The pulling sense of a ligament constraint provides it with the ability to support a load along an axis different from the surface normal, however loads normal to the ligament axis cannot be sustained.

The conditions for force closure require a minimum of seven frictionless fingertips for polyhedral rigid bodies, and an upper limit of 12 frictionless fingertips are required for force closure of non-exceptional rigid bodies. Polyhedral rigid bodies take on the usual definition of solids formed by plane faces, while exceptional rigid bodies

are those with some type of rotational symmetry. In general it is impossible to satisfy force closure requirements for exceptional objects, including spheres and cylinders, using frictionless fingertip contact constraints (Murray, et al., 1994). The unique ability of the model ligaments to carry loads along axes different from the surface normal at the point of insertion, however, allows exceptional bodies to be force closed by a sufficient number of these analogous frictionless fingertip constraints.

Figure 4.19(a) shows a graphical depiction of a relatively simple six-system consisting of pure force wrenches. A basis for the repelling space corresponding to the constraint set shown in Figure 4.19(a) is included in Figure 4.19(b). For this particular example, the basis set of repelling twists is computed in such a manner that results in each twist producing positive virtual work with respect to one wrench and zero virtual work with respect to the remaining wrenches. In general this type of repelling basis

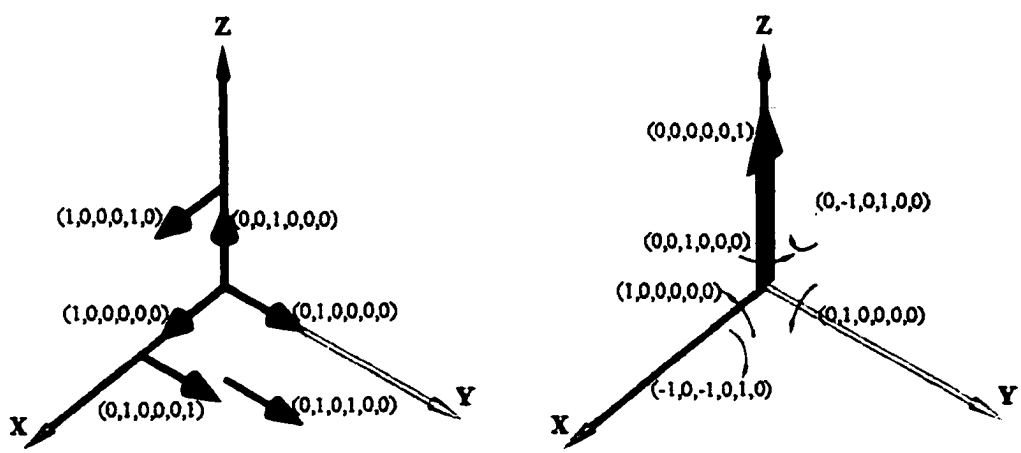


(a) (b)

Figure 4.19 (a) Example constraint set composed of six linearly independent wrenches (six-system). (b) Repelling velocity workspace corresponding to the example six-system of wrench constraints.

representation is possible only when the set of constraining wrenches is linearly independent. It is clear from this example that the six wrenches of the constraining set are linearly independent yet the velocity workspace analysis determines six possible independent, instantaneous trajectories, five rotations and one translation, which do not violate the model constraint conditions. As there is no null space for the set of constraining wrenches, Figure 4.19(b) shows a basis for the entire velocity workspace, allowing the construction of all feasible, instantaneous twists through positive scalar multiplication and addition of the independent basis twists. The resulting repelling velocity workspace for the constraint condition from the displacement workspace of the human knee shown in Figures 4.17(a) and 4.17(b) can be found in Figures 4.20(a) and 4.20(b).

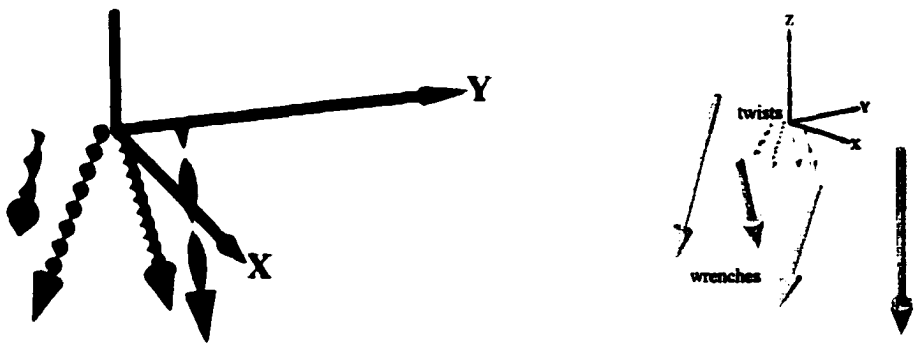


(a) (b)

Figure 4.20 (a) Repelling space (velocity workspace interior) basis twists for four active ligament constraints in the human knee near full extension. (b) Velocity workspace interior basis twists shown with corresponding wrenches of four active ligament constraints in the human knee near full extension.

### 4.3 Geometric Algebra Connection

Consider two points $a$ and $b$ in Euclidean 3-space with homogeneous coordinate representations of Equation 4.3.1.

$$a = [x_a \quad y_a \quad z_a \quad 1] \tag{4.3.1a}$$
$$b = [x_b \quad y_b \quad z_b \quad 1] \tag{4.3.1b}$$

Let $[e_1 \quad e_2 \quad e_3 \quad e_4]$ be a basis for the four-dimensional homogeneous representation of Euclidean 3-space, then $a$ and $b$ may be written in the form of sums as

$$a = x_a e_1 + y_a e_2 + z_a e_3 + e_4 \tag{4.3.2a}$$
$$b = x_b e_1 + y_b e_2 + z_b e_3 + e_4 \tag{4.3.2b}$$

Hestenes and Ziegler (Hestenes and Ziegler, 1991) present some basic definitions of geometric algebra where they define the geometric product $ab$ as

$$ab = a \cdot b + a \wedge b \tag{4.3.3}$$

where $a \cdot b$ is called the inner product and $a \wedge b$ is called the outer product. Substituting the expressions of Equations 4.3.2a and 4.3.2b into the left-hand side of Equation 4.3.3 and expanding, the geometric product may also be described for two points in Euclidean 3-space as

$$\begin{aligned} ab &= (x_a e_1 + y_a e_2 + z_a e_3 + e_4)(x_b e_1 + y_b e_2 + z_b e_3 + e_4) \\ &= x_a e_1 e_4 + y_a e_2 e_4 + z_a e_3 e_4 + e_4 e_4 + x_a z_b e_1 e_3 + y_a z_b e_2 e_3 + z_a z_b e_3 e_3 \\ &\quad + z_b e_4 e_3 + x_a y_b e_1 e_2 + y_a y_b e_2 e_2 + z_a y_b e_3 e_2 + y_b e_4 e_2 + x_a x_b e_1 e_1 \\ &\quad + y_a x_b e_2 e_1 + z_a x_b e_3 e_1 + x_b e_4 e_1 \end{aligned} \tag{4.3.4}$$

Noting

$$e_i e_j = -e_j e_i, \quad i \neq j$$
$$e_i e_j = 1, \qquad i = j$$

Equation 4.3.4 becomes

$$
\begin{aligned}
ab = {} & (x_a x_b + y_a y_b + z_a z_b + 1) + \\
& (x_b - x_a)e_4e_1 + (y_b - y_a)e_4e_2 + (z_b - z_a)e_4e_3 + \\
& (y_a z_b - z_a y_b)e_2e_3 + (z_a x_b - x_a z_b)e_3e_1 + (x_a y_b - y_a x_b)e_1e_2
\end{aligned}
\qquad 4.3.5
$$

Substituting the results from Equation 4.3.5 into Equation 4.3.3, the following relationships can be seen

$$a \cdot b = x_a x_b + y_a y_b + z_a z_b + 1 \qquad 4.3.6a$$

$$
\begin{aligned}
a \wedge b = {} & (x_b - x_a)e_4e_1 + (y_b - y_a)e_4e_2 + (z_b - z_a)e_4e_3 + \\
& (y_a z_b - z_a y_b)e_2e_3 + (z_a x_b - x_a z_b)e_3e_1 + (x_a y_b - y_a x_b)e_1e_2
\end{aligned}
\qquad 4.3.6b
$$

Upon inspection, it is evident that Equation 4.3.6a is the normal incarnation of the scalar or dot product that is commonly associated with vector algebras. Equation 4.3.6b also has the familiar form of Plücker coordinates when the proper basis is assigned. Consider the line containing the points $a$ and $b$ and directed from $a$ to $b$. Then the vector in the direction of that line, passing through the origin is given by

$$[L \quad M \quad N] = [x_b - x_a \quad y_b - y_a \quad z_b - z_a] \qquad 4.3.7$$

The "moment" of the line passing through a and b, about the origin is given by

$$[P \quad Q \quad R] = [x_a \quad y_a \quad z_a] \times [L \quad M \quad N] \qquad 4.3.8a$$

$$[P \quad Q \quad R] = [y_a N - M z_a \quad L z_a - x_a N \quad x_a M - L y_a] \qquad 4.3.8b$$

$$[P \quad Q \quad R] = [y_a z_b - z_a y_b \quad z_a x_b - x_a z_b \quad x_a y_b - y_a x_b] \qquad 4.3.8c$$

The six parameters $[L \quad M \quad N \quad P \quad Q \quad R]$ are said to be the Plücker coordinates of the line from $a$ to $b$. If a basis of the six Plücker coordinates is chosen to be represented by $[e_4e_1 \quad e_4e_2 \quad e_4e_3 \quad e_2e_3 \quad e_3e_1 \quad e_1e_2]$, then the Plücker coordinates of the line from $a$ to $b$ can be written as a sum that is identical to Equation 4.3.6b.

The result is that the outer product of two homogeneous (finite) points in Euclidean 3-space defines the Plücker coordinates of the line containing those points. By carefully choosing the points $a$ and $b$, it is possible to represent a zero pitch screw

(pure force wrench or pure rotation twist) as the outer product of two homogeneous points (or the outer product of two finite vectors passing through the origin). The pure force wrench will act along the screw axis from *a* to *b* while the analogous case of the pure rotation twist will act about that same screw axis from *a* to *b*.

Now consider the same construction for two points at infinity, namely, *c* and *d*. They are given in the summation form as

$$c = [x_c \quad y_c \quad z_c \quad 0] \qquad 4.3.9a$$

$$d = [x_d \quad y_d \quad z_d \quad 0] \qquad 4.3.9b$$

The outer product of *c* and *d* yields

$$c \wedge d = (y_c z_d - z_c y_d)e_2 e_3 + (z_c x_d - x_c z_d)e_3 e_1 + (x_c y_d - y_c x_d)e_1 e_2 \qquad 4.3.10$$

which rewritten in Plücker coordinates is

$$(0,0,0,(y_c z_d - z_c y_d),(z_c x_d - x_c z_d),(x_c y_d - y_c x_d)) \qquad 4.3.11$$

By carefully choosing the points *c* and *d*, it is possible to represent an infinite pitch screw (pure couple wrench or pure translation twist) as the outer product of two homogeneous points at infinity. The axis that the couple is acting about in the case of the wrench is the same as the direction of the translation in the case of the twist and is described by the line passing through the origin and the Cartesian point $(y_c z_d - z_c y_d, z_c x_d - x_c z_d, x_c y_d - y_c x_d)$.

Harkening back to Equation 4.3.3 defining the geometric product of two "regular" vectors, it is evident from Equation 4.3.5 that the result is a multivector composed of scalars and bivectors (components whose basis elements are composed of geometric products of two distinct original basis elements). It is the sum of these bivectors that makeup the exterior products that yield the Plücker coordinates of the

axes under investigation. Hestenes and Sobczyk (Hestenes and Sobczyk, 1984) describe the r-vector part of a multivector $A$ contained in the four-dimensional homogeneous representation of Euclidean 3-space using the following notation

$$A = \langle A \rangle_0 + \langle A \rangle_1 + \langle A \rangle_2 + \langle A \rangle_3 + \langle A \rangle_4 \qquad 4.3.12$$

The subscripts in Equation 4.3.12 represent the grade of the individual r-vector parts. Grade zero represents scalars, grade one includes the four regular vectors (or 1-vectors), grade two includes the six bivectors (or 2-vectors), grade three describes the four trivectors (or 3-vectors), and grade four includes lone pseudoscalar or 4-vector. Using the notation of Equation 4.3.12, the outer product of two 1-vectors is expressed by the grade two part of a multivector and represented by $\langle ab \rangle_2$. Applying this notation to the description of the outer product of Equation 4.3.6b, the following simple wrenches and twists may be defined where $o$ is the point at the Cartesian origin and $a$, $b$, $c$, and $d$ are homogeneous coordinates of points in space.

$W_F = \langle ab \rangle_2$ = pure force acting along $\vec{ab}$ 4.3.13a#

$W_C = \langle cd \rangle_2$ = pure couple normal to the plane sweeping from $\vec{oc}$ to $\vec{od}$ 4.3.13b*

$T_\omega = \langle rs \rangle_2$ = pure rotation about the axis $\vec{rs}$ 4.3.13c#

$T_v = \langle tu \rangle_2$ = pure translation normal to the plane sweeping from $\vec{ot}$ to $\vec{ou}$ 4.3.13d*

\# constructed from finite points ⇒ coefficient of $e_4$ is 1

* constructed from points at infinity ⇒ coefficient of $e_4$ is 0

Under the assumption that the vector $\vec{ab}$ is normal to the plane sweeping from $\vec{oc}$ to $\vec{od}$ ($\vec{rs}$ is normal to the plane sweeping from $\vec{ot}$ to $\vec{ou}$) a general wrench (twist) may be written as the linear combination $W_F + W_C$ ($T_\omega + T_v$). Of course, linear combinations of distinct axes may be employed to form general wrenches or twists.

The resulting cases will, however, always reduce to the general case where the linear and angular axes are coincident as proven by theories of Chasles and Poinsot.

Returning to the identities shown by Hestenes and Sobczyk, the general wrench and general twist may be written as follows

$$\overline{W} = \langle ab \rangle_2 + \langle cd \rangle_2 = \langle ab + cd \rangle_2 \qquad 4.3.14a$$

$$\overline{T} = \langle rs \rangle_2 + \langle tu \rangle_2 = \langle rs + tu \rangle_2 \qquad 4.3.14b$$

It is also useful to comment on the behavior of the pseudoscalar, particularly when interacting with the 2-vector part of a multivector. For the four-dimensional space under investigation here, the pseudoscalar ($I$) is simply the geometric product of all four basis elements $e_1e_2e_3e_4 = e_{1234}$. The shorthand notation omitting the multiple occurrence of the $e$'s is introduced to speed simplification of the following computations. The geometric product of a general bivector and the pseudoscalar is given by

$$(\alpha_1 e_{41} + \alpha_2 e_{42} + \alpha_3 e_{43} + \alpha_4 e_{23} + \alpha_5 e_{31} + \alpha_6 e_{12})(e_{1234}) \qquad 4.3.15$$

Expanding Equation 4.3.15

$$\begin{aligned}
&= (\alpha_1 e_{41} e_{1234} + \alpha_2 e_{42} e_{1234} + \alpha_3 e_{43} e_{1234} + \alpha_4 e_{23} e_{1234} + \alpha_5 e_{31} e_{1234} + \alpha_6 e_{12} e_{1234}) \\
&= (\alpha_1 e_{411234} + \alpha_2 e_{421234} + \alpha_3 e_{431234} + \alpha_4 e_{231234} + \alpha_5 e_{311234} + \alpha_6 e_{121234}) \\
&= (\alpha_1 e_{4234} - \alpha_2 e_{4134} + \alpha_3 e_{4124} + \alpha_4 e_{2124} + \alpha_5 e_{3234} - \alpha_6 e_{34}) \qquad 4.3.16 \\
&= (\alpha_1 e_{23} - \alpha_2 e_{13} + \alpha_3 e_{12} - \alpha_4 e_{14} - \alpha_5 e_{24} - \alpha_6 e_{34}) \\
&= (\alpha_4 e_{41} + \alpha_5 e_{42} + \alpha_6 e_{43} + \alpha_1 e_{23} + \alpha_2 e_{31} + \alpha_3 e_{12})
\end{aligned}$$

Upon comparison of the final result in the manipulations of Equation 4.3.16 with the original bivector in Equation 4.3.15, the action of the pseudoscalar is recognized as simply repositioning the first three coefficients of the bivector with the last three coefficients. Consider the application of the pseudoscalar to a general twist. Now the

usefulness of this operation can be readily seen when the scalar product of a general wrench $(\overline{\beta})$ and this general twist $(\overline{\alpha})$ that has been operated on by the pseudoscalar is computed. The result is the negative of the virtual coefficient used to define the interrelationships of wrenches and twists and to define the velocity workspaces of the human knee.

$$\overline{\beta}\cdot(\overline{\alpha}I)=\begin{bmatrix}\beta_1 e_{41} & \beta_2 e_{42} & \beta_3 e_{43} & \beta_4 e_{23} & \beta_5 e_{31} & \beta_6 e_{12}\end{bmatrix}\begin{bmatrix}\alpha_4 e_{41}\\ \alpha_5 e_{42}\\ \alpha_6 e_{43}\\ \alpha_1 e_{23}\\ \alpha_2 e_{31}\\ \alpha_3 e_{12}\end{bmatrix} \qquad 4.3.17$$

Equation 4.3.17 may be expanded as normal matrix multiplication

$$\overline{\beta}\cdot(\overline{\alpha}I)=\left[\beta_1\alpha_4 e_{4141}+\beta_2\alpha_5 e_{4242}+\beta_3\alpha_6 e_{4343}+\beta_4\alpha_1 e_{2323}+\beta_5\alpha_2 e_{3131}+\beta_6\alpha_3 e_{1212}\right] \qquad 4.3.18$$

until the familiar form of Equation 2.4 is reached

$$\overline{\beta}\cdot(\overline{\alpha}I)=\left[-\beta_1\alpha_4-\beta_2\alpha_5-\beta_3\alpha_6-\beta_4\alpha_1-\beta_5\alpha_2-\beta_6\alpha_3\right]=-\varpi_{\alpha\beta} \qquad 4.3.19$$

Consider $\overline{\beta}=\langle ab+cd\rangle_2$, which is simply the 2-vector part of the sum of the geometric products of the 1-vectors *a* and *b* and the 1-vectors *c* and *d*. The multivector that is the sum of two geometric products, each composed wholly of 0-vectors and 2-vectors, as is the case with $ab+cd$, is itself composed wholly of 0-vectors and 2-vectors. The same argument can be made for a twist $\overline{\alpha}=\langle rs+tu\rangle_2$ and, with a little alteration to the development shown in Equation 4.3.16, its dual $\overline{\alpha}I=\langle rsI+tuI\rangle_2$ can be shown to be the 2-vector part of a multivector composed of only 2-vectors and 4-vectors. The geometric product $(ab+cd)(rsI+tuI)$ is constructed by the

multiplication of a multivector composed of a scalar (0-vector) and a bivector with a multivector composed of a pseudoscalar (4-vector) and another bivector. In general terms, this is shown in Equation 4.3.20 through the multiplication of the multivector $\vec{\gamma}$ with the multivector $\vec{\rho}$.

$$\overline{\gamma\rho} = \left[\begin{bmatrix}\gamma_0\\ \gamma_1\\ \gamma_2\\ \gamma_3\\ \gamma_4\\ \gamma_5\\ \gamma_6\end{bmatrix}^T \begin{bmatrix}1\\ e_{41}\\ e_{42}\\ e_{43}\\ e_{23}\\ e_{31}\\ e_{12}\end{bmatrix}\right]\left[\begin{bmatrix}\rho_0\\ \rho_4\\ \rho_5\\ \rho_6\\ \rho_1\\ \rho_2\\ \rho_3\end{bmatrix}^T \begin{bmatrix}e_{1234}\\ e_{41}\\ e_{42}\\ e_{43}\\ e_{23}\\ e_{31}\\ e_{12}\end{bmatrix}\right] \qquad 4.3.20$$

Expanding Equation 4.3.20 yields an expression composed of one scalar (0-vector), six bivectors (2-vectors), and one pseudoscalar (4-vector). The scalar part of the geometric product given in Equation 4.3.20 is identical to Equation 4.3.19, providing a more general way to express the virtual coefficient.

$$\varpi = -\langle (ab + cd)(rsI + tuI) \rangle_0 \qquad 4.3.21$$

This construction of the virtual coefficient allows the application of extended screw theory to the familiar notions of forces without any detailed knowledge of screws, wrenches, or twists or even Plücker coordinates. All that is necessary to determine the constraint relationship between the forces acting on a rigid body and any instantaneous velocity is a set of points describing the direction and coordinates of those forces and velocities.

For example, consider the case of a force acting along the axis from the homogeneous point $a = (0,1,0,1)$ through the point $b = (0,1,1,1)$ with a couple acting

normal to the plane swept out from the point at infinity, $c = (1,0,0,0)$, to the point at infinity, $d = (0,1,0,0)$. The resulting wrench defined by Equation 4.3.14a is developed in Equation 4.3.22.

$$\begin{aligned} \overline{W} &= \langle ab + cd \rangle_2 \\ &= \langle (e_2 + e_4)(e_2 + e_3 + e_4) + (e_1)(e_2) \rangle_2 \\ &= \langle 2 + e_{43} + e_{23} + e_{12} \rangle_2 \\ &= e_{43} + e_{23} + e_{12} \end{aligned} \qquad 4.3.22$$

To assist in drawing parallels to the previous discussions, the screw coordinates of the wrench given in Equation 4.3.22 are $(0 \;\; 0 \;\; 1 \;\; 1 \;\; 0 \;\; 1)$. Now consider the simple twist of pure translation parallel to the wrench axis. This instantaneous velocity screw should produce positive virtual work as it is in the direction of the force delivered by the constraining wrench. Since the twist is pure translation, there is no axis of rotation to be defined by the points at infinity r and s, meaning any axis is applicable as long as the magnitude of the rotation is zero. For consistency, let that axis be coincident with the axis of the constraining wrench. This is a purely arbitrary selection and has no consequence on the results of the example. The homogeneous points at infinity defining this fictitious axis of rotation are given from $r = (0,1,0,0)$ and $s = (0,1,1,0)$. The translation is described as occurring perpendicular to the *x-y* plane in the positive *z*-direction or equivalently normal to the plane swept out by the vectors from the origin to the points $t = (1,0,0,0)$ and $u = (0,1,0,0)$, respectively. The resulting twist defined by Equation 4.3.14b is developed in Equation 4.3.23.

$$\begin{aligned}\overline{T} &= \langle 0rs + tu \rangle_2 \\ &= \langle 0 + (e_1)(e_2) \rangle_2 \\ &= \langle e_{12} \rangle_2 \\ &= e_{12}\end{aligned} \qquad 4.3.23$$

The zero scalar multiple of the geometric product *rs* is included to accommodate the absence of an instantaneous angular velocity. As before, to keep in touch with the previous, non-geometric algebra based development, the screw coordinates of the twist given in Equation 4.3.23 are $(0 \quad 0 \quad 0 \quad 0 \quad 0 \quad 1)$. Constructing the virtual coefficient using Equation 4.3.21 the correct classification of this twist is confirmed as repelling exhibiting a positive virtual coefficient.

$$\begin{aligned}\varpi &= -\langle (ab + cd)(rsI + tuI) \rangle_0 \\ &= -\langle (2 + e_{43} + e_{23} + e_{12})(e_{12}e_{1234}) \rangle_0 \\ &= -\langle -1 + e_{41} + e_{42} + 3e_{43} + e_{12} + e_{1234} \rangle_0 \\ &= 1\end{aligned} \qquad 4.3.24$$

Consider a second, slightly more complicated twist with respect to the constraining wrench of Equation 4.3.22. Also, to demonstrate an added feature of this technique, let the specification of the twist be such that the axis defining the infinitesimal rotation is not parallel to the direction of pure translation. Let the twist be described by a pure infinitesimal rotation about the axis from $r = (0,2,1,1)$ to $s = (0,1,0,1)$ and a pure infinitesimal translation perpendicular to the plane swept out by the vectors from the origin to the points $t = (1,0,-1,0)$ and $u = (1,-1,0,0)$, respectively. The resulting twist defined by Equation 4.3.14b is developed in Equation 4.3.25.

$$
\begin{aligned}
\overline{T} &= \langle rs + tu \rangle_2 \\
&= \langle (2e_2 + e_3 + e_4)(e_2 + e_4) + (e_1 - e_3)(e_1 - e_2) \rangle_2 \\
&= \langle 4 - e_{42} - e_{43} - 2e_{23} - e_{31} - e_{12} \rangle_2 \\
&= -e_{42} - e_{43} - 2e_{23} - e_{31} - e_{12}
\end{aligned}
\qquad 4.3.25
$$

Continuing the evidence for comparison with the screw coordinates, the twist coordinates of the result of Equation 4.3.25 are $(0,-1,-1,-2,-1,-1)$. Computation of the virtual work using the screw coordinate method yields a negative value as shown in Equation 4.3.26. The coinciding calculation using geometric algebra is shown in Equation 4.3.27, yielding the same conclusion that was drawn from the screw coordinate computation. Both methods indicate that this particular twist is a member of the contrary space of the constraining wrench.

$$
\overline{W} \cdot \overline{T}^* = \begin{bmatrix} 0 & 0 & 1 & 1 & 0 & 1 \end{bmatrix} \begin{bmatrix} -2 \\ -1 \\ -1 \\ 0 \\ -1 \\ -1 \end{bmatrix}
\qquad 4.3.26
$$

$$
\varpi_{\overline{WT}} = -2
$$

$$
\begin{aligned}
\varpi_{\overline{WT}} &= -\langle (ab + cd)((rs + tu)(I)) \rangle_0 \\
&= -\langle (2 + e_{43} + e_{23} + e_{12})((4 - e_{42} - e_{43} - 2e_{23} - e_{31} - e_{12})(e_{1234})) \rangle_0 \\
&= -\langle 2 - 2e_{41} - e_{42} + 3e_{43} - 2e_{23} - e_{31} + 3e_{12} + 12e_{1234} \rangle_0 \\
\varpi_{\overline{WT}} &= -2
\end{aligned}
\qquad 4.3.27
$$

Figures 4.21(a) and 4.21(b) include graphical representations for the wrench and twists described in the two examples.

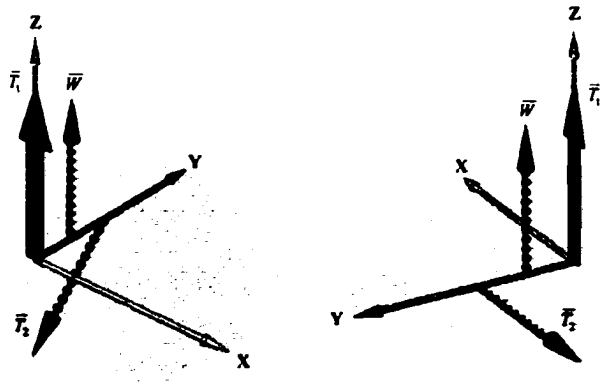


Figure 4.21 (a) Perspective view of the wrench and twists discussed in the example geometric product studied, (b) A second view of the wrench and twists cited in the example constructions.

# CHAPTER 5. CONCLUSIONS AND RECOMMENDATIONS

## 5.1 Conclusions

The evolution of mankind from primal, animalistic origins to a more civilized cooperation and coexistence has permitted the shift from pursuing physical activities for mere survival to more quality-of-life based athletic pursuits and socially rooted recreational sports. Advancement of technology, shifting of cultural expectations, and better understanding of human physiology have all contributed to the evolution of the study of human biomechanics, predominantly motivated by a desire to minimize the more negative aspects of physical exertion. The human knee joint is a popular topic of concern due to its size, complexity, and, particularly, its frequency of injury. This dissertation presents the application of well-known kinematic analysis techniques to study a model of the human knee focusing on ligament function and surface interaction.

Building on classical works of those such as Chasles, Poinsot, and Ball, along with more contemporary achievements of, among others, Hunt, Ohwovoriole, Murphy, Zhang, and Omeltchenko, the concept of velocity workspaces has been defined and explored for an initial model of the passive constraint system of the human knee. While addressing this task, a method for determining the fixed orientation displacement workspaces for the same model of the human knee was achieved. Extracting key parameters necessary for defining the model of the passive constraint system of the human knee joint through the use of clinical imaging techniques was also investigated for the construction of workspaces *in vivo*. While this particular task was not rigorously verified, the data indicate that construction of the model using this method would be a viable gateway to the implementation of workspace analysis in a clinical setting.

The computation of fixed orientation displacement workspaces of the human knee incorporates both the contributions of ligament constraints as well as surface contact constraints to map out the boundaries of the displacement of the tibia relative to the femur. It is believed that this is the first time that both ligament constraints and surface contact constraints have been included together to study three-dimensional workspaces of the human knee joint. Workspace analysis of robotic mechanisms having constraints analogous to the model of the human knee joint explored in this research is also believed to be previously unaddressed. The characteristic irregularity and complexity of the geometry of the human knee joint, calling for the exploration of nontraditional methods of obtaining and implementing model parameters, is the most prevalent factor that distinguishes this displacement workspace research from comparable works in archival literature.

### 5.1.1 A Note on the Variable Orientation Displacement Workspace

Assuming that the VODW is determined for all possible positions and orientations of the human knee joint model, the most difficult task is to succinctly communicate the myriad of information contained in such a space. From a clinical perspective, other than as a visual aid during communication with the physician or as some type of metric for classification purposes, the VODW, in its current form, is not specific enough to offer significant benefits on an individual patients basis when presented in its entirety. Diagnostically, VODWs falter in that the palpating examinations for ligament and meniscal injuries are performed at either fixed relative orientations (anterior drawer, posterior drawer, Lachman, etc.) between the tibia and femur or along specific paths (pivot shift, McMurray's test, etc.) (Dandy and Edwards,

1998; Miller, 1997), not necessarily represented by the exterior surfaces of the VODW boundary. The fact that the VODW boundary is composed of the maximum displacements of the tibia relative to the femur causes its validity to be directly linked to the accuracy of the information used to model the geometric constraints, such as ligament and cartilage deformation, when computed using energy minimization methods. The portion of total system energy stored by each ligament or surface contact constraint is directly dependent on the relative values of the material properties assumed for each modeled structure. Varying the percentage of energy absorbed in a given structure will have an effect on the spatial parameters (position and orientation) of the minimum energy workspace point. If the relative behavior of the model parameters does not coincide with that of their counterparts *in vivo*, then the construction of the VODW reduces to an interesting exercise. Realistically, the VODW itself may be inaccurate when the kinematics of the knee are considered under the constraint of additional parameters known to affect the knee, but not considered in the VODW construction. These include the constraints imposed by other less universal ligamentous bodies, active muscular contraction, and surrounding capsular tissues. For those tasks that the VODW could be most useful, inaccuracies are unacceptable but also unavoidable when modeling the human anatomy.

From a computational perspective, the VODW presents unique problems as well. To assure that a point on the VODW boundary is reachable without violating the model parameters en route, all constraints must be evaluated simultaneously. This is particularly a problem when the model includes both surface constraints and ligament constraints. The possibilities of any number of contact points being active as well as the

possibility of multiple orientations contributing to the computed boundary point introduce complexities into the discrete computational stability of the workspace detection. The occurrence of two or more distinct orientations at single position on the VODW boundary can lead to problems not only in the ambiguity of the current point, but also in the computation of adjacent points. Depending on the step size and direction chosen for the discrete shift to compute the next position, the VODW could arrive at orientations near any of the multiple orientations of the previous point without regard to the previously chosen condition. This could lead to the following of an interior contour, corrupting the VODW, or should the algorithm be forced to maintain continuity with previous orientations, the subsequent point could coincide with the preceding point, stalling the computation indefinitely.

Some authors have gotten around the questions associated with arbitrary surface geometries by modeling the contact area of the tibia and femur as smooth mathematical functions (Wismans, et al., 1980) or by limiting their study to prosthetic components with regular geometries (Chen, et al., 2000). Both studies assumed two-point contact for their surface constraints. Expanding such studies to include the effects of ligament interference and wrapping around modeled bone surfaces is another area of concern when attempting to cover all possibilities of even the simplest of models. As the structures of the knee move relative to one another, particularly the tibia and femur, ligaments will wrap around some surfaces, momentarily shortening the rest length for the ligament. The trajectory taken through the VODW, as a ligament is wrapping over some structure, affects over what region of the surface that ligament conforms.

Perhaps the most difficult problem associated with computing the VODW is simply the possibility for multiple orientations to exist at a single point. In Omeltchenko's computation of the VODW, conditions have appeared where the orientations of adjacent points showed significant variations, questioning the continuity of the space (Omeltchenko, 1997). If continuity is forced, then the trajectory that is taken to arrive at that point can have the dominant effect on the orientation chosen to represent the VODW at that point. Measurement error and resolution can influence the choice of one orientation over another, creating situations that are not representative of the motion of the joint model, yet thrust to the forefront as a valid motion.

With all of these negative arguments towards the VODW, the successful definition and accurate generation of such a space holds the most promise for characterizing human knee motion based solely on geometry. The widely varying parameters of the human knee, within the general population, such as intercondylar notch width, ligament insertion sites, ligament lengths, meniscal geometry, and cartilage thickness all contribute to the VODW conception. It has the potential to serve as a metric addressing the controversy of a universal coordinate system for the human knee joint and provide a conduit to link the study of the effects of seemingly disconnected joint parameters. From a design perspective, however the VODW would be most useful in evaluating the performance and capabilities of prosthetics or planned surgical procedures.

The current deficiency in the development of VODWs is a lack of acceptable techniques for extracting key system parameters from living subjects in conjunction with inadequate statistically significant data accurately estimating associated properties

of these data. The development and construction of a velocity workspace, however, requires some type of input constraint set. Since there is not a well-established and widely accepted representation of the "typical" passive constraint system of the human knee, the definition of meaningful velocity workspaces is dependent on the application of legitimate data from a real human knee joint. Without such, this investigation accomplishes little beyond a look at various properties of a rather unique mechanism that may be called a knee but has few other connections to reality. With that in mind, the most basic type of displacement workspace, providing three-dimensional constraint set information, is the fixed-orientation displacement workspace. Given the developmental nature of this research, the inherent (and circumventable) complexities introduced by VODWs, and the need for clinical relevance, fixed-orientation displacement workspaces (FODWs) were employed to determine the constraint set information necessary to define velocity workspaces of the human knee. VODWs can be constructed by taking Boolean unions of multiple FODWs, give rise to the continuity concerns as dictated by the order that the unions are performed. This construction loses nothing in the form of kinematic data when compared to the energy-based method, but does pay a price through computational inefficiency.

### 5.1.2 Velocity Workspaces

Calling on the results of the fixed orientation workspace analysis, specifically the contributions of the modeled structures to the constraint of the tibia, a method was presented to determine the possible instantaneous displacements (velocities) the tibia might assume without contradicting the modeled constraints. Significant findings during the development of this method include: (1) The characteristics of the boundary

of multi-dimensional velocity workspaces can always be linked back to the behavior of the underlying two-systems comprising the space; (2) With the constraints of the knee model interpreted herein, a total of twelve independent, frictionless fingertip like constraints are necessary to completely force close the tibia, effectively rendering the tibia and femur into a single rigid body; (3) The detection of contrary spaces affords the identification of instantaneous motions of the tibia relative to the femur that will violate model parameters and could lead to mechanical failure of one or more of the structures in the knee joint model; (4) Preliminary constructions using cadaver data yield promising results, showing expected elements among the velocity workspace bases.

It is well known that screw systems can be characterized by reciprocity and/or linear independence. Hunt introduces general $n$-systems as any group of $n$ linearly independent screws, not all belonging to the same $(n-1)$-system. He also notes that it is equivalent, and, in the case of higher order systems, easier to investigate the properties of reciprocal systems as a means of garnering information about a given screw system (Hunt, 1978). With the construction of the velocity workspace, both of these assertions provide usable information regarding the constraint condition and possible motion of the modeled joint. The characterization of $n$-systems based on their underlying $(n-1)$-systems can be propagated down to the interaction of independent 1-systems, which is simply the behavior or 2-systems. This is a way of breaking down the complexities and intricacies of higher order systems for the purposes of characterization, analysis, and design.

The current implementation of the model includes four ligament constraints and the possibility of any number of surface constraints. As both the ligament and surface

constraints are analogous to the frictionless fingertip model often employed in grasp analysis, results from well-established force closure studies may be applied to the knee joint model. The first relationship that should be recognized is that the current model of the human knee should never reach force closure as all constraints are provided through passive or reactive means. To achieve force closure would indicate a configuration of the joint where motion would be theoretically impossible, eliminating the main function of the joint. The second observation from this perspective is that complete force closure is not a requirement for stability. The components of the knee joint, given the appropriate constraints, may be placed in configurations that will put the rigid bodies in static equilibrium, indicating the forces acting on the tibia relative to the femur are balanced. Conceding that these balancing forces are contributed by the co-contraction of muscular contraction across the knee joint, their inclusion could progress the model closer to the force closed condition. Such a condition is desirable in the human knee or its prosthetic replacement so the joint would have, at a minimum, preliminary resistance to any externally promoted forces.

The separate detection of the reciprocal and repelling basis screws is convenient for expressing the boundary (reciprocal) and interior (repelling) regions of the velocity workspaces. An additional feature of this separation is the immediate determination of the contrary space by multiplying the repelling bases by negative scalars. Complete identification of the contrary space can be accomplished by specifying the twists that act in the opposite sense along the constraining wrench screw axes. These exercises afford the identification of twists that will meet with resistance from the system constraints and that represent the most immediate potential for damage to the

constraining structures. Used in conjunction with kinematic data, twists realized from specific human motions such as running, jumping, and stopping can be compared to the contrary bases to help identify motions similar to those threatening the passive structures within a joint model. The approach can also be employed in the design of prosthetic components to predict wear characteristics or to create implants that will yield in a prescribed manner in an effort to avoid more catastrophic modes of failure. Presented with a set of twists that are to be avoided, a new face emerges for design, analysis, and evaluation of factors surrounding the human knee joint.

The example construction undertaken using the UMN cadaver data set, while promising in its prediction of instantaneous motion, provides only a slight introduction to the validation of the workspace analysis methods developed in this research. Ideally, *in vivo* kinematic data, radiological imaging, and harvested joint specimens, all from a common subject would be sufficient data to validate these works. Radiological imaging is necessary to accomplish the construction of the knee model, leading to the workspace analyses. Fixing the joint specimens in some type of mechanism that would allow measurement of spatial position and orientation variations in concert with constraint force activity would provide an environment for validating the displacement workspace boundary computations. Mimicking the kinematic data with the same mechanism would provide sufficient data for constraint determination, leading to verification of velocity workspace analyses through comparison of the permitted twists, contained within the workspaces, with those exhibited in the recorded motions.

It is readily acknowledged that such a data set will likely never exist as to be absolutely perfect, all three data collections would occur very near each other

chronologically. That is, the joint specimens would need to be harvested soon after the imaging and kinematic data collection to ensure joint parameters did not undergo significant change through age or injury in the interim. Feasible, alternatives for validation include the application of the methods to non-human test subjects, such as those belonging to the canine or equine families, with similar joint structures. The main concession made in this substitution is that feedback normally acquired in the kinematic data collection would not be available to the same extent as with human subjects. Construction of a duplicate knee from the radiological imaging data on the kinematic data test subject through some type of total knee arthroplasty on a cadaver specimen would also approach the ideal validation data set in a practical manner, with the validation of the duplicate knee construction as the main concession.

### 5.1.3 Geometric Algebra

The complexity and abstract nature of screw theory is one of the primary reasons more researchers do not take advantage of its inherent benefits for scientific investigation. Many feel that the time and energy required to become comfortable with its representation and various properties far exceeds the advantages of using such a mathematical tool. The investigation into geometric algebra was primarily motivated out of an attempt to find a method of harnessing the advantages of extended screw theory in a manner that did not require extensive mathematical or geometric expertise.

The ease with which key parameters of extended screw theory, such as the virtual coefficient and the pitch of a screw, fall out of computations performed within the geometric algebra is a powerful argument for the adoption of this representation for applications of screw theory in general. The computation of numerical valued screws is

much more intuitive in the geometric algebra and programming of the geometric product is reduced to polynomial multiplication with easily recognized substitutions. The previous method for specifying screw axes, first by finding a line's Plücker coordinates, followed by the modification to incorporate the pitch in the description of the screw is replaced by an algebraic product that maintains the integrity of the construction without the need for more complex entities like the cross product. Accommodations are automatically included in the algebra for the special case of infinite pitch screw axes without any special treatment, requiring only basic math skills to compute the screw coordinates for the corresponding axis.

Included in this research is but a scratch on the surface of what geometric algebra embodies. The representation of Euclidean 3-space using the four dimensional, homogeneous coordinates is but one vector space that constructs a useful geometric algebra. Other researchers, most notably Hestenes (Hestenes, et al., 1999), have employed a conformal model of Euclidean 3-space embedded in the geometric algebra generated by a five-dimensional basis. The representation is constructed to undertake more sophisticated geometric endeavors, however for the simple tasks depicted in this research, the improvements do not warrant the addition of the fifth dimension.

## 5.2 Recommendations and Future Research

There are several ways the methods presented in this research may be altered to produce improved results. The primary recommended improvement is the inclusion of the articular cartilage and menisci in the construction of the tibia and femur surface geometries. The degeneration of cartilage and damage to menisci are often causes of pain and disability associated with the human knee, underscoring their need for normal

joint performance. As such, their contributions to constraints should be included in the construction of both the displacement and velocity workspaces. Radiological imaging and data reduction software are sufficiently advanced to handle such tasks, allowing the augmentation of the bone surfaces to include cartilage and meniscal structures. For the sake of the construction of velocity workspaces, these structures may be modeled as rigid bodies without prejudice as the velocity workspaces consist of infinitesimal twists. Resistance to the compression of the cartilage involves the expulsion of fluid through a porous matrix, requiring finite time spans to deform the structure, which are not encountered in the instantaneous analysis of velocity workspaces.

Improvements to the ligament constraints may also be implemented through modeling of the multiple bundle structure of ligaments. In this scenario, individual ligament constraints would be realized as multiple filaments, which could share or transfer loads currently interpreted as solitary pure force wrenches throughout the range of motion. Boeree and Ackroyd characterize the appearance of an intact ACL as having two or three longitudinal bands (Boeree and Ackroyd, 1992), while Draganich, et al. found placing a 180° twist in ACL replacement grafts resulted in near isometric motions in cadaver knees (Draganich, et al., 1996). Twists along the length of the ligaments as well as consideration of the overall insertion area would be more readily studied through the multiple bundle models and data collection would be minimally complicated. Verification of bundle detection methods using radiological imaging or some other type of *in vivo* data collection would be necessary prior to implementing such improvements in order to assure that such parameters may be extracted in a clinical setting.

Another concept that should be explored is the construction of the FODW as an intersection of a set of volumes rather than surfaces. Assigning a tolerance to the ligament lengths would produce a spherical shell with a finite thickness while employing deformable models of the surface contact areas would arrive at the same type of boundary with an associated thickness. Addressing the controversy of defining a rest length for ligaments *in vivo*, the ligaments could be considered "pre-strained" in every configuration with their contribution to the overall constraint conditions weighted according to the location of the tibia along each of the ligament tolerances. The ability of the surface to deform would accommodate kinematic data that initiated under load and continued on through various loading conditions. The tolerances could also provide avenues for employing more complex contact models such as soft-fingertips or multiple hard-fingertip contact constraints for each contact "point".

The displacement and velocity workspace analyses have shown themselves to be tools best suited for use in conjunction with kinematic data acquisition and radiological imaging at their current level of development. As research continues and the knowledge base expands, spatial modeling will inevitably depose current, highly invasive techniques for data collection and notoriously indeterminate, statistics based analyses as the preferred means of exploring the mechanics of human motion. It is believed that the workspace analysis tools explored in this research will establish accessible directions toward achieving that capability.

# REFERENCES


AAOS. (1997). "6 Million a Year Seek Medical Care For Knees." American Academy of Orthopaedic Surgery (AAOS).

Abdel-Malek, K., Adkins, F., Yeh, H.-J., and Haug, E. (1997). "On the Determination of Boundaries to Manipulator Workspaces." *Robotics and Computer-Integrated Manufacturing*, 13(1), 63-72.

Abdel-Malek, K., Yeh, H.-J., and Khalrallah, N. (1999). "Workspace, Void, and Volume Determination of the General 5DOF Manipulator." *Mechanics of Structures and Machines*, 27(1), 89-115.

Ackerman, M. J. (2000). "The Visible Human Project." National Library of Medicine 8600 Rockville Pike, Bethesda, MD 20894.

Agrawal, S. K., and Garimella, R. (1994). "Workspace Boundaries of Free-floating Open and Closed Chain Planar Manipulators." *Journal of Mechanical Design*, 116(1), 105-110.

Amis, A. A., and Dawkins, G. P. C. (1991). "Functional Anatomy of the Anterior Cruciate Ligament: Fibre Bundle Actions Related to Ligament Replacements and Injuries." *The Journal of Bone and Joint Surgery*, 73-B(2), 260-267.

Andriacchi, T. P., Mikosz, R. P., Hampton, S. J., and Galante, J. O. (1983). "Model Studies of the Stiffness Characteristics of the Human Knee Joint." *Journal of Biomechanics*, 16(1), 23-29.

Anton, H. (1977). *Elementary Linear Algebra*, John Wiley & Sons, New York.

Arendt, E., and Dick, R. (1995). "Knee Injury Patterns Among Men and Women in Collegiate Basketball and Soccer." *The American Journal of Sports Medicine*, 23(6), 694-701.

Audesirk, T., and Audesirk, G. (1996). *Biology, Life on Earth*, Prentice-Hall, Inc., Upper Saddle River.

Ball, S. R. S. (1900). *A Treatise on the Theory of Screws*, Cambridge University Press, Cambridge CB2 2RU, UK.

Barrett, H. H., and Swindell, W. (1981). *Radiological Imaging: The Theory of Image Formation, Detection, and Processing*, Academic Press, New York.

Beggs, J. S. (1983). *Kinematics*, Hemisphere Publishing Corporation, Washington.

Bendjaballah, M. Z., Shirazi-Adl, A., and Zukor, D. J. (1997). "Finite Element Analysis of Human Knee Joint in Varus-Valgus." *Clinical Biomechanics*, 12(3), 139-148.

Bicchi, A., Melchiorri, C., and Balluchi, D. (1995). "On the Mobility and Manipulability of General Multiple Limb Robots." *IEEE Transactions on Robotics and Automation*, 11(2), 215-228.

Blacharski, P. A., Somerset, J. H., and Murray, D. G. (1975). "A three-dimensional study of the kinematics of the human knee." *Journal of Biomechanics*, 8, 375-384.

Blankevoort, L., Huiskes, R., and de Lange, A. (1991a). "Recruitment of Knee Joint Ligaments." *Journal of Biomechanical Engineering*, 113, 94-103.

Blankevoort, L., Kuiper, J. H., Huiskes, R., and Grootenboer, H. J. (1991b). "Articular Contact in a Three-Dimensional Model of the Knee." *Journal of Biomechanics*, 24(11), 1019-1031.

Boeree, N. R., and Ackroyd, C. E. (1992). "Magnetic Resonance Imaging of Anterior Cruciate Ligament Rupture." *The Journal of Bone and Joint Surgery [Br]*, 74-B(4), 614-616.

Boisgard, S., Geiger, B., and Michel, H. (1994). "A Study of 3D Kinematics of the Knee Joint." *First International Symposium on Medical Robotics and Computer-Assisted Surgery*, 121-125.

Bradley, W., and Tosteson, H. (1982). "Basic Physics of NMR." Nuclear Magnetic Resonance Imaging in Medicine, A. R. Margulis, ed., Igaku-Shoin Medical Publishers, New York, 11-29.

Brand, R. A. (1986). "Knee Ligaments: A New View." *Journal of Biomechanical Engineering*, 108, 106-110.

Brown, G. A. (1990). "Load-Bearing Role of the Human Knee Meniscus," Doctoral, Massachusetts Institute of Technology, Cambridge, MA.

Buckwalter, J. A. (1999). "Evaluating Methods of Restoring Cartilaginous Articular Surfaces." *Clinical Orthopaedics and Related Research*, 367S, S224-S238.

Bulca, F., Angeles, J., and Zsombor-Murray, P. J. (1999). "On the workspace determination of spherical serial and platform mechanisms." *Mechanism and Machine Theory*, 34, 497-512.

Bylski-Austrow, D. I., Ciarelli, M. J., Kayner, D. C., Matthews, L. S., and Goldstein, S. A. (1994). "Displacements of the Menisci Under Joint Load: An *In Vitro* Study in Human Knees." *Journal of Biomechanics*, 27(4), 421-431.

Bylski-Austrow, D. I., Grood, E. S., Hefzy, M. S., Holden, J. P., and Butler, D. L. (1990). "Anterior Cruciate Ligament Replacements: A Mechanical Study of Femoral Attachment Location, Flexion Angle at Tensioning, and Initial Tension." *Journal of Orthopaedic Research*, 8(4), 522-531.

Bylski-Austrow, D. I., Malumed, J., Meade, T., and Grood, E. S. (1993). "Knee Joint Contact Pressure Decreases After Chronic Meniscectomy Relative to the Acutely Meniscectomized Joint: A Mechanical Study in the Goat." *Journal of Orthopaedic Research*, 11(6), 796-804.

Cai, M.-S., and Rovetta, A. (1990). "A New Algorithm for Workspace Analysis for Robot Manipulators." *Meccanica*, 25, 40-46.

Calhoun, P. S., Kuszyk, B. S., Heath, D. G., Carley, J. C., and Fishman, E. K. (1999). "Three-Dimensional Volume Rendering of Spiral CT Data: Theory and Method." *Radiographics*, 19, 745-764.

Ceccarelli, M. (1995). "A Synthesis Algorithm for Three-Revolute Manipulators by Using an Algebraic Formulation of Workspace Boundary." *Journal of Mechanical Design*, 117, 298-302.

Ceccarelli, M., and Vinciguerra, A. (1995). "On the Wordspace of General 4R Manipulators." *The International Journal of Robotics Research*, 14(2), 152-160.

Chan, S. C. N., and Seedhom, B. B. (1999). "'Equivalent geometry' of the knee and the prediction of tensions along the cruciates: an experimental study." *Journal of Biomechanics*, 32, 35-48.

Chen, E., Ellis, R. E., and Bryant, J. T. (2000). "A Strain-Energy Model of Passive Knee Kinematics for the Study of Surgical Implantation Strategies." *Medical Image Computing and Computer-Assisted Intervention (MICCAI)*, Pittsburg, PA, 1086-1095.

Crowninshield, R., Pope, M. H., and Johnson, R. J. (1976). "An Analytical Model of the Knee." *Journal of Biomechanics*, 9, 397-405.

Crowninshield, R. D. (1978). "Use of Optimization Techniques to Predict Muscle Forces." *Journal of Biomechanical Engineering*, 100, 88-92.

Dandy, D. J., and Edwards, D. J. (1998). *Essential Orthopaedics and Trauma*, Churchill Livingstone, New York.

Davidson, J. K., and Hunt, K. H. (1987a). "Rigid Body Location and Robot Workspaces: Some Alternative Manipulator Forms." *Journal of Mechanisms, Transmissions, and Automation in Design*, 109(2), 224-232.

Davidson, J. K., and Hunt, K. H. (1987b). "Robot Workspace of a Tool Plane: Part 1--A Ruled Surface and Other Geometry." *Journal of Mechanisms, Transmissions, and Automation in Design*, 109, 50-60.

Davidson, J. K., and Pingali, P. (1987). "Robot Workspace of a Tool Plane: Part 2--Computer Generation and Selected Design Conditions for Dexterity." *Journal of Mechanisms, Transmissions, and Automation in Design*, 109, 61-73.

Donahue, T. H., Hull, M. L., Rashid, M. M., and Jacobs, C. R. (2000). "Finite Element Model of te Human Knee Joint to Study Tibio-Femoral Contact Mechanics." *Advances in Bioengineering*, Orlando, Florida, 155-156.

Donaldson, W. F. I., Warren, R. F., and Wickiewicz, T. (1985). "A comparison of acute anterior cruciate ligament examinations. Initial versus examination under anesthesia." *The American Journal of Sports Medicine*, 13(1), 5-10.

Draganich, L. F., Hsieh, Y.-F., and Reider, B. (1996). "Strategies for Attachment Site Locations and Twist of the Intraarticular Anterior Cruciate Ligament Graft." *The American Journal of Sports Medicine*, 24(3), 342-349.

Duck, F. A. (1990). *Physical Properties of Tissue, A Comprehensive Reference Book*, Academic Press, New York.

Ebert-Uphoff, I., and Chirikjian, G. S. (1995). "Efficient Workspace Generation for Binary Manipulators with Many Actuators." *Journal of Robotic Systems*, 12(6), 383-400.

Ellis, R. E. (2000). "From Scans to Sutures: Robotics Methods for Computer-Enhanced Surgery." Robotics Research : The Ninth International Symposium, D. E. Koditschek, ed., Springer-Verlag, New York, New York, 350.

Etzel, K. R., and McCarthy, J. M. (1999). "Interpolation of Spatial Displacements Using the Clifford Algebra of $E^4$." *Journal of Mechanical Design*, 121(1), 39-44.

Fiala, T. G. S., Novelline, R. A., and Yaremchuk, M. J. (1993). "Comparison of CT Imaging Artifacts from Craniomaxillofacial Internal Fixation Devices." *Plastic and Reconstructive Surgery*, 92(7), 1227-1232.

Fischer, I. S. (1998). *Dual-Number Methods in Kinematics, Statics, and Dynamics*, CRC Press, New York.

Fleming, B. C., Beynnon, B. D., Nichols, C. E., Johnson, R. J., and Pope, M. H. (1993). "An in vivo comparison of anterior tibial translation and strain in the anteromedial band of the anterior cruciate ligament." *Journal of Biomechanics*, 26(1), 51-58.

Frank, C. B., and Shrive, N. G. (1994). "Ligament." Biomechanics of the Musculo-Skeletal System, W. Herzog, ed., John Wiley and Sons, Inc., New York, NY, 106-132.

Frankel, V. H., Berstein, A. H., and Brooks, D. B. (1971). "Biomechanics of internal derangement of the knee. Pathomechanics as determined by analysis of the instant centers of motion." *The Journal of Bone and Joint Surgery*, 53-A(5), 945-962.

Freudenstein, F., and Woo, L. S. (1969). "Kinematics of the Human Knee Joint." *Bulletin of Mathematical Biophysics*, 31, 215-232.

Fuller, J., Liu, L.-J., Murphy, M. C., and Mann, R. W. (1997). "A comparison of lower-extremity skeletal kinematics measured using skin- and pin-mounted markers." *Human Movement Science*, 16(2/3), 219-242.

Fuller, J. E., Omeltchenko, A., Butler, J., and Murphy, M. C. (2000). "Visualization of the effects of varying anterior cruciate ligament rest lengths using the total reachable workspace concept." *CAOS*, Bern, Switzerland.

Fung, Y. C. (1993). *Biomechanics, Mechanical Properties of Living Tissues*, Springer-Verlag, Inc., New York.

Furia, J. P., Lintner, D. M., Saiz, P., Kohl, H. W., and Noble, P. (1997). "Isometry Measurements in the Knee With the Anterior Cruciate Ligament Intact, Sectioned, and Reconstructed." *The American Journal of Sports Medicine*, 25(3), 346-352.

Fuss, F. K. (1989). "Anatomy of the Cruciate Ligaments and Their Function in Extension and Flexion of the Human Knee Joint." *The American Journal of Anatomy*, 184, 165-176.

Gibson, C. G., and Hunt, K. H. (1990a). "Geometry of Screw Systems--1, Screws: Genesis and Geometry." *Mechanism and Machine Theory*, 25(1), 1-10.

Gibson, C. G., and Hunt, K. H. (1990b). "Geometry of Screw Systems--2, Classification of Screw Systems." *Mechanism and Machine Theory*, 25(1), 11-27.

Gil, J., Li, G., Kanamori, A., and Woo, S. L.-Y. (1998). "Development of a 3D Computational Human Knee Joint Model." *Advances in Bioengineering*, Anaheim, California, 1-2.

Godest, A.-C., de Cloke, C. S., Taylor, M., Gregson, P. J., Keane, A. J., Sathasivan, S., and Walker, P. S. (2000). "A computational model for the prediction of total knee replacement kinematics in the saggital plane." *Journal of Biomechanics*, 33, 435-442.

Goldman, A. J., and Tucker, A. W. (1956). "Polyhedral Convex Cones." Linear Inequalities and Related Systems, A. W. Tucker, ed., Princeton University Press, Princeton, New Jersey, 19-40.

Goldstein, H. (1980). *Classiscal Mechanics*, Addison-Wesley Publishing Company, Reading, Massachusetts.

Gosselin, C. M., and Guillot, M. (1991). "The Synthesis of Manipulators with Prescribed Workspace." *Journal of Mechanical Design*, 113(4), 451-455.

Gosselin, C. M., Lavoie, E., and Toutant, P. (1992). "An Efficient Algorithm for the Graphical Representation of the Three-Dimensional Workspace of Parallel Manipulators." *Robotics, Spatial Mechanisms, and Mechanical Systems*, DE-Vol. 45, 323-328.

Gray, H. (1995). *Anatomy, Descriptive and Surgical*, Barnes & Noble, New York.

Grood, E. S., Hefzy, M. S., and Lindenfield, T. N. (1989). "Factors affecting the region of most isometric femoral attachments; Part I: The posterior cruciate ligament." *The American Journal of Sports Medicine*, 17(2), 197-207.

Grood, E. S., and Suntay, W. J. (1983). "A Joint Coordinate System for the Clinical Description of Three-Dimensional Motions: Application to the Knee." *Journal of Biomechanical Engineering*, 105, 136-144.

Guillet, G. L. (1956). *Guillet's Kinematics of Machines*, John Wiley & Sons, New York.

Gupta, K. C. (1986). "On the Nature of Robot Workspace." *The International Journal of Robotics Research*, 5(2), 112-121.

Gupta, K. C., and Roth, B. (1982). "Design Considerations for Manipulator Workspace." *Journal of Mechanical Design*, 104(3), 704-711.

Hamilton, S. W. R. (1969). *Elements of Quaternions*, Chelsea Publishing Company.

Hardt, D. E. (1978). "Determining Muscle Forces in the Leg During Normal Human Walking--An Application and Evaluation of Optimization Methods." *Journal of Biomechanical Engineering*, 100, 72-78.

Harrington, I. J. (1976). "A Bioengineering Analysis of Force Actions at the Knee in Normal and Pathological Gait." *Biomedical Engineering*, 11(5), 167-72.

Haug, E. J., Luh, C.-M., Adkins, F. A., and Wang, J.-Y. (1995). "Numerical Algorithms for Mapping Boundaries of Manipulator Workspaces." *Journal of Mechanical Design*, 118(2), 228-234.

Hefzy, M. S., and Abdel-Rahman, E. M. (2000). "Three-Dimensional Dynamic Anatomical Modeling of the Human Knee Joint." Musculoskeletal Models and Techniques, C. Leondes, ed., CRC Press, New York.

Hefzy, M. S., and Cooke, T. D. V. (1996). "Review of knee models: 1996 Update." *Applied Mechanics Review*, 49(10), S187-S193.

Hefzy, M. S., and Grood, E. S. (1988). "Review of knee models." *Applied Mechanics Reviews*, 41(1), 1-13.

Hestenes, D. (1987). *New Foundations for Classical Mechanics*, D. Reidel Publishing Company, Boston, MA.

Hestenes, D., Li, H., and Rockwood, A. (1999). *A Unified Algebraic Framework for Classical Geometry*, Springer, Berlin.

Hestenes, D., and Sobczyk, G. (1984). *Clifford Algebra to Geometric Calculus*, D. Reidel Publishing Company, Boston, MA.

Hestenes, D., and Ziegler, R. (1991). "Projective Geometry with Clifford Algebra." *Acta Applicandae Mathematicae*, 23, 25-63.

Hight, T. K., Piziali, R. L., and Nagel, D. A. (1979). "A Dynamic, Nonlinear Finite-Element Model of a Human Leg." *Journal of Biomechanical Engineering*, 101(August), 176-184.

Hildebrand, F. H., and Johnson, C. G. (1970). *Finite Mathematics*, Prindle, Weber & Schmidt, Inc., Boston, Massachusetts.

Hoyle, K. m. c. (1996). "Characteristics of Injuries and Illnesses Resulting in Absences from Work, 1994." *USDL-96-163*, United States Department of Labor, Bureau of Labor Statistics, Washington, DC.

Huang, S., and Schimmels, J. M. (1998). "The Bounds and Realization of Spatial Stiffnesses Achieved with Simple Springs Connected in Parallel." *IEEE Transactions on Robotics and Automation*, 14(3), 466-475.

Huang, S., and Schimmels, J. M. (2000). "The Eigenscrew Decomposition of Spatial Stiffness Matrices." *IEEE Transactions on Robotics and Automation*, 6(2), 146-156.

Huang, T., Wang, J., and Whitehouse, D. J. (1999). "Closed Form Solution to Workspace of Hexapod-Based Virtual Axis Machine Tools." *Journal of Mechanical Design*, 121, 26-31.

Hunt, K. H. (1978). *Kinematic Geometry of Mechanisms*, Oxford University Press, Oxford.

Ji, Z. (1994). "Workspace Analysis of Stewart Platforms via Vertex Space." *Journal of Robotic Systems*, 11(7), 631-639.

Kane, T. R., and Scher, M. P. (1970). "Human Self-rotation by Means of Limb Movements." *Journal of Biomechanics*, 3, 39-49.

Karger, A. (1996). "Singularity Analysis of Serial Robot-Manipulators." *Journal of Mechanical Design*, 118, 520-525.

Katz, J. W., and Fingeroth, R. J. (1986). "The diagnostic accuracy of ruptures of the anterior cruciate ligament comparing the Lachman test, the anterior drawer sign, and the pivot shift test in acute and chronic knee injuries." *The Amercian Journal of Sports Medicine*, 14(1), 88-91.

Kelly, M. A., Fithian, D. C., Chern, K. Y., and Mow, V. C. (1990). "Structure and Function of the Meniscus: Basic and Clinical Implications." *Biomechanics of Diarthrodial Joints*, S. L.-Y. Woo, ed., Springer-Verlag, New York, 191-211.

Kieffer, J., and Litvin, F. L. (1991). "Swept Volume Determination and Interference Detection for Moving 3-D Solids." *Journal of Mechanical Design*, 113(4), 456-463.

King, A. I. (1984). "A Review of Biomechanical Models." *Journal of Biomechanical Engineering*, 106, 97-104.

Kuipers, J. B. (1999). *Quaternions and Rotation Sequences*, Princeton University Press, Princeton, New Jersey.

Kumar, A., and Patel, M. S. (1986). "Mapping the Manipulator Workspace Using Interactive Computer Graphics." *The International Journal of Robotics Research*, 5(2), 122-130.

Kumar, A., and Waldron, K. J. (1981). "The Workspaces of a Mechanical Manipulator." *Journal of Mechanical Design*, 103, 665-672.

Langrana, N. A., Leppard, D., Alexander, H., and Weiss, A. (1982). "Kinematics of the Knee--A Computer Graphics Model." *ASME Technical Report 82-DET-40*, 1-8.

Lanzendorf, E. J. (1988). "Determination of Material Properties of Ligamentous Tissues in the Human Knee," Master of Science, Massachusetts Institute of Technology, Boston, MA.

LaPrade, R. F., and Burnett, Q. M. I. (1994). "Femoral Intercondylar Notch Stenosis and Correlation to Anterior Cruciate Ligament Injuries." *The American Journal of Sports Medicine*, 22(2), 198-203.

Lasenby, A., Doran, C., and Gull, S. (1993). "Grassmann calculus, pseudoclassical mechanics, and geometric algebra." *Journal of Mathematical Physics*, 34(8), 3683-3712.

Lasenby, J., Lasenby, A. N., and Doran, C. J. L. (2000). "A unified mathematical language for physics and engineering in the 21st century." *Philosophical transactions of the Royal Society of London. Series A, Mathematical and physical sciences*, 358, 21-39.

Latombe, J.-C. (1991). *Robot Motion Planning*, Kluwer Academic Publishers, Bonston, MA.

Lee, J. (2001). "A structured algorithm for minimum $l_\infty$-norm solutions and its application to a robot velocity workspace analysis." *Robotica*, 19, 343-352.

Lee, T. W., and Yang, D. C. H. (1983). "On the Evaluation of Manipulator Workspace." *Journal of Mechanisms, Transmissions, and Automation in Design*, 105, 70-77.

Lewis, J. L., and Lew, W. D. (1978). "A Method for Locating and Optimal "Fixed" Axis of Rotation for the Human Knee Joint." *Journal of Biomechanical Engineering*, 100, 187-193.

Lewis, J. L., Lew, W. D., Engebretsen, L., Hunter, R. E., and Kowalczyk, C. (1990). "Factors Affecting Graft Force in Surgical Reconstruction of the Anterior Cruciate Ligament." *Journal of Orthopaedic Research*, 8(4), 514-521.

Lord, P. J. (1994). "Computer Aided Intertrochanteric Osteotomy Planning and Surgery Simulation," Doctoral, Massachusetts Institute of Technology, Cambridge, MA.

Madhani, A., and Dubowsky, S. (1992). "Design and Motion Planning of Multi-Limb Robotic Systems: The Force-Workspace Approach." *Robotics, Spatial Mechanisms, and Mechanical Systems*, 45.

Martelli, S., Joukhadar, A., Zaffagnini, S., Marcacci, M., Lavallee, S., and Champleboux, G. (1996). "A Fiber-Based ACL Model for Geometrical and Mechanical Simulations." *RR2924*, Institut National de Recherche en Informatique et en Automatique, Montbonnot Saint Martin, France.

Masory, O., and Wang, J. (1992). "Workspace Evaluation of Stewart Platforms." *Robotics, Spatial Mechanisms, and Mechanical Systems*, 45, 337-346.

McLeod, W. D., and Cross, M. J. (1974). "Knee Joint Axis of Rotation." *27th ACEMB*, Philadelphia, Pennsylvania.

Merlet, J.-P. (1995). "Determination of the Orientation Workspace of Parallel Manipulators." *Journal of Intelligent and Robotic Systems*, 13, 143-160.

Merlet, J.-P. (1997). "Designing a Parallel Manipulator for a Specific Workspace." *The Inernational Journal of Robotics Research*, 16(4), 545-556.

Merlet, J.-P. (1998a). "Efficient Computation of the extremum of the Articular Velocities of a Parallel Manipulator in a Translation Workspace." *IEEE International Conference on Robotics and Automation*, Leuven, Belgium, 1976-1981.

Merlet, J.-P. (1998b). "Efficient estimation of the extremal articular forces of a parallel manipulator in a translation workspace." *IEEE International Conference on Robotics and Automation*, Leuven, Belgium, 1982-1987.

Merlet, J.-P., Gosselin, C. M., and Mouly, N. (1998). "Workspaces of Planar Paralel Manipulators." *Mechanism and Machine Theory*, 33(1/2), 7-20.

Mihalko, W. M., and Krackow, K. A. (1999). "Posterior Cruciate Ligament Effects on the Flexion Space in Total Knee Arthroplasty." *Clinical Orthopaedics and Related Research*(360), 243-250.

Miller, R. H. I. (1997). "Knee Injuries." Campbell's Operative Orthopaedics, S. T. Canale, ed., Mosby, St. Louis, MO, 1113-1170.

Minns, R. J. (1981). "Forces at the Knee Joint: Anatomical Considerations." *Journal of Biomechanics*, 14, 633-643.

Morgan, T. G., and Murphy, M. C. (1997). "Thresholding on Bone Density for the Identification of Ligament Insertion Sites of the Human Knee." 381-386.

Morrison, J. B. (1970). "The Mechanics of the Knee Joint in Relation to Normal Walking." *Journal of Biomechanics*, 3, 51-61.

Mow, V. C., Hou, J. S., Owens, J. M., and Ratcliffe, A. (1990). "Biphasic and Quasilinear Viscoelastic Theories for Hydrated Soft Tissues." *Biomechanics of Diarthrodial Joints*, S. L.-Y. Woo, ed., Springer-Verlag, New York, 215-260.

Murphy, M. C. (1990). "Geometry and the Kinematics of the Normal Human Knee," Doctor of Philosophy, Massachusetts Institute of Technology, Cambridge.

Murphy, M. C., and Mann, R. W. (1988). "A Method for Estimating the Total Fredom of the Knee." *ASME Winter Annual Meeting*, Chicago, IL, 55-65.

Murphy, M. C., and Mann, R. W. (1990). "Estimation of the Number of Degrees of freedom in the Normal *in vivo* Human Knee." *Winter Annual Meeting of ASME*, Dallas, TX, 23-29.

Murray, M. P., Seireg, A., and Scholz, R. C. (1967). "Center of gravity, center of pressure, and supportive forces during human activities." *Journal of Applied Physiology*, 23(6), 831-838.

Murray, R. M., Li, Z., and Sastry, S. S. (1994). *A Mathematical Introduction to Robotic Manipulation*, CRC Press, Inc., Boca Raton, Florida.

N.C.A.A. (1999). "Injury Surveillance System." The National Collegiate Athletic Association, 700 W. Washington Street, P.O. Box 6222, Indianapolis, Indiana 46206-6222.

N. E. M. A. (2000). "Digital Imaging and Communications in Medicine (DICOM)." Global Engineering Documents, Englewood, CO, USA.

Nigg, B. M., and Herzog, W. (1994). "Biomechanics of the Musculo-skeletal System." John Wiley & Sons, New York, 578.

Nissan, M. (1980). "Review of Some Basic Assumptions in Knee Biomechanics." *Journal of Biomechanics*, 13, 375-381.

Noyes, F. R. (1986). "Levels of Knee Joint Research. How do We Bridge the Gap." *Journal of Biomechanical Engineering*, 108, 100-105.

Ohwovoriole, M. S. (1980). "An Extension of Screw Theory and its Application to the Automation of Industrial Assemblies," Doctor of Philosophy, Stanford University.

Ohwovoriole, M. S., and Roth, B. (1981). "An Extension of Screw Theory." *Journal of Mechanical Design*, 103(3), 725-735.

Omeltchenko, A. (1997). "An Energy-Based Method for Evaluating Constraint Recruitment in the Knee," Masters Thesis, Louisiana State University, Baton Rouge, LA.

Omeltchenko, A., and Murphy, M. C. (1998). "An energy-based method for elucidating the constraints in the human knee." *Transactions of the 44th Annual Meeting of the Orthopaedic Research Society*, New Orleans, LA, 1112.

Ortiz, G. J., Schmotzer, H., Bernbeck, J., Graham, S., Tibone, J. E., and Vangsness Jr., C. T. (1998). "Isometry of the Posterior Cruciate Ligament, Effects of Functional Load and Muscle Force Application." *The American Journal of Sports Medicine*, 26(5), 663-668.

Patriarco, A. G., Mann, R. W., Simon, S. R., and Mansour, J. M. (1981). "An Evaluation of the Approaches of Optimization Models in the Prediction of Muscle Forces During Human Gait." *Journal of Biomechanics*, 14(8), 513-525.

Pennock, G. R., and Clark, K. J. (1990). "An Anatomy-Based Coordinate System for the Description of the Kinematic Displacements in the Human Knee." *Journal of Biomechanics*, 23(12), 1209-1218.

Phillips, J. (1984). *Freedom in Machinery: Introducing Screw Theory*, Cambridge University Press, New York, New York.

Phillips, J. (1990). *Freedom in Machinery: Screw Theory Exemplified*, Cambridge University Press, New York, New York.

Piziali, R. L., Seering, W. P., Nagel, D. A., and Schurman, D. J. (1980). "The Function of the Primary Ligaments of the Knee in Anterior-Posterior and Medial-Lateral Motions." *Journal of Biomechanics*, 13, 777-784.

Pope, M. H., Crowninshield, R., Miller, R., and Johnson, R. (1976). "The Static and Dynamic Behavior of the Human Knee *in Vivo*." *Journal of Biomechanics*, 9, 449-452.

Race, A., and Amis, A. A. (1996). "Loading of the two bundles of the posterior crucialte ligament: An analysis of bundle function in A-P Drawer." *Journal of Biomechanics*, 29(7), 873-879.

Rao, A. C., and Anne, J. (1998). "Topology Based Characteristics of Kinematic Chains: Work Space, Rigidity, Input-joint and Isomorphism." *Mechanism and Machine Theory*, 33(5), 625-638.

Rasband, W. (2000). "ImageJ." National Institutes of Health.

Rath, E., and Richmond, J. C. (2000). "The menisci: basic science and advances in treatment." *British Journal of Sports Medicine*, 34, 252-257.

Ribitsch, V. O. (1990). "Viscoelastic Behaviour of Synovial Fluids and Artificial Replacements." *Biomechanics of Diarthrodial Joints*, S. L.-Y. Woo, ed., Springer-Verlag, New York, 287-304.

Rimon, E., and Burdick, J. W. (1995a). "A configuration Space Analysis of Bodies in Contact--I. 1st Order Mobility." *Mechanism and Machine Theory*, 30(6), 897-912.

Rimon, E., and Burdick, J. W. (1995b). "A configuration Space Analysis of Bodies in Contact--II. 2nd Order Mobility." *Mechanism and Machine Theory*, 30(6), 913-928.

Röhrle, H., Scholten, R., Sigolotto, C., Sollbach, W., and Kellner, H. (1984). "Joint Forces in the Human Pelvis-Leg Skeleton During Walking." *Journal of Biomechanics*, 17(6), 409-424.

Romanes, G. J. (1986). *Cunningham's Manual of Practical Anatomy*, Oxford University Press, New York.

Romdhane, L. (1994). "Orientation workspace of fully parallel mechanisms." *European Journal of Mechanics A - Solids*, 13(4), 541-553.

Roth, B. (1976). "Performance Evaluation of Manipulators From a Kinematic Viewpoint." *Performance Evaluation of Programmable Robots and Manipulators*, NBS Special Publications No. 459, 39-61.

Roth, B. (1983). "Screws, Motors, and Wrenches that Cannot be Bought in a Hardware Store." *Robotics Research, The First International Symposium*, Bretton Woods, NH, 679-693.

Schreiber, S. (1997). "The displacement workspace of the human knee joint," Doctoral, Technischen Universität Darmstadt, Darmstadt, Germany.

Scion Corporation (2000). "Scion Image.", 82 Worman's Mill Ct., Suite H, Frederick, MD 21701.

Seely, F. B., and Ensign, N. E. (1933). *Analytical Mechanics for Engineers*, John Wiley and Sons, Inc., New York, NY.

Seireg, A., and Arvikar, R. J. (1973). "A Mathematical Model for Evaluation of Forces in Lower Extremeties of the Musculo-Skeletal System." *Journal of Biomechanics*, 6, 313-326.

Selig, J. M. (1996). *Geometrical Methods in Robotics*, Springer, New York.

Sen, D., and Mruthyunjaya, T. S. (1999). "Synthesis of workspaces of planar manipulators with arbitrary topology using shape representation and simulated annealing." *Mechanism and Machine Theory*, 34, 391-420.

Shoemaker, S. C., and Markolf, K. L. (1985). "Effects of Joint Load on the Stiffness and Laxity of Ligament-Deficient Knees." *The Journal of Bone and Joint Surgery*, 67-A(1), 136-146.

Shrive, N. G., and Frank, C. B. (1994). "Articular Cartilage." Biomechanics of the Musculo-Skeletal System, W. Herzog, ed., John Wiley and Sons, Inc., New York, NY, 79-105.

Sidles, J. A., Larson, R. V., Garbini, J. L., Downey, D. J., and Matsen, F. A. I. (1988). "Ligament Length Relationships in the Moving Knee." *Journal of Orthopaedic Research*, 6(4), 593-610.

Sisk, T. D. (1987). "Knee Injuries." Campbell's Operative Orthopaedics, A. H. Crenshaw, ed., The C. V. Mosby Company, St. Louis, 2283-2483.

Smith, P. G., and Kane, R. R. (1968). "On the dynamics of the human body in free fall." *Journal of Applied Mechanics*, 35, 167-168.

Spanos, J., and Kohli, D. (1985). "Workspace Analysis of Regional Structures of Manipulators." *Journal of Mechanisms, Transmissions, and Automation in Design*, 107, 216-222.

Stoianovici, D., Whitcomb, L. L., J.H., A., R.H., T., and L.R., K. (1998). "A Modular Surgical Robotic System for Image Guided Percutaneous Procedures." *Lecture Notes in Computer Science*, 1496, 404-410.

Sugimoto, K., and Duffy, J. (1981a). "Determination of Extreme Distances of a Robot Hand - 1. A General Theory." *Journal of Mechanical Design*, 103(3), 631-636.

Sugimoto, K., and Duffy, J. (1981b). "Determination of Extreme Distances of a Robot Hand - Part 2: Robot Arms with Special Geometry." *Journal of Mechanical Design*, 103(4), 776-783.

Sugimoto, K., Duffy, J., and Hunt, K. H. (1982). "Special Configurations of Spatial Mechanisms and Robot Arms." *Mechanism and Machine Theory*, 17(2), 119-132.

Sutherland, C. J., and Gayou, D. E. (1996). "Artifacts and Thresholding in X-Ray CT of a Cortical Bone and Titanium Composite." *Journal of Computer Assisted Tomography*, 20(3), 496-503.

Taxt, T., and Lundervold, A. (1994). "Multispectral Analysis of the Brain in Magnetic Resonance Imaging." *IEEE Workshop on Biomedical Image Analysis*, Seattle, Washington, 33-42.

Tewes, D. P., Fritts, H. M., Fields, R. D., Quick, D. C., and Buss, D. D. (1997). "Chronically Injured Posterior Cruciate Ligament." *Clinical Orthopaedics and Related Research*, 335, 224-232.

Torzilli, P. A., Asakari, E., and Jenkins, J. T. (1990). "Water Content and Solute Diffusion Properties in Articular Cartilage." *Biomechanics of Diarthrodial Joints*, S. L.-Y. Woo, ed., Springer-Verlag, New York, 363-390.

Töyräs, J., Lyyra-Laitinen, T., Niinimäki, M., Lindgren, R., Nieminen, M. T., Kiviranta, I., and Jurvelin, J. S. (2001). "Estimation of the Young's modulus of articular cartilage using an arthroscopic indentation instrument and ultrasonic measurement of tissue thickness." *Journal of Biomechanics*, 34, 251-256.

Tsai, L.-W. (1999). *Robot Analysis: The Mechanics of Serial and Parallel Manipulators*, John Wiley & Sons, New York.

Tsai, M. J., and Lee, H. W. (1993). "On the Special Bases of Two- and Three-Screw Systems." *Journal of Mechanical Design*, 115(3), 540-546.

van den Bogert, A. J. (1994). "Analysis and Simulation of Mechanical Loads on the Human Musculoskeletal System: A Methodological Overview." *Exercise and Sport Sciences Reviews*, 22, 23-51.

Viidik, A. (1990). "Structure and Function of Normal and Healing Tendons and Ligaments." *Biomechanics of Diarthrodial Joints*, S. L.-Y. Woo, ed., Springer-Verlag, New York, New York, 3-38.

Wheeless, C. R. I. (2001). "Wheeless' Textbook of Orthopaedics."

Wismans, J., Veldpaus, F. E., Janssen, J., Huson, A., and Struben, P. (1980). "A Three-Dimensional Mathematical Model of the Knee-Joint." *Journal of Biomechanics*, 13, 677-685.

Woo, S. L.-Y., Weiss, J. A., and MacKenna, D. A. (1990). "Biomechanics and Morphology of the Medial Colateral and Anterior Cruciate Ligaments." *Biomechanics of Diarthrodial Joints*, S. L.-Y. Woo, ed., Springer-Verlag, New York, 63-104.

Woo, S. L.-Y., and Young, E. P. (1991). "Structure and Function of Tendons and Ligaments." *Basic Orthopaedic Biomechanics*, W. C. Hayes, ed., Raven Press, New York, 199-244.

Yamamoto, K., Hirokawa, S., and Kawada, T. (1998). "Strain Distribution in the Ligament Using Photoelasticity. A Direct Application to the Human ACL." *Medical Engineering and Physics*, 20, 161-168.

Yang, A. T. (1974). "Calculus of Screws." Basic Questions of Design Theory, W. R. Spillers, ed., Elsevier, New York, 266-281.

Yang, D. C. H., and Lee, T. W. (1983). "On the Workspace of Mechanical Manipulators." *Journal of Mechanisms, Transmissions, and Automation in Design*, 105(March), 62-70.

Yang, F.-C., and Haug, E. J. (1994a). "Numerical Analysis of the Kinematic Dexterity of Mechanisms." *Journal of Mechanical Design*, 116, 119-126.

Yang, F.-C., and Haug, E. J. (1994b). "Numerical Analysis on the Kinematic Working Capability of Mechanisms." *Journal of Mechanical Design*, 116, 111-118.

Zhang, M.-L. (1995). "Mapping the displacement workspace of the human knee," Masters Thesis, Louisiana State University, Baton Rouge, LA.

Zhang, M. and Murphy, M.C. (1995) "Mapping the displacement workspace of the human knee," *Proceedings of the 19th Annual Meeting of the American Society of Biomechanics*, Palo Alto, CA, August 1995, p. 257.

Zhang, S. J., Howard, D., and Sanger, D. J. (1996a). "Workspaces of a walking machine and their graphical representation. Part II: static workspaces." *Robotica*, 14(2), 219-226.

Zhang, S. J., Sanger, D. J., and Howard, D. (1996b). "Workspaces of a walking machine and their graphical representation. Part I: kinematic workspaces." *Robotica*, 14(1), 71-79.

# APPENDICES

## Appendix A Quaternions

### A.1 Basic Properties

A quaternion, $\mathbf{q}$, is a four dimensional vector that may be represented as a 4-tuple or equivalently as the sum of a scalar and vector quantities as shown in Equation A.1.

$$\mathbf{q} = (q_0, q_1, q_2, q_3) = q_0 + q_1\vec{\mathrm{i}} + q_2\vec{\mathrm{j}} + q_3\vec{\mathrm{k}} \qquad \text{A.1}$$

Some properties of the elements in Equation A.1 are listed in the following expressions.

$$\{q_0, q_1, q_2, q_3\} \in \Re \qquad \text{A.2a}$$

$$\{\vec{\mathrm{i}}, \vec{\mathrm{j}}, \vec{\mathrm{k}}\} \in \text{orthonormal quaternion basis} \qquad \text{A.2b}$$

$$\vec{\mathrm{i}}^2 = \vec{\mathrm{j}}^2 = \vec{\mathrm{k}}^2 = ijk = -1 \qquad \text{A.2c}$$

$$ij = k, ji = -k, jk = i, kj = -i, ki = j, ik = -j \qquad \text{A.2d}$$

Two quaternions, $\mathbf{p}$ and $\mathbf{q}$, are said to be equivalent if and only if they satisfy all of the relationships given in Equations A.3a-A.3d.

$$q_0 = p_0 \qquad \text{A.3a}$$

$$q_1 = p_1 \qquad \text{A.3b}$$

$$q_2 = p_2 \qquad \text{A.3c}$$

$$q_3 = p_3 \qquad \text{A.3d}$$

The sum of two quaternions, $\mathbf{p}$ and $\mathbf{q}$, is given by Equation A.4.

$$\mathbf{q} + \mathbf{p} = (q_0 + p_0) + (q_1 + p_1)\vec{\mathrm{i}} + (q_2 + p_2)\vec{\mathrm{j}} + (q_3 + p_3)\vec{\mathrm{k}} \qquad \text{A.4}$$

The product of a scalar, $a$ and quaternion, $\mathbf{q}$, is given by Equation A.5.

$$a\mathbf{q} = aq_0 + aq_1\vec{\mathrm{i}} + aq_2\vec{\mathrm{j}} + aq_3\vec{\mathrm{k}} \qquad \text{A.5}$$

The product of two quaternions, $\mathbf{p}$ and $\mathbf{q}$, is given by Equation A.6.

$$\mathbf{qp} = (q_0p_0 - q_1p_1 - q_2p_2 - q_3p_3) + (q_0p_1 + q_1p_0 + q_2p_3 - q_3p_2)\vec{i} + (q_0p_2 + q_2p_0 + q_3p_1 - q_1p_3)\vec{j} + (q_0p_3 + q_3p_0 + q_1p_2 - q_2p_1)\vec{k} \quad \text{A.6}$$

The complex conjugate of a quaternion, $\mathbf{q}$, is given by Equation A.7.

$$\mathbf{q}^* = q_0 - q_1\vec{i} - q_2\vec{j} - q_3\vec{k} \quad \text{A.7}$$

Useful properties of the complex conjugate are included in Equations A.8a and A.8b.

$$\mathbf{q} + \mathbf{q}^* = 2q_0 \quad \text{A.8a}$$

$$(\mathbf{pq})^* = \mathbf{q}^*\mathbf{p}^* \quad \text{A.8b}$$

This leads to the definition of the Norm, $N(\mathbf{q})$, of a quaternion, $\mathbf{q}$, given by Equation A.9.

$$N(\mathbf{q}) = \sqrt{\mathbf{q}^*\mathbf{q}} = \sqrt{q_0^2 + q_1^2 + q_2^2 + q_3^2} \quad \text{A.9}$$

Bringing together the norm and complex conjugate, the inverse, $\mathbf{q}^{-1}$, of a quaternion, $\mathbf{q}$, is given by Equation A.10.

$$\mathbf{q}^{-1} = \frac{\mathbf{q}^*}{N^2(\mathbf{q})} \quad \text{A.10}$$

If the norm of a quaternion is equal to 1, the quaternion is said to be a unit quaternion and by Equation A.10, the inverse of a unit quaternion can be seen to be its complex conjugate. (Kuipers, 1999)

**A.2 Quaternions as Rotations**

Given some point $p$ in three-dimensional space, written as a sum of the orthonormal unit vectors of Equation A.2b, and a unit quaternion $\mathbf{q}$ of the form of Equation A.11, then Equation A.12 represents a rotation of the point $p$ about the axis defined by $\bar{u}$ through the angle $\theta$.

$$\begin{gathered} \mathrm{q} = \cos\left(\frac{\theta}{2}\right) + \sin\left(\frac{\theta}{2}\right)\vec{u} \\ \vec{u} = \left(x\vec{i} + y\vec{j} + z\vec{k}\right), \text{a unit vector} \\ \theta, x, y, z \in \Re \end{gathered} \qquad \text{A.11}$$

$$p' = \mathrm{q}p\mathrm{q}^{*} \qquad \text{A.12}$$

The following example shows a simple rotation of the Cartesian point $p = (5,0,0)$ 90° about the positive Cartesian y-axis. The unit quaternion is given in Equation A.13.

$$\begin{aligned} \mathrm{q} &= \cos(45°) + \sin(45°)\left(0\vec{i} + \vec{j} + 0\vec{k}\right) \\ \mathrm{q} &= \frac{1}{\sqrt{2}}\left(1 + \vec{j}\right) \end{aligned} \qquad \text{A.13}$$

The rotation is then carried out as shown in Equation A.14 resulting in the expected transformed point $p' = (0,0,-5)$.

$$\begin{aligned} p' &= \frac{1}{\sqrt{2}}\left(1 + \vec{j}\right)\left(5\vec{i} + 0\vec{j} + 0\vec{k}\right)\frac{1}{\sqrt{2}}\left(1 - \vec{j}\right) \\ &= \frac{1}{2}\left(1 + \vec{j}\right)\left(5\vec{i}\right)\left(1 - \vec{j}\right) \\ &= \frac{1}{2}\left(5\vec{i} + 5\vec{j}\vec{i}\right)\left(1 - \vec{j}\right) \\ &= \frac{1}{2}\left(5\vec{i} - 5\vec{k} - 5\vec{i}\vec{j} + 5\vec{k}\vec{j}\right) \\ &= \frac{1}{2}\left(5\vec{i} - 5\vec{k} - 5\vec{k} - 5\vec{i}\right) \\ &= -5\vec{k} \end{aligned} \qquad \text{A.14}$$

## Appendix B Plücker and Screw Coordinates

Consider a unit vector $\bar{\mathbf{v}} = v_x\bar{\mathbf{i}} + v_y\bar{\mathbf{j}} + v_z\bar{\mathbf{k}}$ in the usual Cartesian coordinate system (where $(\bar{\mathbf{i}}, \bar{\mathbf{j}}, \bar{\mathbf{k}})$ represent the orthonormal unit vectors of the Cartesian frame) that passes through the point $\mathbf{p} = (p_x, p_y, p_z)$. The vector from the origin to $\mathbf{p}$ is given by $\bar{\mathbf{p}} = p_x\bar{\mathbf{i}} + p_y\bar{\mathbf{j}} + p_z\bar{\mathbf{k}}$. The Plücker coordinates (or line coordinates) of the line through the point $\mathbf{p}$ in the direction of $\bar{\mathbf{v}}$ are given by the six quantities $(L, M, N, P, Q, R)$ defined by Equation B.1. (Ohwovoriole, 1980)

$$\begin{bmatrix} L \\ M \\ N \\ P \\ Q \\ R \end{bmatrix} = \begin{bmatrix} \bar{\mathbf{v}} \\ \bar{\mathbf{p}} \times \bar{\mathbf{v}} \end{bmatrix} = \begin{bmatrix} v_x \\ v_y \\ v_z \\ p_y v_z - p_z v_y \\ p_z v_x - p_x v_z \\ p_x v_y - p_y v_x \end{bmatrix} \qquad \text{B.1}$$

Multiplication of the Plücker coordinates by a scalar has the same effect as scaling the unit vector by the same magnitude. With this realization, the Plücker coordinates may now be defined by the location of any two distinct points lying along a line as the line defined by Plücker coordinates remains invariant under scalar multiplication. Consider two points $\mathbf{p}$ and $\mathbf{r}$ in space given by $\mathbf{p} = (p_x, p_y, p_z)$, and $\mathbf{r} = (r_x, r_y, r_z)$. The Plücker coordinates $(L, M, N, P, Q, R)$ of the line that contains the two points are given by

$$\begin{bmatrix} L \\ M \\ N \\ P \\ Q \\ R \end{bmatrix} = \frac{1}{\sqrt{(r_x - p_x)^2 + (r_y - p_y)^2 + (r_z - p_z)^2}} \begin{bmatrix} r_x - p_x \\ r_y - p_y \\ r_z - p_z \\ p_y r_z - p_z r_y \\ p_z r_x - p_x r_z \\ p_x r_y - p_y r_x \end{bmatrix} \quad \text{B.2}$$

Of the six variables defining the Plücker coordinates, only four are independent. $L$, $M$, and $N$ are proportional to the direction cosines of the line, causing only two to be independent. The parameters $P$, $Q$ and $R$ define the "moment" of the line about the origin, manifested by a line through the origin, perpendicular to the line defined by the Plücker coordinates. Mathematically this restriction is expressed as Equation B.3.

$$LP + MQ + NR = 0 \quad \text{B.3}$$

Associating a pitch $(\lambda)$, which characterizes some metric of length, with a line in space defines a screw axis. The pitch describes the ratio of a linear displacement parallel to the line in space to an angular displacement about the line in space. The screw axis may be defined using Plücker coordinates as described in Equation B.4. These six parameters define Ball's screw coordinates, five of which are independent.

$$\begin{bmatrix} \$_1 \\ \$_2 \\ \$_3 \\ \$_4 \\ \$_5 \\ \$_6 \end{bmatrix} = \begin{bmatrix} L \\ M \\ N \\ P + \lambda L \\ Q + \lambda M \\ R + \lambda N \end{bmatrix} \quad \text{B.4}$$

Similar to Plücker coordinates for lines, screw coordinates used to define screw axes are also invariant under scalar multiplication. Scalar multiplication of screw coordinates effectively reduces to scalar multiplication of the Plücker coordinates

defining the line along which the screw is defined. The pitch is not altered. Only when a sixth independent parameter is specified, defining the intensity or magnitude of the screw displacement, does scalar multiplication have an effect. With the intensity defined, the screw coordinates now define a finite screw displacement, and it is this intensity that is affected by a scalar multiplication.

The pitch of a screw may be extracted from screw coordinates through the use of Equation B.5, which is a direct result of the application of the condition described by Equation B.3.

$$\lambda = \frac{\$_1\$_4 + \$_2\$_5 + \$_3\$_6}{\$_1^{\,2} + \$_2^{\,2} + \$_3^{\,2}} \qquad \text{B.5}$$

As is shown by Equation B.4, a zero pitch screw reduces to the Plücker coordinates of the line defining the screw axis. An infinite pitch screw has for its first three coordinates, all zeros, $\$_1=0$, $\$_2=0$, and $S_3=0$, and for its last three coordinates, $\$_4$, $\$_5$, and $S_6$, values proportional to the direction cosines of line at infinity, normal to the screw axis.

Twists are infinitesimal screw displacements and may be designated by screw coordinates that define a screw axis. A zero pitch twist represents a pure, infinitesimal rotation, while an infinite pitch twist represents a pure, infinitesimal translation.

Wrenches are the combination of a force along an axis with a couple about the same axis and may be represented with screw coordinates. A zero pitch wrench corresponds to a pure force while an infinite pitch wrench corresponds to a pure couple.

## Appendix C Geometric Algebra

The basis for the construction of geometric algebras is the definition of the geometric product (also known as the Clifford product) of two vectors. The geometric product of an $n$-dimensional vector space over the real numbers must satisfy three basic axioms. These include the associative rule, distributive rule, and contraction rule and are shown in Equations C.1a, C.1b, and C.1c respectively.

$$a(bc) = (ab)c \qquad \text{C.1a}$$

$$a(b+c) = ab + ac \qquad \text{C.1b (1)}$$

$$(b+c)a = ba + ca \qquad \text{C.1b (2)}$$

$$a^2 = |a|^2 \qquad \text{C.1c}$$

Both distributive rules are necessary as the geometric product is not generally commutative while the contraction rule is required for the space to be considered Euclidean.

Often it is useful to divide the geometric product of two Euclidean vectors $\bar{\mathbf{a}}$ and $\bar{\mathbf{b}}$, expressed herein as $\bar{\mathbf{a}}\bar{\mathbf{b}}$, into symmetric and antisymmetric parts. Doing so gives the general expression shown in Equation C.2 for the geometric product of the vectors $\bar{\mathbf{a}}$ and $\bar{\mathbf{b}}$.

$$\bar{\mathbf{a}}\bar{\mathbf{b}} = \bar{\mathbf{a}} \cdot \bar{\mathbf{b}} + \bar{\mathbf{a}} \wedge \bar{\mathbf{b}} \qquad \text{C.2}$$

Geometric algebras can be constructed from the products of any finite dimension vector space, however for the sake of usefulness, familiarity and simplicity, the following example construction will be carried out using a nonhomogeneous representation for the three-dimensional Euclidean vector space. Here, $\bar{\mathbf{a}} \cdot \bar{\mathbf{b}}$ is the standard scalar or dot product of the two (three-dimensional) vectors $\bar{\mathbf{a}}$ and $\bar{\mathbf{b}}$, and $\bar{\mathbf{a}} \wedge \bar{\mathbf{b}}$ is called the outer or wedge product of the two vectors $\bar{\mathbf{a}}$ and $\bar{\mathbf{b}}$. The outer

product or wedge product gives rise to a new class of vectors called bivectors. Extending the notion that a vector can be interpreted as an oriented line segment in three dimensions, a bivector can be analogously interpreted as an oriented plane segment in three-dimensional Euclidean space, while a trivector can be interpreted as a "directed" volume in three-dimensional Euclidean space. Figure C.1 gives a graphical representation of vectors $\vec{\mathbf{a}}, \vec{\mathbf{b}}$, and $\vec{\mathbf{c}}$, along with the bivector $\vec{\mathbf{a}} \wedge \vec{\mathbf{b}}$ in a general Cartesian reference frame denoted by $i, j$, and $k$.

Consider the following example using the Cartesian basis vectors given in Equation C.3:

$$\begin{aligned} \vec{i} &= e_1 \\ \vec{j} &= e_2 \\ \vec{k} &= e_3 \end{aligned} \qquad \text{C.3}$$

The geometric algebra generated by these basis vectors has the following eight basis elements:

$$\{1, e_1, e_2, e_3, e_{23}, e_{31}, e_{12}, e_{123}\}$$

consisting of a scalar $(1)$, three vectors $(e_1, e_2, e_3)$, three bivectors $(e_{23}, e_{31}, e_{12})$ and a trivector $(e_{123})$, which represents the pseudoscalar for this particular geometric algebra.

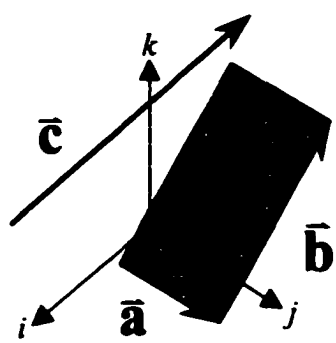


Figure C.1 Visual interpretation of vectors and bivectors

Defining the two Cartesian vectors $\bar{\mathbf{a}}$ and $\bar{\mathbf{b}}$ as in Equations C.4a and C.4b, then the geometric product of those two vectors is computed as shown in Equation C.5.

$$\bar{\mathbf{a}} = a_1 e_1 + a_2 e_2 + a_3 e_3 \qquad \text{C.4a}$$

$$\bar{\mathbf{b}} = b_1 e_1 + b_2 e_2 + b_3 e_3 \qquad \text{C.4b}$$

As the geometric algebra is not, in general, commutative, the order of the multiplication among vectors must be preserved. The scalar coefficients, however, are commutative with respect to multiplication and can be manipulated as such for convenience.

$$\begin{aligned}\bar{\mathbf{a}}\bar{\mathbf{b}} = {} & a_1 b_1 e_1 e_1 + a_1 b_2 e_1 e_2 + a_1 b_3 e_1 e_3 + a_2 b_1 e_2 e_1 + a_2 b_2 e_2 e_2 \\ & + a_2 b_3 e_2 e_3 + a_3 b_1 e_3 e_1 + a_3 b_2 e_3 e_2 + a_3 b_3 e_3 e_3\end{aligned} \qquad \text{C.5}$$

The basis unit vectors defined in the base Cartesian frame are anticommutative in the geometric algebra with respect to multiplication allowing the simplifications and substitutions found in Equations C.6a, C.6b, C.6c, and C.6d to be applied to Equation C.5.

$$e_2 e_3 = -e_3 e_2 = e_{23} \qquad \text{C.6a}$$

$$e_3 e_1 = -e_1 e_3 = e_{31} \qquad \text{C.6b}$$

$$e_1 e_2 = -e_2 e_1 = e_{12} \qquad \text{C.6c}$$

$$e_1 e_1 = e_2 e_2 = e_3 e_3 = 1 \qquad \text{C.6d}$$

The expression for the geometric product originally defined in Equation C.2 for the general geometric algebra is now seen in Equation C.7, expanded for the familiar, Euclidean three-dimensional vector space.

$$\bar{\mathbf{a}}\bar{\mathbf{b}} = (a_1 b_1 + a_2 b_2 + a_3 b_3) + (a_2 b_3 - a_3 b_2) e_{23} + (a_3 b_1 - a_1 b_3) e_{31} + (a_1 b_2 - a_2 b_1) e_{12} \qquad \text{C.7}$$

From Equation C.7 explicit expressions can be extracted for the inner (scalar) and outer (wedge) products of two (one)-vectors in Euclidean space as shown in Equations C.8 and C.9 respectively.

$$\bar{\mathbf{a}}\cdot\bar{\mathbf{b}} = (a_1b_1 + a_2b_2 + a_3b_3) = \frac{1}{2}(\bar{\mathbf{a}}\bar{\mathbf{b}} + \bar{\mathbf{b}}\bar{\mathbf{a}}) \qquad \text{C.8}$$

$$\bar{\mathbf{a}}\wedge\bar{\mathbf{b}} = (a_2b_3 - a_3b_2)e_{23} + (a_3b_1 - a_1b_3)e_{31} + (a_1b_2 - a_2b_1)e_{12} = \frac{1}{2}(\bar{\mathbf{a}}\bar{\mathbf{b}} - \bar{\mathbf{b}}\bar{\mathbf{a}}) \qquad \text{C.9}$$

The even sub-algebra spanned by the basis of the geometric algebra generated by the three-dimensional (nonhomogeneous) Euclidean vector space consists of all linear combinations involving the zero-dimensional scalar basis and the two-dimensional basis bivector elements. The most striking feature of this sub-algebra is that it is a representation for the quaternion algebra discussed in Appendix A. In fact, one of the main motivations behind Hamilton's development of quaternions was the investigation of the quotient of vectors, which he notes "must be conceived as some converse act to geometric multiplication". (Hamilton, 1969) Within this even sub-algebra, the scalar corresponds to the scalar part of a quaternion while the bivectors are analogous to the three right versors defining the basis of the vector part of the quaternion (*I, J, K*). The versors are written in capitals to distinguish them from the previous Cartesian basis vectors (*i, j, k*).

Hamilton fully recognized this implication in his development and discussion of quaternions, showing that the product of two vectors was itself a quaternion with the scalar and vector parts given by the right hand sides of Equations C.8 and C.9, respectively. (Hamilton, 1969) The basis elements give above, however are not identical to the right versors defined by Hamilton. The bivectors $\{e_{23}, e_{31}, e_{12}\}$ maintain the familiar property of squaring to –1, however as shown in Equation C.10, the product

of the three basis bivectors in the order analogous to their Hamiltonian representation does not result in the same –1 as the right versors in Hamilton's original development do.

$$e_{23}e_{31}e_{12} = e_{233112} = e_2e_3^2e_1^2e_2 = e_2^2 = 1 \neq -1 \qquad \text{C.10}$$

This difference comes from the fact that Hamilton defined his basis by using the idea of the vector quotients whereas geometric algebra employs the idea of the geometric product to obtain its basis set. Figure C.2 is a regeneration of the reference coordinate system that Hamilton uses to define his basis within his development of quaternions. (Hamilton, 1969)

Using the same unit vectors (OI, OJ, and OK) the analogous geometric algebra bases may be constructed as shown in the Equations of C.11. The ternary product may then be computed in the terms of the geometric algebra representation as shown in Equation C.12, recalling the contraction rule of Equation C.1c.

$$\begin{aligned} e_{23} &= (-\mathrm{OJ})(\mathrm{OK}) \\ e_{31} &= (\mathrm{OK})(\mathrm{OI}) \\ e_{12} &= (\mathrm{OI})(-\mathrm{OJ}) \end{aligned} \qquad \text{C.11}$$

$$\begin{aligned} e_{23}e_{31}e_{12} &= (-\mathrm{OJ})(\mathrm{OK})(\mathrm{OK})(\mathrm{OI})(\mathrm{OI})(-\mathrm{OJ}) \\ &= (-\mathrm{OJ})(\mathrm{OK})^2(\mathrm{OI})^2(-\mathrm{OJ}) \\ &= (-\mathrm{OJ})|\mathrm{OK}|^2|\mathrm{OI}|^2(-\mathrm{OJ}) \\ &= (-\mathrm{OJ})(1)(1)(-\mathrm{OJ}) \\ &= (-\mathrm{OJ})(-\mathrm{OJ}) \\ &= (\mathrm{OJ})^2 \\ &= |\mathrm{OJ}|^2 \\ &= 1 \end{aligned} \qquad \text{C.12}$$

$$i = \frac{OK}{OJ} = \frac{-OJ}{OK} = \frac{-OK}{-OJ} = \frac{OJ}{-OK}$$
$$j = \frac{OI}{OK} = \frac{-OK}{OI} = \frac{-OI}{-OK} = \frac{OK}{-OI}$$
$$k = \frac{OJ}{OI} = \frac{-OI}{OJ} = \frac{-OJ}{-OI} = \frac{OI}{-OJ}$$

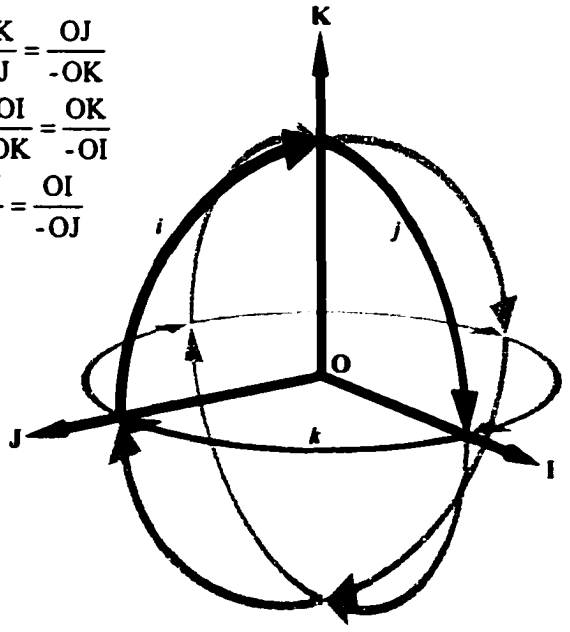


$$ijk = \frac{OK}{OJ} \cdot \frac{OI}{OK} \cdot \frac{OJ}{OI}$$
$$= \frac{-OJ}{OK} \cdot \frac{OK}{-OI} \cdot \frac{-OI}{OJ}$$
$$= \frac{-OJ}{OJ}$$
$$= -1$$

Figure C.2 Hamilton's $i, j$, and $k$ basis unit versors

Care should be taken when simplifying a sequence of vector quotients written in Hamilton's left-handed notation. Notice that a numerator may cancel (in the sense of combining fractions) only with a denominator to the immediate left, but not with one to the immediate right. The geometric algebra basis vectors also exhibit this feature but it is presented as the more widely recognized property of anticommutativity.

The basic properties and features included in this appendix represent but an introduction to the power and completeness of geometric algebras. The observation that the quaternion algebra resides in the geometric algebra generated by nonhomogeneous Euclidean three-space gives an indication of the potential that geometric algebra representations may hold. The fact that the construction was performed by simple algebraic manipulations with minimal restrictions suggests straightforwardness in the use of such representations. The works of Hestenes (Hestenes, 1987; Hestenes, et al., 1999; Hestenes and Ziegler, 1991), Etzel and McCarthy (Etzel and McCarthy, 1999),

Lasenby, et al. (Lasenby, et al., 1993) and Lasenby, et al. (Lasenby, et al., 2000) are suggested references for more rigorous discussions of geometric algebras, their properties, and for some intriguing applications.

# VITA

John Eric Fuller was born and raised in Shreveport, Louisiana. Following his graduation from Captain Shreve High School in 1991, John followed in the footsteps of his only sibling, enrolling in Louisiana State University, from where he earned a Bachelor's of Science degree in Mechanical Engineering in the Spring of 1995. Unable to get the bayou out of his blood, John returned to LSU to pursue a lifelong ambition of earning a Doctorate. After another six and a half years at LSU, John finally realized this objective in the Fall semester of 2001, earning a Doctor of Philosophy in Mechanical Engineering degree focusing his research on the biomechanics of the human knee. Having spent a sum total of ten and a half years at an institution of higher learning, John will pursue a research-oriented career in a nonacademic setting following his graduation from LSU.

# DOCTORAL EXAMINATION AND DISSERTATION REPORT

**Candidate:** John Eric Fuller

**Major Field:** Mechanical Engineering

**Title of Dissertation:** Development and Characterization of Velocity Workspaces for the Human Knee

**Approved:**

Major Professor and Chairman

Dean of the Graduate School

**EXAMINING COMMITTEE:**

**Date of Examination:**

October 3, 2001